Establishment of Performance-Based Specifications for the Structural Use of Locally Available Macro-Synthetic Fibres
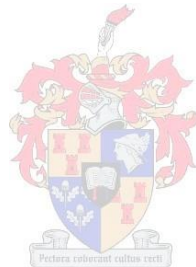
by

Courtney Megan Odendaal

Thesis presented in partial fulfilment of the requirements for the degree
Master of Engineering at Stellenbosch University

Supervisor: Prof. William Peter Boshoff

Faculty of Engineering

March 2015

Declaration

By submitting this thesis/dissertation electronically, I declare that the entirety of the work contained therein is my own, original work, that I am the sole author thereof (save to the extent explicitly otherwise stated), that reproduction and publication thereof by Stellenbosch University will not infringe any third party rights and that I have not previously in its entirety or in part submitted it for obtaining any qualification.

…………………………………………… Signature

Date: December 2014

Summary

FRC (Fibre-reinforced concrete) has become a common form of secondary and even primary reinforcing in some applications throughout the world. In South Africa, the structural applications are limited primarily to steel fibres while cheaper, lighter and more durable synthetic fibres have been side-lined due to low stiffnesses.

The purpose of this research project is to investigate the behaviour of synthetic fibre-reinforced concrete (SynFRC) using fibres which are locally available in South Africa, and to propose a performance-based specification and test method for the use of these fibres.

In order to achieve this, single fibre pull-out tests were performed on four locally available polypropylene fibres. It was found that the average bond stresses of the fibres are influenced primarily by the fibre cross sectional shape, longitudinal geometry and surface treatment, and secondarily by the aspect ratio. The W/C ratio had little effect on the single fibre performance of non-treated fibres, but appeared to have a slight effect on the single fibre performance of the surface treated fibre. From the experimental results, the highest fibre bond stress will be generated by using a fibre with an X-shaped cross section, longitudinal crimping and applying a surface treatment to this fibre. It also appears that the bond stress distribution for flat fibres is close to uniform, while the bond stress distribution for non-flat crimped fibres has a high mechanical interlock component at the surface end.

Macro-mechanical performance tests were performed by means of the BS EN 14651 (2007) three point beam bending test and the ASTM C1550 (2012) Round Determinate Panel Test (RDPT). These tests were selected following a thorough literature review. The RDPT was found to be more consistent and able to identify trends which the three point beam bending test could not. In addition, the three point beam bending test's most popular output, the $R_{e,3}$ value tended to be misleading with varying W/C ratios, and it is recommended that the equivalent flexural tensile strength be used instead if the three point beam bending test is used.

The macro-mechanical testing showed that increasing the fibre dosage did increase post-cracking performance. The flat fibres' performance was significantly better than that of the non-flat fibres, and also increased at a faster rate with increasing fibre dosage. The post-cracking performance decreased with increasing W/C ratios and increasing aggregate sizes. The macro-mechanical performance was inversely proportionate to the single fibre performance. The macro-mechanical performance decreased with increasing fibre bond stress, and increased with increasing equivalent diameter, which equates to fewer fibres in a set volume of fibres.

Finally, basic principles were developed from the data. These principles were used to predict the RDPT and three point beam bending test performance parameters based on fibre dosage, single fibre

properties (bond stress and equivalent diameter), W/C ratio and aggregate size from the available data. The principles can be further refined with more experimental data.

Opsomming

Vesel-gewapende beton word regoor die wêreld as 'n algemene vorm van sekondêre en selfs primêre versterking gebruik. In Suid-Afrika is die strukturele toepassings hoofsaaklik tot staal vesels beperk, terwyl goedkoper, ligter en meer duursame sintetiese vesels vermy word as gevolg van lae styfhede.

Die doel van hierdie navorsingsprojek is om die gedrag van sintetiese-veselversterktebeton (SynFRC) te ondersoek deur gebruik te maak van vesels wat in Suid-Afrika beskikbaar is, en 'n prestasie-gebaseerdespesifikasie en toetsmetode vir die gebruik van sintetiese vesels voor te stel.

Enkelveseluittrektoetse is op vier plaaslik beskikbare polipropileen vesels uitgevoer. Daar is gevind dat die gemiddelde verbandspanning van die vesel hoofsaaklik deur die vesel deursnee vorm, lengte meetkunde en oppervlak behandeling beïnvloed word, en tweedens deur die aspek verhouding beïnvloed. Die W/C-verhouding het min effek op die enkelveselprestasie van nie-behandelde vesels, maar het 'n effek op die enkeleveselprestasie van die oppervlak-behandelde vesel gehad. Die eksperimentele resultate wys dat die hoogste vesel verbandspanning deur 'n vesel met 'n X-vormige deursnit, lengte krimping en toepassing van 'n oppervlak behandeling gegenereer sal word. Dit blyk ook dat die verbandspanningverspreiding vir 'n plat vesel naby aan uniform is, terwyl die verbandspanningverspreiding vir 'n nie-plat gekrimpde vesel 'n hoë meganiese grendeling komponent op die oppervlak ente het.

Makro-meganiese prestasietoetse is uitgevoer deur middel van die BS EN 14651 (2007) driepuntbalkbuigtoets en die ASTM C1550 (2012) RDPT. Hierdie toetse is ná 'n deeglike literatuuroorsig gekies. Die RDPT is meer konsekwent en is in staat om neigings te identifiseer wat die driepuntbalkbuigingtoets nie kan nie. Daarbenewens, met wisselende W/C verhoudings, is die driepuntbalkbuigtoets se gewildste resultaat, die $R_{e,3}$-waarde geneig om misleidend te wees. Dit word aanbeveel dat die ekwivalentebuigtreksterkte in plaas van die $R_{e,3}$-waarde as die drie punt balk buig toets resultaat gebruik word.

Die makro-meganiesetoets het getoon dat die verhoging van die veseldosis 'n toename in na-krakingprestasie veroorsaak. Die plat vesels se prestasie was aansienlik beter as die van nie-plat vesels, en het met 'n toenemende veseldosis teen 'n vinniger koers verhoog. Die na-krakingprestasie het met toenemende W/C en die verhoging van die klip grootte afgeneem. Die makro-meganieseprestasie was omgekeerd eweredig aan die enkelveselprestasie. Die makro-meganieseprestasie het met toenemende vesel band stres verminder, en het met 'n toenemende gelykstaande deursnee (wat gelykstaande is aan minder vesel in 'n stel volume van vesel) vergroot.

Ten slotte is basiese beginsels uit die data ontwikkel. Hierdie beginsels is gebruik om die RDPT en driepuntbalkbuigtoets prestasieparameters gebaseer op veseldosis, enkelveseleienskappe

(verbandspanning en ekwivalentediameter), W/C-verhouding en klip grootte van die beskikbare data te voorspel. Die beginsels kan met meer eksperimentele data verder verfyn word.

Acknowledgements

I would like to thank the following people for their assistance:

- The staff of the laboratory and the workshop of the Civil Engineering Department for their assistance during the many months of casting and testing
- The fibre suppliers, Geotex, Chryso and Fibsol
- Philip Frost for assisting me with the single fibre pull-out tests
- My parents for affording me the opportunities in life to be able to attend university
- My supervisor, Prof Billy Boshoff, for his guidance and support

TABLE OF CONTENTS

List of Figures

List of Tables

List of Symbols

b	Beam width
CMOD	Crack mouth opening displacement
$D^f_{bz,i}$	Energy absorption up to deflection i
d_e	Equivalent fibre diameter
δ	Deflection
δ_L	Deflection at LOP
$F_{applied}$	Applied load
$F_{eq,i}$	Equivalent force corresponding to deflection i
$F_{fracture}$	Force required for fibre fracture
F_j	Applied load corresponding to CMOD j
F_L	Maximum applied load
F_p	Peak load (Four point beam bending)
$F_{r,bond}$	Resisting force from interfacial shear bond stress
f_1	First peak strength (Four point beam bending)
f_{ctm}	Axial tensile strength
$f_{eq,3}$	Third equivalent flexural tensile strength
$f_{eq,j}$	Equivalent flexural tensile strength corresponding to deflection i
f_p	Peak strength (Four point beam bending)
$f_{R,j}$	Residual flexural tensile strength corresponding to CMOD j
h_b	Unnotched beam height
h_{sp}	Notched beam height
LOP	Limit of proportionality
l_b	Beam span

l_c	Critical fibre length
l_d	Developed fibre length
l_e	Embedded fibre length
l_f	Cut fibre length
λ	Fibre aspect ratio (l_f / d_e)
MOR	Modulus of rupture
m_f	Mass of fibres
P_1	First peak load (Four point beam bending)
P_p	Peak load (Four point beam bending)
φ	Fibre snubbing angle
$R_{e,3}$	Third equivalent flexural tensile strength ratio
$R^D_{T,150}$	Equivalent flexural tensile strength ratio (Four point beam bending)
$R_{e,i}$	Equivalent flexural tensile strength ratio corresponding to deflection i
σ_f	Fibre tensile strength
$T_{D,150}$	Energy absorption up to $l_b/150$ (Four point beam bending)
τ	Interfacial shear bond stress
τ_{ave}	Average interfacial shear bond stress
W	RDPT energy absorption up to 40 mm

CHAPTER 1
Introduction

Concrete is a versatile material used in many everyday structures. It consists of a mixture of cement, water and aggregate to which other materials such as admixtures and cement replacement materials may be added (Illston & Domone, 2001).

Concrete has a low tensile strength in comparison to its compressive strength, and suffers brittle failure in direct and flexural tension. This has traditionally been compensated for by the inclusion of high tensile strength steel bar reinforcing. However, steel bar reinforcing has significant drawbacks such as a lack of durability in corrosive environments, high transportation and labour costs, and being labour and time-intensive. Fibre reinforced concrete (FRC) has been developed as a partial solution to these problems.

FRC is defined by the American Concrete Institute (ACI) as concrete containing discrete randomly-orientated fibres, and has been researched and used globally for the past century (Concrete Society, 2003). Standards and publications have been produced by, amongst others, the American Society for Testing and Materials (ASTM) International, the British Standards Institute (BSI) and the British Concrete Society detailing the benefits and usage of FRC.

Synthetic fibres are a viable solution for the replacement of traditional steel reinforcing and the popular steel fibre reinforced concrete (SFRC) as they are cheap, lightweight and inert, and thus durable.

Globally, synthetic fibre reinforced concrete (SynFRC) is used in a wide range of applications where crack control and post-cracking performance are of importance (ACI Committee 544, 1996).

1

Applications include industrial floors, roads, pavements, shotcrete for tunnel linings, slope stabilisation and precast segments (ERMCO, 2012 and Euclid Chemical Company, 2007).

In South Africa, SynFRC is generally avoided due to a lack of guidelines on the usage thereof, the lower stiffness of synthetic fibres when compared to steel fibres and research to back suppliers' claims. The primary objective of this research is to increase confidence in SynFRC by establishing performance based specifications for SynFRC using locally available macro-synthetic fibres by testing the fibres in various international test setups and determining various single fibre properties. The approach to achieving this objective is contained in the layout of this report.

Chapter 2 contains a theoretical background of FRC and the globally available tests to measure the performance thereof.

Chapter 3 determines the single fibre properties of four locally available fibres using a single fibre pull-out test method.

Chapter 4 compares two performance tests and the influence of fibre type, dosage, water-cement (W/C) ratio and aggregate size on the output parameters thereof.

Chapter 5 develops guidelines for the prediction of the performance parameters based on the trends and relations of the experimental data from Chapters 3 and 4. The guidelines are demonstrated by formulating equations based on the available data.

The research significance of this study is outlined below

- The effect of certain factors affecting single fibre behaviour will be established.
- The reliability of various macro-mechanical tests will be established.
- The performance of various locally available fibres on a macro-mechanical level and how they are affected by W/C ratio, aggregate size, fibre type and dosage will be determined, thus allowing comparison with other synthetic fibres.
- Any links between single fibre properties and macro-mechanical properties will be established.   .

CHAPTER 2

FRC Background

This chapter contains a general background on fibres for reinforcement, descriptions of FRC behaviour on single fibre and macro-mechanical levels, and in-depth discussions of popular international performance measurement methods.

2.1. General Overview of Fibres

2.1.1. Historical perspective

Since ancient times, fibres such as straw and horse hair have been used to reinforce brittle building materials such as mud bricks and plaster. In the early 1900s, asbestos fibres were popularised as highly durable reinforcing for cement products such as corrugated roofing sheets and pressure pipes. Asbestos fibre popularity decreased after they were established to be carcinogenic, and with this came the development of alternate fibres, namely steel fibres in the 1950s, glass fibres in Russia in the 1960s, and large scale synthetic fibre research in the 1980s (ACI Committee 544, 1996; Hannant, 1978).

2.1.2. Usage of fibres

Most publications stress that fibres are intended as secondary reinforcement, and should not be considered as influencing the pre-cracking behaviour. ACI Committee 544 (1996) reasoned that fibre distribution variance could result in low fibre content in critical areas, which would severly compromise structural integrity. Hannant (2002) agrees with the notion of fibres being a secondary reinforcement, although it is possible for the cracked concrete to carry a higher flexural tensile load than the uncracked section.

2.1.3. Steel fibres

Standards such as ASTM A820 (2011) and BS EN 14889-1 (2006) have standardised steel fibres for use in concrete. Steel fibres are popular due to their high stiffness (approximately 200 GPa) and tensile strength (between 0.5 GPa and 3 GPa). These fibres are typically available in lengths of 25 mm to 60 mm and aspect ratios (λ, defined as the fibre length divided by the fibre diameter) of 30 to 100 (Concrete Society, 2007).

Steel fibres are known to increase post-cracking load-bearing capacity (Soutsos et al., 2012; Buratti et al., 2011). However, this can only happen while the surrounding cement matrix's alkalinity remains high and passively protects the steel fibres. Carbonation reduces the cement matrix pH and if corroding agents such as water, oxygen and chlorides are present, fibre corrosion causes spalling to occur near the surface. If the crack widths are limited, the dispersed nature of the fibres limits the corrosion to the surface. When crack widths are not limited and post-crack load bearing fibres are exposed, the failure mode changes from ductile fibre pull-out to potentially catastrophic brittle fibre fracture (Illston & Domone, 2001; Concrete Society 2007).

2.1.4. Micro-synthetic fibres

Micro-synthetic fibres have been defined by ACI Concrete Terminology (2013) as fibres with an equivalent diameter (d_e) of less than 0.3 mm, though they are typically even smaller. Micro-synthetic fibres enhance the plastic state properties of concrete by improving the homogenity of the concrete mix which reduces early age cracking caused by bleeding and segregation, as well as by intercepting micro cracks before they can become visible macro cracks (Hannant, 2002).

2.1.5. Macro-synthetic fibres

A wide range of fibres including polypropylene, nylon, carbon, polyethylene, acrylic, aramid and polyester fibres have been developed in the petro-chemical and textile industry from organic polymers. Some of these fibres, such as carbon, are disadvantaged by factors such as economical inefficiency (Hannant, 1978; ACI Committee 544, 1996).

Polymeric synthetic fibres for use in concrete are also standardised, such as in BS EN 14889-2 (2006) which focuses on polyolefin fibres (polypropylene, polyster, nylon, aramid and acrylic fibres).

Polymeric synthetic fibres are generally chemically inert and bond mechanically with the surrounding cement matrix. Actions such as fibre crimping and twisting increase the mechanical advantage.

Macro-synthetic fibres are significantly larger than their micro counterparts, with lengths between 15 mm and 60 mm and equivalent diameters of between 0.3 mm and 1.0 mm. Macro-synthetic fibres have been developed as an alternative to steel fibre reinforcing to provide post crack flexural strength

and ductility, as well as minimising drying shrinkage cracks (Hathaway, 2007). Figure 1 shows the difference in physical size of micro- (hair-like) and macro- synthetic fibres.
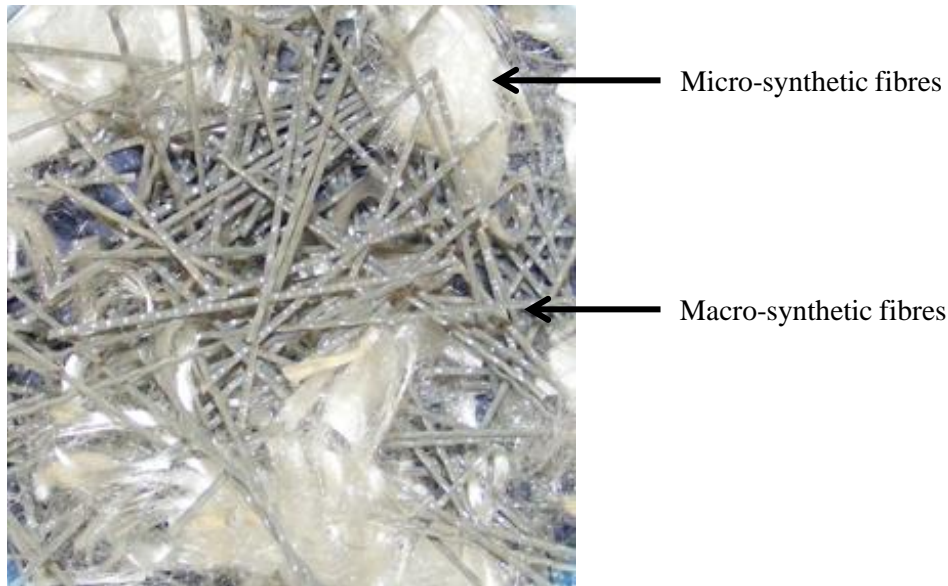
Figure 1: Physical difference between micro- and macro- synthetic fibres

Polypropylene fibres are the most popular synthetic fibres for use in concrete, both globally and locally. Although it has a low stiffness (approximately 5 GPa), its high tensile strength (0.5 GPa) and low cost saw it being researched as a concrete additive as early as 1965 (Beaudoin, 1990). It is also durable, as shown by the research of Hannant (1998).

2.2. FRC Behaviour and Performance

Concrete structures are generally reinforced with steel bar reinforcing for tension caused by flexure, as stated by Hannant (1978) and the ACI Committee 544 (1996).

2.2.1. Uncracked FRC behaviour and performance measurement

Uncracked FRC strength is based on the matrix strength, due to the low volume fibres added. The volume of fibres added is usually less than 1 %, with 2 % by volume seen as a relatively high dosage. Even at these higher dosages, the fibres make up such a small percentage of the matrix that their contribution to the uncracked performance is insignificant. This is confirmed by various studies, including Richardson (2005) and Soutsos et al. (2012).

The flexural tensile strength of conventionally reinforced and unreinforced concrete is quantified by the Modulus of Rupture (MOR), which is a measure of the first-crack strength of the concrete. The MOR is determined by standardised three and four point beam bending tests, specifically in South Africa by SANS 5864 (2006). These tests employ simple beam theory to determine the flexural stress at failure or first crack from the applied loadings and beam dimensions.

Commonly used fibre dosages do not have a significant effect on the pre-cracking flexural strength of concrete, as stated by the Concrete Society (2003) and ACI Committee 544 (1996) and confirmed by, amongst others, Richardson (2005) and Soutsos et al. (2012). Richardson (2006) also found that the compresive strength decreases with an increase in fibre dosage. Thus, traditional flexural tests are not suitable to demonstrate the advantages of fibres, which are evident after cracking.

2.2.2. Single fibre behaviour

When concrete cracks, the load is transferred from the cement matrix to the fibres by mechanical bonding, friction or chemical bonding. A simplified explanation of the single fibre behaviour when subjected to tensile loading follows, based on the following assumptions:

- Fibres are aligned with the stress and uniformly distributed throughout the matrix
- Behaviour of both the matrix and fibres is elastic up until failure
- The fibre-matrix interface is uniform and continuous

When the force is transferred from the cement matrix to the fibres, an interfacial shear bond stress (τ) develops between the cement-based matrix and the fibre, indicated in green in Figure 2.
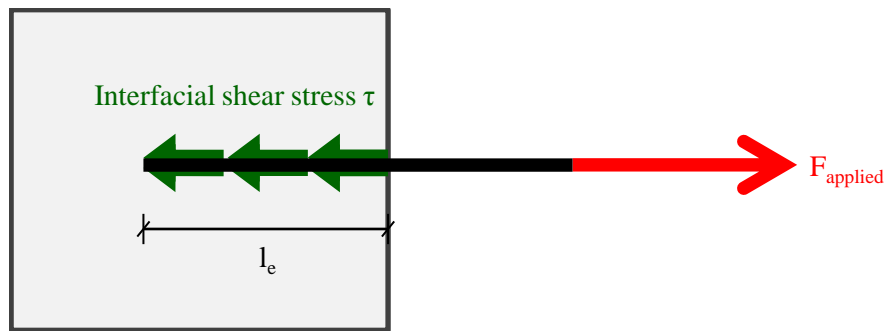
Figure 2: Load transfer between cement-based matrix and fibre

The resisting force ($F_{r,bond}$) offered by the shear stress over the embedded fibre length (l_e) can be written as

$$F_{r,bond} = \tau \times \pi \times d_e \times l_e \qquad [1]$$

where d_e is the equivalent fibre diameter.

The force required for fibre fracture ($F_{fracture}$) can be written as

$$F_{fracture} = \sigma_f \times \frac{\pi d_e^2}{4} \qquad [2]$$

where σ_f is the fibre tensile strength.

6

FRC can fail in various ways, the most common of which is fibre pull-out, which will occur if $F_{r,bond}$ is less than $F_{fracture}$. If $F_{r,bond}$ is larger than $F_{fracture}$, fibre fracture will occur, leading to brittle failure of the composite (Beaudoin, 1990; Hannant, 1978).

The critical embedded fibre length (l_c) is defined as the maximum length of fibre which will allow fibre pull-out as opposed to fibre fracture. This length is obtained by equating Equations [1] and [2] to obtain

$$l_c = \frac{\sigma_f d_e}{4\tau} \qquad\qquad\qquad [3]$$

It is ideal for fibre pull-out to occur as opposed to fibre fracture. For this to occur, a fibre has to pull out on at least one side of a crack, implying that the critical length should not be embedded on both sides simultaneously. For this to be possible, fibre lengths should be limited to a maximum of twice the critical length.

The above explanation of single fibre behaviour assumes a constant bond stress over the embedded fibre length. In reality, this bond stress is not constant over the fibre length and is comprised of an elastic bond stress, a frictional bond stress which develops as fibre pull-out occurs and any mechanical bond stress (Brandt, 2009). The τ used in Equations [1] and [3] is therefore actually an average bond stress (τ_{ave}) acting over the embedded length.

2.2.3. Factors influencing interfacial bond stress

Three primary methods exist for enhancing the bond stress of a fibre. The first is transition zone densification, which can be achieved by, for example, adding silica fume to the matrix, thus providing more cement matrix as opposed to free water for the fibre to bond with. Although this has been shown to enhance the interfacial bond stress region of metal and carbon fibres, the chemical inertness of polymeric synthetic fibres disallows this effect (Li et al., 1994).

Secondly, various deformations can be applied to the fibres, such as fibrillation, crimping and twisting in order to enhance the mechanical bond.

The final bond stress improvement method is chemical surface treatment of the fibre, which removes hydrogen atoms from the polymer backbone of the fibre and replaces them with polar groups. This enhances reactivity and improves the adhesion between the fibres and cement matrix (Singh et al., 2004).

2.2.4. Fibre snubbing

The fibre snubbing effect is the increase in maximum pull-out force when a fibre is pulled out at an angle (φ) as opposed to being pulled out in an aligned fashion (Figure 3).

As the fibre is being pulled out of the concrete at an angle, a normal force is exerted on the fibre to cause the direction change. This normal force translates to a perpendicular frictional force, which provides an extra component to the bond stress resistance. Synthetic fibre snubbing is generally not as pronounced as that of stiffer steel fibres (Li et al., 1990).
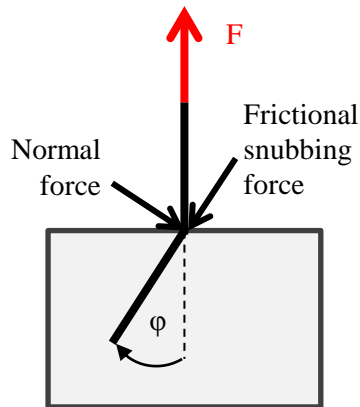
Figure 3: Fibre snubbing angle

2.2.5. Post-cracking FRC behaviour

In normal concrete (depicted by the purple line in Figure 4) the load-bearing capacity drops sharply once the concrete has cracked. In FRC, the load carried by the concrete is transferred to the fibres during cracking. Depending on the fibre dosage, the composite will experience either strain hardening or strain softening (depicted by red and green lines in Figure 4 respectively). Strain hardening occurs when the fibres carry a higher load than that which the composite did prior to cracking, and conversely strain softening occurs when the fibres carry a lower load than what the composite did prior to cracking. Polymeric synthetic fibres generally tend to exhibit strain softening behaviour at typical dosages due to their lower stiffnesses.

Several studies (Won et al., 2006; Cengiz & Turanli, 2004 and Soutsos et al., 2012) have shown a significant increase of the toughness (energy absorption capability of a material) of FRC over conventional concrete.

2.2.6. Factors affecting post-cracking FRC performance

It is generally accepted that an increase in fibre dosage results in an increase in the post cracking performance parameters. The fibre material also affects the performance with steel fibres generally outperforming synthetic fibres at the same dosage (Buratti et al.,2011; Soutsos et al., 2012 and Won et al., 2006).
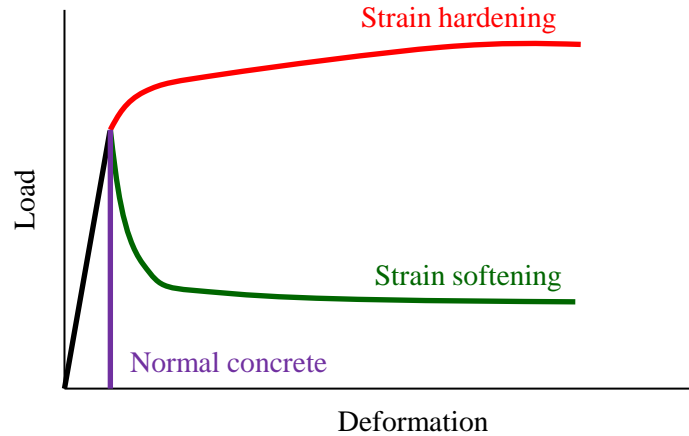
Figure 4: Depiction of strain softening and strain hardening behaviour of FRC, adapted from ACI Committee 544 (1996)

Figure 5 shows results from the research of Soutsos et al. (2012) which shows the improvement in post-cracking three point beam bending test performance when increasing synthetic fibre dosage from 4.6 kg.m^{-3} (black line) to 5.3 kg.m^{-3} (red line).
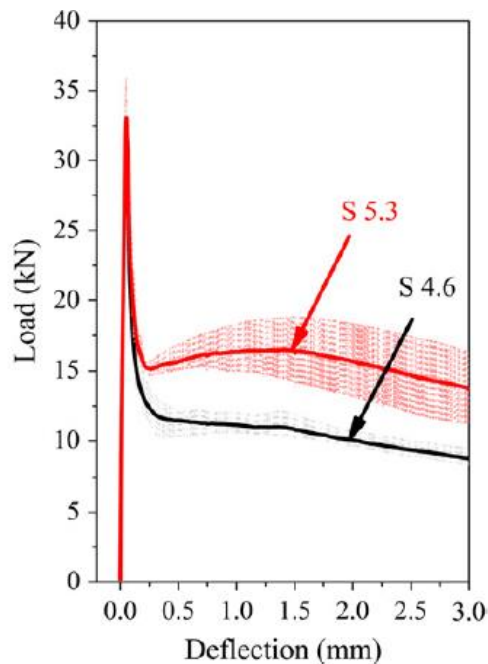
Figure 5: Typical three point beam bending results for synthetic fibres (Soutsos et al., 2012)

An increase in coarse aggregate size will negatively affect the fibre distribution, as shown in Figure 6. The less uniform fibre distribution over cracks will result in fewer fibres being able to consistently bridge the cracks and provide post-cracking load carrying capacity.

9
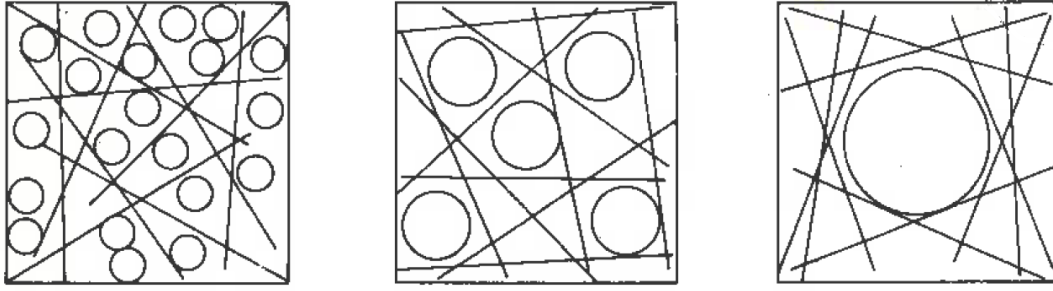
Figure 6: Effect of coarse aggregate size on fibre distribution (Hannant, 1978)

The W/C ratio is another factor known to affect the post cracking performance of concrete. Nallathambi et al. (1984) and Lin (1992) found that an increasing W/C ratio causes a decrease in post-cracking performance parameters. A lower W/C ratio also has the advantage of increasing the matrix strength and decreasing the free moisture in the matrix which could aid the transport of corrosive materials (Concrete Society, 2007).

Other factors relating to single fibre properties and mix design may also influence post-cracking behaviour.

2.3. Three Point Beam Bending Test

2.3.1. Setup
The three point beam bending test for FRC, documented by BS EN 14651 (2007) and recommended by the 2010 Model Code, is shown schematically in Figure 7.

The test method involves a simply supported beam with a notch of 25 mm, a cross sectional area of 150 x 150 mm and a span (l_b) of 500 mm. At 28 days, a central load is applied in the centre of the beam using an actuator at a rate controlled by either the crack mouth opening displacement (CMOD) or the beam deflection (δ). The test is terminated once a specified CMOD or deflection is reached. The following values of interest can be determined from this test.

2.3.2. Limit of proportionality (LOP)
The LOP is calculated using the maximum applied load (F_L) in the CMOD interval of 0 to 0.05 mm, and elastic beam theory. The LOP is not equivalent to the MOR of traditional flexural tests, as the MOR is based on the loading at the first crack, whilst the LOP can be obtained from loading after the first crack, for example in strain hardening concrete. The LOP is given by

$$LOP = \frac{3F_L l_b}{2bh_{sp}^2} \qquad\qquad [4]$$

where b is the specimen width and h_{sp} the distance between the tip of the notch and the top of the specimen.

10
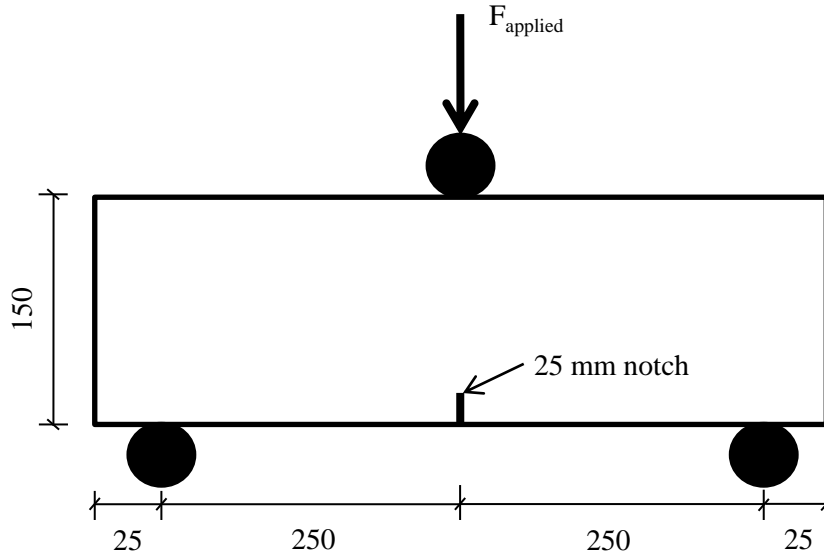
Figure 7: Schematic setup of the three point beam bending test as per BS EN 14651 (2007)

2.3.3. Residual flexural tensile strengths (f_{R,j})

Residual flexural tensile strengths ($f_{R,j}$) are strengths calculated using the applied loading at specified CMODs. The values for the various CMODs and their corresponding loads (F_j) are shown in Figure 8.
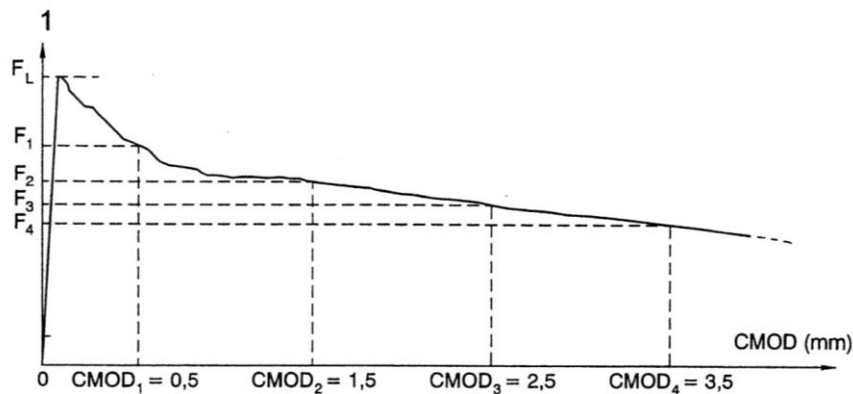
Figure 8: BS EN 14651 (2007) CMODs and corresponding force determination

The $f_{R,j}$ corresponding to a particular CMOD can be calculated using the corresponding force F_j and elastic beam theory:

$$f_{R,j} = \frac{3F_j l_b}{2bh_{sp}^2} \, , \qquad j = 1, 2, 3, 4 \tag{5}$$

2.3.4. Equivalent flexural tensile strengths (f_{eq,i}) and ratios

BS EN 14651 (2007) does not explicitly define equivalent flexural tensile strengths ($f_{eq,i}$). RILEM TC 162 (2002) describes the process of determining $f_{eq,i}$ based on the load-deflection diagram.

11

The energy absorption capacity ($D^f_{BZ,i}$) is defined as the area under the load-deflection curve up to a specified deflection. Figure 9 depicts the concept for determining the third equivalent flexural tensile strength, $f_{eq,3}$. The energy absorption $D^f_{BZ,3}$ is the energy absorption up to a deflection of δ_3 (2.65 mm past the deflection at which the LOP was reached (δ_L)). The energy absorption is divided into two parts – energy absorption of plain concrete (i.e. with no influence of fibres) indicated by the unshaded area, and energy absorption of the fibres indicated by the shaded area. The energy absorption of the fibres is used to determine an equivalent force ($F_{eq,3}$), which will give a rectangular block with an area equal to $D^f_{BZ,3}$.
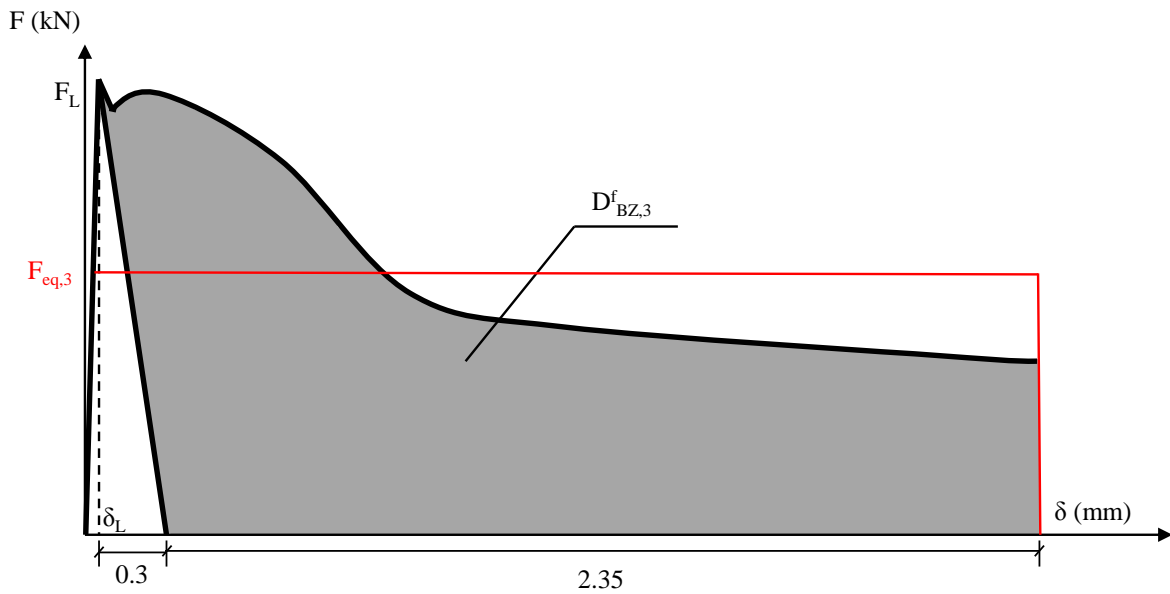
Figure 9: Load-deflection diagrams for determination of $f_{eq,3}$ (RILEM, 2002)

Any equivalent force can be determined as:

$$F_{eq,i} = \frac{D^f_{BZ,i}}{\delta - 0.15} \quad i = 2,3 \tag{6}$$

and then used to calculate $f_{eq,i}$ at a particular deflection:

$$f_{eq,i} = \frac{3\,F_{eq,i}l_b}{2bh^2_{sp}} \quad i = 2,3 \tag{7}$$

The equivalent flexural tensile strength ratio $R_{e,3}$, would then be determined as:

$$R_{e,3} = \frac{f_{eq,3}}{LOP} \tag{8}$$

12

2.3.5. Disadvantages

This test method is not intended for fibres longer than 60 mm, as this is the maximum typical fibre length (ERMCO, 2012), or for aggregate larger than 32 mm. The aggregate size limitation could be due to the negative effect increasing aggregate size has on fibre dispersion.

The primary disadvantage of the three point beam bending test is a high result scatter. This is well documented by Buratti et al. (2011), Parmentier et al. (2008) and Vandewalle et al. (2008). The high result scatter is attributed to the variability of fibre distribution over such a small cross sectional area.

Buratti et al. (2011) found that the scatter of stiffer steel fibres was significantly higher than that of the less stiff macro-synthetic fibres (Figure 10). This was attributed to the synthetic fibres dispersing more homogenously throughout the concrete during mixing than the steel fibres.
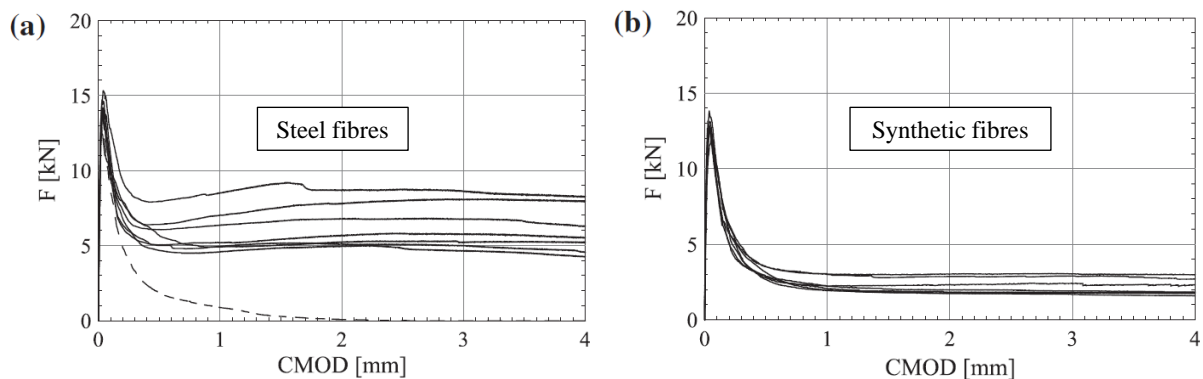
Figure 10: Scatter of three point bending test results for steel fibres (left) and macro-synthetic fibres (right) (Buratti et al., 2011).

Another possible disadvantage of the three point beam bending test is that a lower LOP (induced by, for example, a higher W/C ratio) results in a misleading higher $R_{e,3}$ value (as per Equation [8]), even if the fibre dosage and thus post-cracking performance as indicated by equivalent flexural tensile strengths is similar.

2.4. Four Point Beam Bending Tests

2.4.1. Setup

The basic test setup for the four point unnotched beam bending test (Figure 11) (also known as the third point loading beam bending test) has been standardised by ASTM C78 (2010). The standard utilises two preferred beam sizes – 100 x 100 x 350 mm (span 300 mm) and 150 x 150 x 500 mm (span 450 mm).

Two standards which use this setup, ASTM C1609 (2012) and ASTM C1399 (2010) are described in the following sections.

2.4.2. ASTM C1609: Equivalent flexural tensile strength ratio

ASTM C1609 (2010) utilises the normal four point bending test, but measures the deflection up to at least $l_b/150$ of the span (3 mm for 450 mm beam and 2 mm for a 300 mm beam), while monitoring the load and net deflection. Figure 12 shows a typical load versus net deflection curve, as obtained from the standard.

The first peak strength (f_1) can be calculated as:

$$f_1 = \frac{P_1 l_b}{b h_b^2} \tag{9}$$

where P_1 is the first peak load and h is the depth of the specimen.

Similarly, the peak strength f_p can be calculated using the peak load P_P, if required.
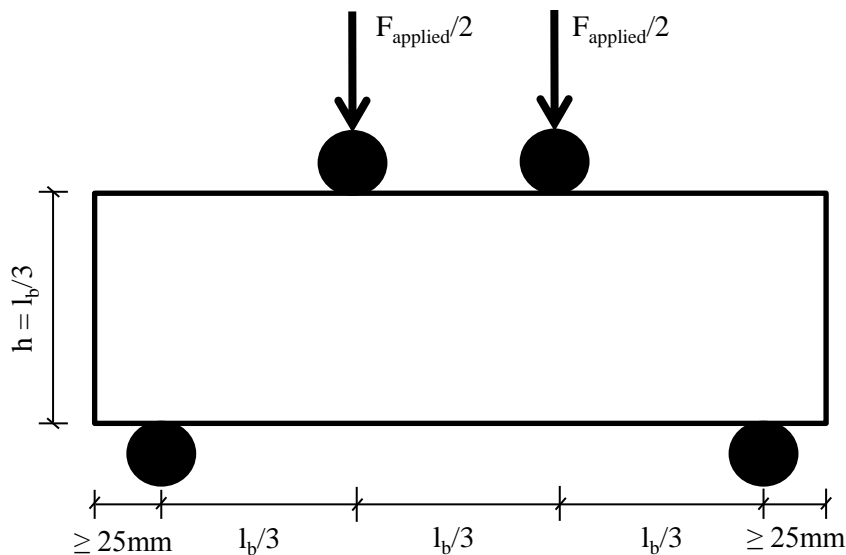
Figure 11: Schematic of the ASTM C78 (2010) four point beam bending test setup

The equivalent strength ratio $R^D_{T,150}$ is calculated using the first peak load:

$$R^D_{T,150} = \frac{150\,T^D_{150}}{f_1 b h_b^2} \times 100 \tag{10}$$

where T^D_{150} is the area under the load deflection curve up to $l_b/150$,

Residual flexural tensile stresses are also specified at various deflections, as in Section 2.3.3.

2.4.3. ASTM C1399: Residual flexural tensile strengths

The experimental setup of ASTM C1399 (2010) is similar to that of ASTM C78 (2010). An initial loading cycle is applied up until the first crack, and once the beam has cracked, the load is removed and reapplied to obtain a second load-deflection. The average residual stress is determined using the
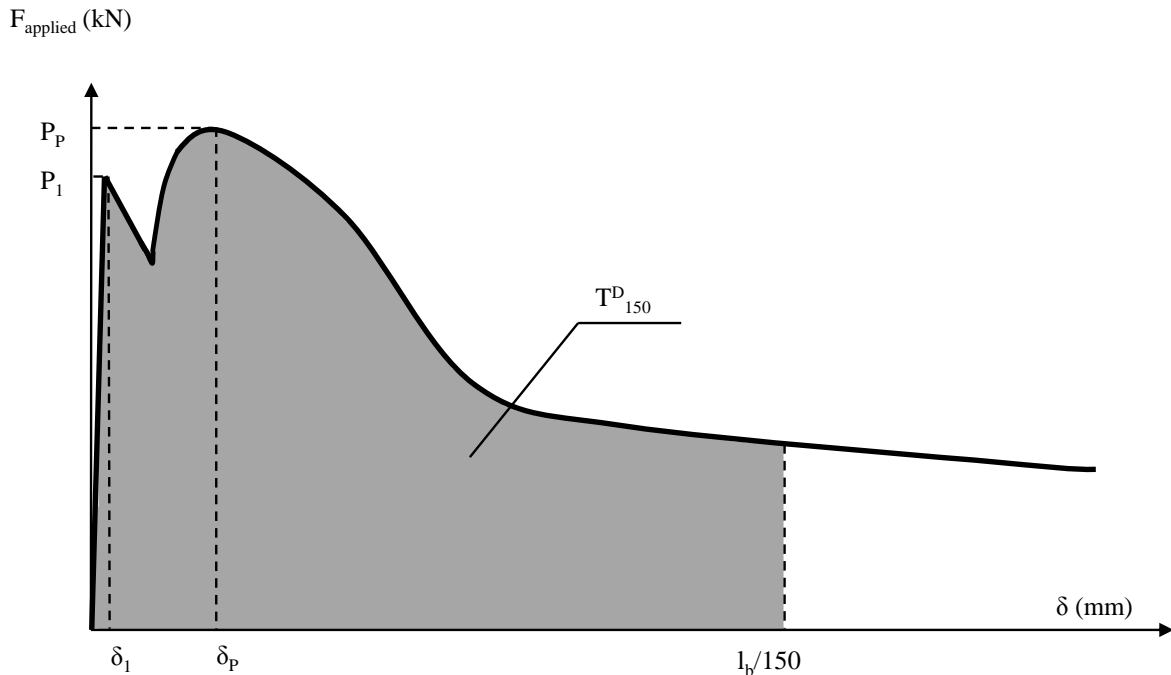
Figure 12: ATSM C1609 (2012) typical load versus net deflection curve

average of load values at specified deflection values on the reloading curve (0.5 mm, 0.75 mm, 1.0 mm, 1.25 mm).

2.4.4 Toughness indices tests

Various toughness index test methods such as ASTM C1018 (1997) were used to quantify toughness. ASTM C1018 (1997) employed the ASTM C78 (2010) test setup, and defined a method for determining first crack strength (MOR), the corresponding deflection, as well as various toughness indices based on areas determined by multiples of the first crack deflections. However, these standards have been withdrawn or are no longer available.

A possible reason for the withdrawal of the standard is, as stated by Mindess et al. (1994), that the results were strongly influenced by the test procedure and method of analysis used, for example the method of determination of the first crack and deflection measurement.

2.4.5. Disadvantages

The test standards (SANS 5864, 2006) warn that the results of the four point beam bending test will be lower than that of the three point beam bending test. This is due to there being a larger region for the crack to occur – the entire middle third of the beam instead of being forced at a particular point, and thus allowing for the selection of a weaker spot along the span for the crack to occur.

Many researchers, including Parmentier et al. (2008), Chao et al. (2011) and Bernard (2002) have reported high result scatter when using the four point beam bending test, as opposed to round panel test, which is described next.

15

2.5. Round Determinate Panel Test (RDPT)

2.5.1. Setup

The ASTM C1550 Round Determinate Panel Test (RDPT) (Figure 13) was developed as a solution to the high scatter of beam test results. The RDPT subjects a round 800 mm diameter panel with a 75 mm thickness, symmetrically supported at three points, to a central point load applied with a hemispherical end. As with the beam bending tests, a load deflection curve is plotted, and the energy absorbed up to specific deflections can be used for comparative purposes. A successful sample is regarded as one in which three evenly sized cracks occur between the supports, and two successful samples constitute a set.

Figure 13: RDPT setup

2.5.2. Potential problems and advantages

The standard specifies a tedious load-deflection adjustment procedure if the loading piston deflection is used to measure the central deflection of the panel. A simple solution is to measure the deflection directly on the tensile (bottom) surface of the panel. A second potential problem is the occurrence of beam-like failure, as opposed to the desired failure mode, as there is no way to predict if this will occur. This could lead to an entire sample set having to be recast.

The RDPT has a significantly higher crack area than any of the beam bending tests, which reduces result scatter. Another advantage of this test is its biaxial flexural behaviour, which is similar to that of in-situ structures.

2.6. EFNARC Panel Tests

EFNARC (1996) proposed a simply supported square panel test consisting of a 600 x 600 x 100 mm plate with a centrally applied load, shown schematically in Figure 14. The central deflection rate is

specified as 1.5 mm per minute, and testing is terminated at a central deflection of 25 mm. The energy absorption capacity is then determined as the area under the load deflection curve, as for the RDPT. EFNARC (1996) also specifies energy classes, as shown in Table 1. This test was a precursor to the RDPT, and is primarily used for shotcrete.
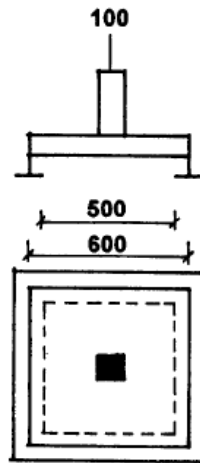
Figure 14: EFNARC square panel test setup

Table 1: EFNARC (1996) energy classes

Toughness classification	Energy absorption in joule for deflection up to 25 mm
a	500
b	700
c	1000

2.7. Wedge Splitting Test (WST)

The wedge splitting test (WST) developed by NT Build 511 (2005), involves applying a vertical splitting load to a notched FRC 150 mm or 200 mm cube. The CMOD and applied load are monitored and can be used to determine the splitting force, as well as fracture energy (energy required to open a unit area of crack surface) and residual tensile stresses. However, the test documentation itself admits that the coeffcient of variation can be anything from 5 to 40 percent, and attributes it to the usual factors of fibre distribution, fibre content and fibre length.

2.8. Correlation between Tests

Several studies have been done on the correlation of the tests mentioned above. The most relevant are discussed in the following sections.

2.8.1. Correlation of RDPT and EFNARC panel tests

Bernard (2002) produced Figure 15, showing a strong linear correlation ($R^2 = 0.9$) between EFNARC square panel tests and ASTM RDPT tests. The correlation was obtained at an EFNARC panel deflection of 25 mm and an RDPT deflection of 40 mm, with the relationship of 1000 J at 25 mm on the EFNARC test being equal to 400 J at 40 mm on the RDPT.
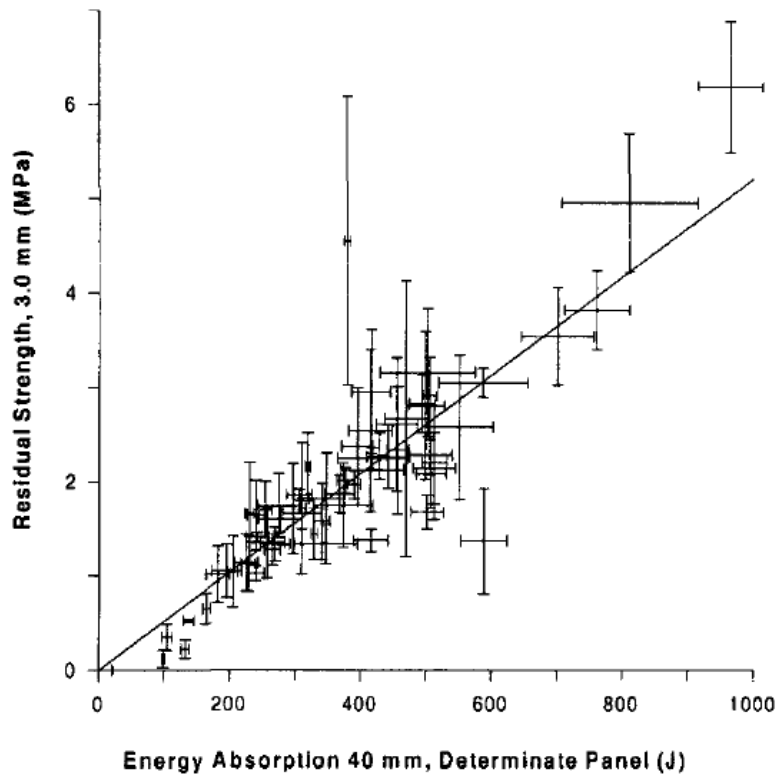
Figure 15: RDPT and EFNARC correlations (Bernard, 2002)

2.8.2. Relation between three point beam bending test and RDPT

Parmentier et al. (2008) conducted three point bending tests, and compared the residual stresses to the ASTM RDPT energy values at the same crack opening. The initial results using steel fibres (Figure 16) showed a promising correlation, although the authors did express doubt over whether the correlation could be attributed to the fibre dosage or the fibre type. The authors particularly stated that when the macro-synthetic fibre results were added the correlation was not as promising.

2.9. Concluding Summary

FRC behaviour is complex at best, and new FRC research is being undertaken every day. Although several test methods for quantifying FRC behaviour exist, the two most viable ones for SynFRC appear to be three point beam bending test due to its familiarity and apparent lower scatter when using synthetic fibres, and the RDPT due to its significantly lower result scatter.
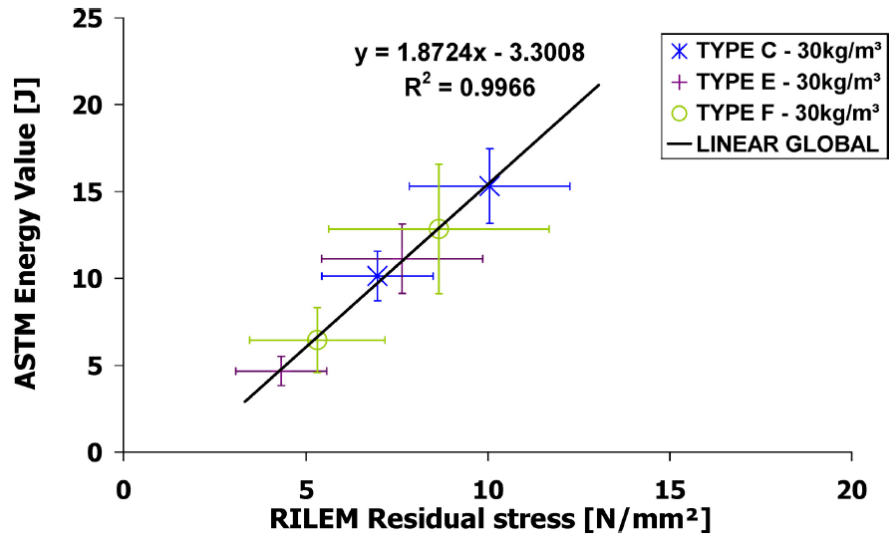
Figure 16: (Parmentier et al., 2008) Correlation between ASTM RDPT tests and RILEM three point beam bending tests

CHAPTER 3

Single Fibre Pull-out Experiments

Single fibre pull-out tests were performed on four locally available macro-synthetic fibres to determine the maximum pull-out force, average bond stress and critical length of each fibre. From the tests the effects of the W/C ratio, cross-sectional shape and aspect ratio on the average bond stress were determined. The snubbing effect was also investigated.

The main obstacles with single fibre pull-out tests are that they are not standardised, the generally high variation due to the small sample surface area, and the difficulty in preparing these fine and sensitive samples.

3.1. Materials

3.1.1. Fibres

Single fibre pull-out tests were performed on four locally available polypropylene fibres (Figure 17) with a relative density (RD) of between 0.88 and 0.92 (as per the material information sheets).

The equivalent fibre diameter (d_e) is defined in BS EN 14889-2 (2006) as the diameter of a circle with an area equal to the mean cross sectional area of the fibre. A scale with a resolution of 0.0001 g was used to weigh 20, 40 and 50 fibres of each type of fibre. As the fibre lengths were known, the equivalent diameters of each fibre could be determined using:
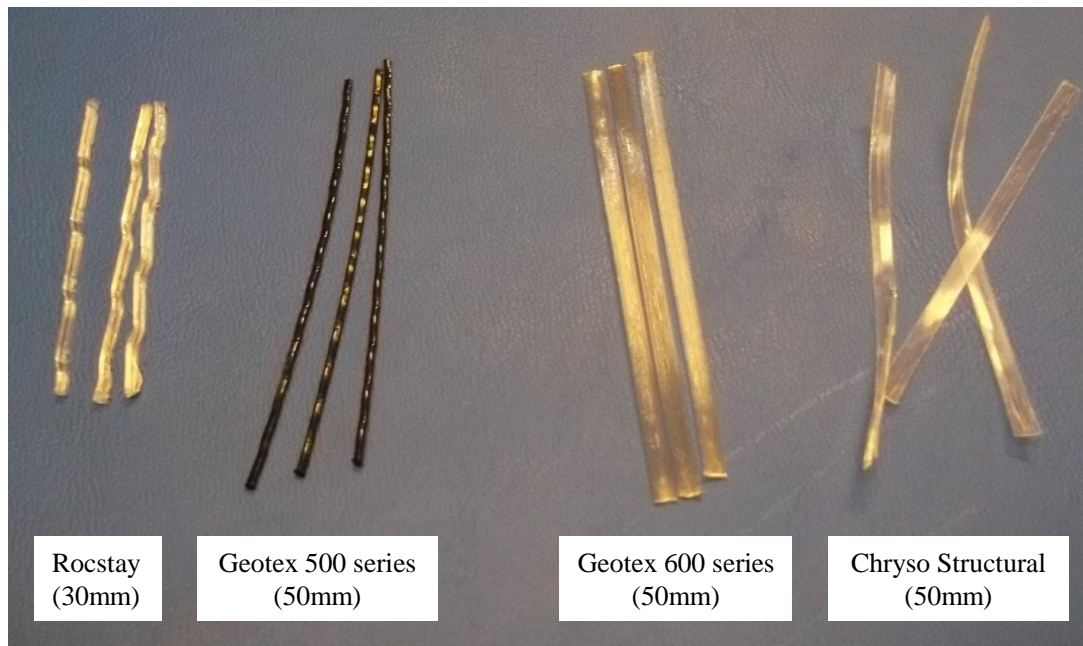
Figure 17: Fibres used in tests

$$d_e = \sqrt{\frac{4000 m_f}{RD\pi l_d}}$$
[11]

where m_f is the total mass of fibres in grams and l_d is the total length of fibres weighed in mm. Detailed measurements and calculations are available in Appendix A.

The aspect ratio (λ) of a fibre is equal to:

$$\lambda = \frac{l_f}{d_e}$$
[12]

The fibres are typically cut to lengths (l_f) as chosen by the supplier. Longer length fibres were specifically cut for the purpose of achieving deeper embedment lengths in the single fibre pull-out experiments. Longer length fibres are not typically available, as they can negatively influence the concrete workability.

Two rounds of testing were conducted on the Rocstay fibres after a discrepancy in the cross-sectional size between the fibres used in some of the single fibre pull-out tests and the macro-mechanical tests was noted. The first round of single fibre pull-out testing was conducted using fibres which had a larger equivalent diameter than the fibres used in the macro-mechanical tests (Chapter 4). The second round of single fibre testing utilised fibres which had the same equivalent diameter as the fibres used in the macro-mechanical tests. The fibres used for the longer embedment length single fibre pull-out had the same equivalent diameter as the fibres used in the second round of single fibre pull-out testing and macro-mechanical tests.

21

The Geotex 500 series fibres also had a geometrical discrepancy between the fibres used for the shorter length and longer length single fibre pull-out experiments. The Geotex 500 series fibres are crimped (Figure 17). However, the mechanical crimping deformation of the longer length fibres was not as pronounced as the shorter typical cut length fibres. This was again only noted after results indicated a discrepancy (Figure 30).

The fibre geometries (cross-sectional shape and longitudinal geometry), typical cut lengths, equivalent diameters and aspect ratios (both supplied and measured), supplied fibre tensile strengths (σ_f) and theoretical maximum breaking forces (according to the supplied fibre tensile strength and measured equivalent diameters) are summarised in Table 2.

3.1.2. Cement

A CEM I 52.5N supplied by Pretoria Portland Cement was used, with a relative density of 3.14. Although the production of this particular cement was discontinued approximately halfway through the project, enough was still available for testing to be completed using the same cement.

3.1.3. Fine aggregate

A fine natural sand, locally known as Malmesbury Sand with a relative density of 2.62 was used. Three batches of sand were used throughout the project. Each batch was graded according to SANS 1083 (2006). The gradings (Figure 18) were found to be similar and therefore not expected to influence the test results.
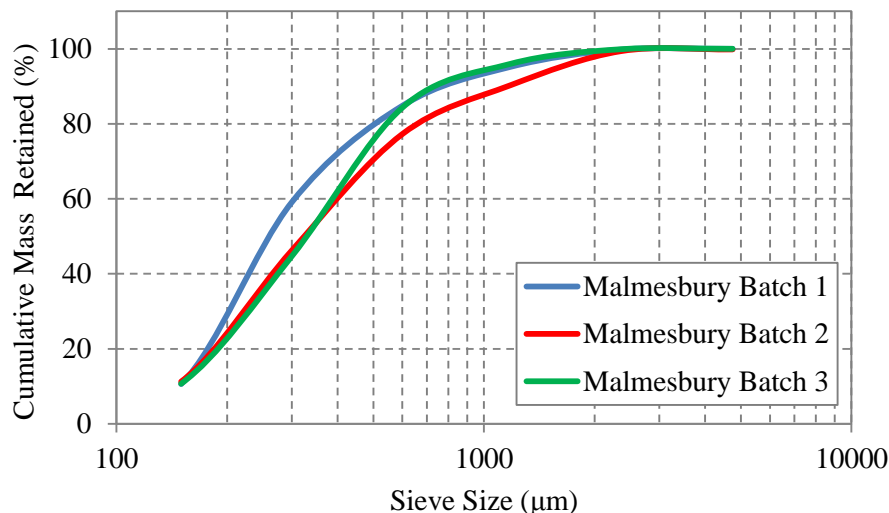
Figure 18: Fine aggregate gradings

3.1.4 Coarse aggregate

6 mm Greywacke aggregate (also known as Malmesbury Shale) with a relative density of 2.8 and a compacted bulk density (CBD) of 1563 kg.m^{-3} was used. It is identifiable by its blue-grey colouring and angular shape.

22

Table 2: Fibre properties

Fibre name	Cross sectional shape	Longitudinal geometry	l_f (mm)	d_e – Supplier (mm)	d_e – Measured (mm)	d_e - Longer length - Measured (mm)	λ - Supplier	λ - Measured	λ - Longer length - Measured	σ_f (MPa)	Theoretical maximum force (N)
Rocstay CXO 50/30 SS (Set 1)	X	Crimped	30	0.8	0.998	0.703	37.5	30.1	42.6	300	235
Rocstay CXO 50/30 SS (Set 2)	X	Crimped	30	0.8	0.701	0.703	37.5	42.8	42.6	300	116
Geotex 500 series	Oval	Crimped	50	0.9	0.760	0.767	55.5	65.8	65.2	295	134
Geotex 600 series	Rectangular	Flat fibrillated	50	0.8	0.907	-	62.5	55.1	-	275	178
Chryso Structural	Rectangular	Flat tape (Crypsinated)	50	0.79	0.615	-	63.3	81	-	336	100

23

3.2. Test Program

The single fibre test program comprised testing all four fibres described in Section 3.1.1 at W/C ratios of 0.4, 0.5 and 0.6, and embedment lengths as follows:

- The Rocstay fibre was tested at multiples of a third of its typical length (30 mm)
- The other fibres were tested at multiples of a quarter of its typical length (50 mm)

The embedment lengths are detailed in Table 3.

Table 3: Embedment length descriptions

Embedment length (mm)	Rocstay	Geotex 500 series	Geotex 600 series	Chryso Structural
L1	10	12.5	12.5	12.5
L2	20	25	25	25
L3	30	37.5	37.5	37.5
L4	40	50	50	45

The snubbing effect (Section 2.2.4) was investigated using a constant embedment length of two thirds of the typical cut fibre length for the Rocstay fibres (20 mm) and half of the typical cut fibre length for the other fibres (25 mm), a W/C ratio of 0.5, and snubbing angle variations of 0°, 30° and 60°.

The mix designs per cubic metre for the three different W/C ratios are given in Table 4.

Table 4: Single fibre pull-out experiment mix designs, all values in $kg.m^{-3}$

Mix number	Water	Cement	W/C ratio	6 mm Aggregate	Sand
M1	240	400	0.6	781.5	926.2
M2	240	480	0.5	781.5	859.4
M3	240	600	0.4	781.5	759.3

Although the inclusion of coarse aggregate could potentially increase the result variation, it is unrealistic and unrepresentative of everyday concrete to not use coarse aggregate.

3.3. Sample Preparation, Casting and Curing

Eight samples were prepared for each single fibre mix variation. Specimen moulds were prepared by halving a standard 100 x 100 mm cube mould with an oiled wooden separator, which yielded samples

24

of approximately 100 x 100 x 40 mm. The dry constituents were mixed for 60 seconds before the mix water was added, and allowed to mix in for 120 seconds. Slump tests were performed according to SANS 5862-1 (2006).

The moulds were filled to the brim and compacted using a vibrating table. Concrete was then either added or removed to bring the sample to level with the mould edge. The fibres were inserted into the centre of the wet concrete up to the relevant pre-marked embedment length. A schematic of a halved cube mould with two samples is shown in Figure 19. Note the fibre is not to scale.
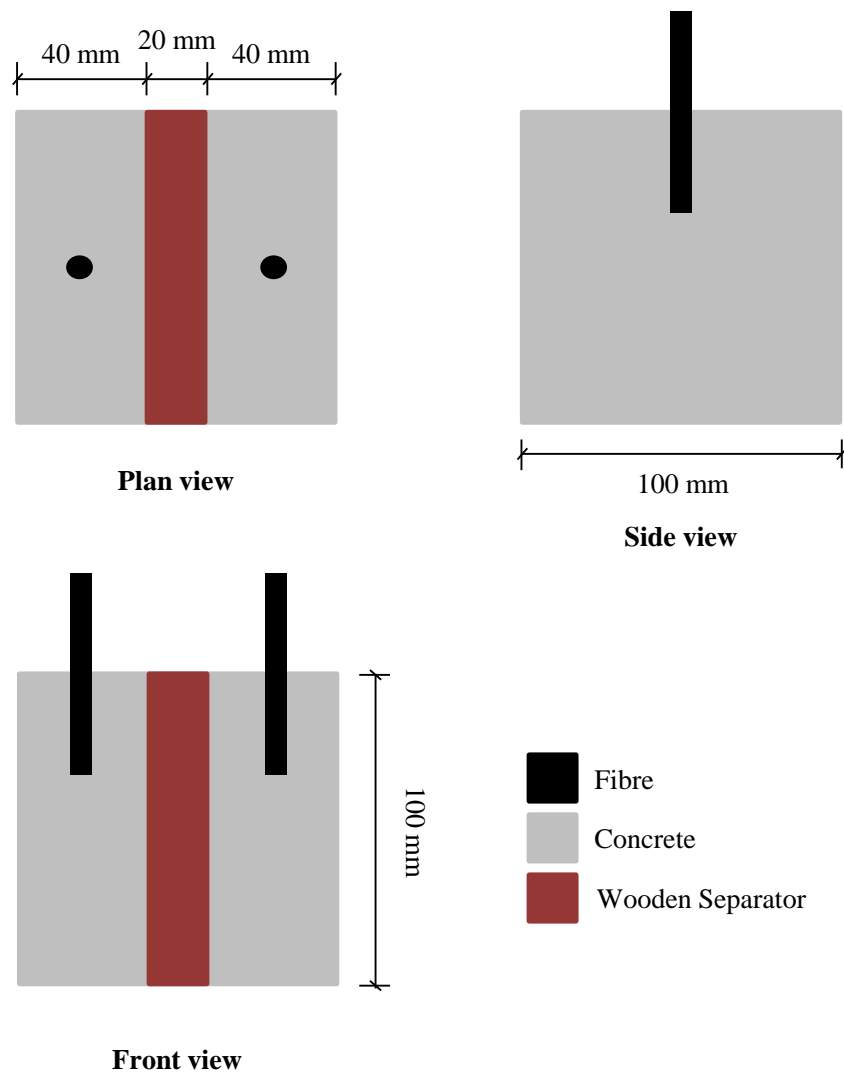
Figure 19: Schematic of single fibre sample preparation. Note the fibre is not to scale.

Various problems were encountered during fibre insertion. In order to determine where the middle of the sample was, measurements were taken with a ruler and the fibre inserted within 2 mm of the centre in each direction. The fibres were also visually inspected from all directions to ensure verticality. The stiffer Rocstay and Geotex 500 series fibres allowed for the discovery of aggregate

25

particles during insertion. The fibre would bend noticeably if coarse aggregate particle was encountered, thus allowing it to be moved away from the centre.

The Geotex 600 series and Chryso Structural fibres were not stiff enough to be inserted alone, and had to be inserted with a stiffer fibre which was then removed and the specimen lightly recompacted.

For the snubbing angle effect experiments, the flat fibres were inserted into the concrete with an orientation such that they would bend about their strong axis when being pulled out. Figure 20 schematically shows a flat rectangular fibre cross section, with strong and weak axis bending indicated.
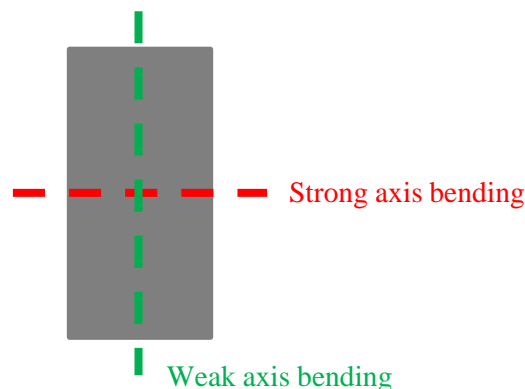
Figure 20: Cross-section of a flat rectangular fibre with strong and weak axis bending indicated

The samples were allowed to set in a temperature controlled chamber at 23°C for 24 hours, and then placed in a curing tank at 22°C until testing at 28 days.

3.4. Test Setup

The single fibre pull-out test setup is shown in Figure 21. The tests were performed in a Zwick Z250 Materials Testing Machine. Hydraulic clamps held the bottom part of the concrete specimen. The fibre clamp gripped the fibre protruding from the concrete, as close to the concrete as possible for consistency. Two HBM Linear Variable Differential Transformers (LVDTs) were used to measure pull-out displacement. The size of the LVDTs depended on the fibre embedment length. 50 mm LVDTs were used for embedment lengths less than 40 mm and 100 mm LVDTs were used for embedment lengths of 40 mm or more. The HBM load cell used has a capacity of 250 kg. The pull-out tests were performed at a constant crosshead displacement rate of 0.2 mm.s^{-1}

3.4.1. Fibre clamps

A drill chuck, shown in Figure 21, was used as a fibre clamp for the non-flat Rocstay and Geotex 500 series fibres. The drill chuck was unable to grip the flat Geotex 600 series and Chryso Structural fibres. A separate clamp (Figure 22) with rounded edges was manufactured for gripping these fibres.

26
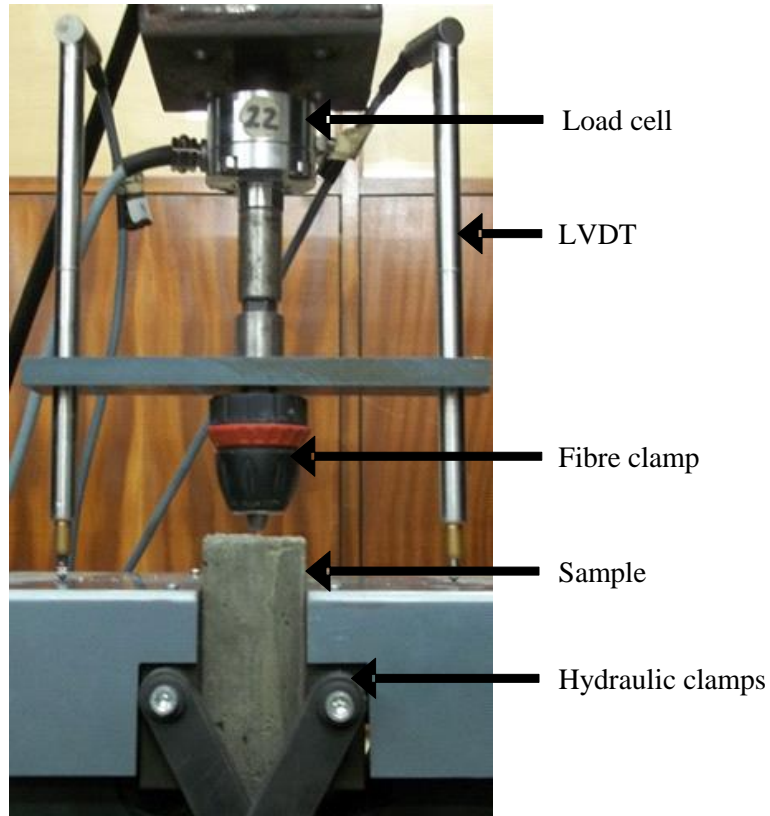
Figure 21: Single fibre pull-out test setup

For both fibre clamps, permanent marker was used to mark the fibres at the clamp-fibre interface to ensure the fibres were not slipping out of the clamp during testing.

Figure 22: Fibre clamp with rounded edges

3.5. Results

Detailed results of the single fibre pull-out test results in terms of pull-out forces and bond stresses can be found in Appendix B. Appendix B includes minimum and maximum values, the average, standard deviation, coefficients of variation (COV) and the characteristic (95 % confidence value) of the results. The results in terms of compressive strength, workability, average pull-out force and bond stress values, and COVs is presented in the following sections.

3.5.1. Compressive strength and workability

Compressive strength tests (fully detailed results in Appendix C) were performed on each mix according to SANS 5863 (2012). Figure 23 summarises the results of the compressive strength tests as the average and COV of each W/C ratio. The COV is a normalised measure of a sample's variation which is determined by dividing the standard deviation by the average.
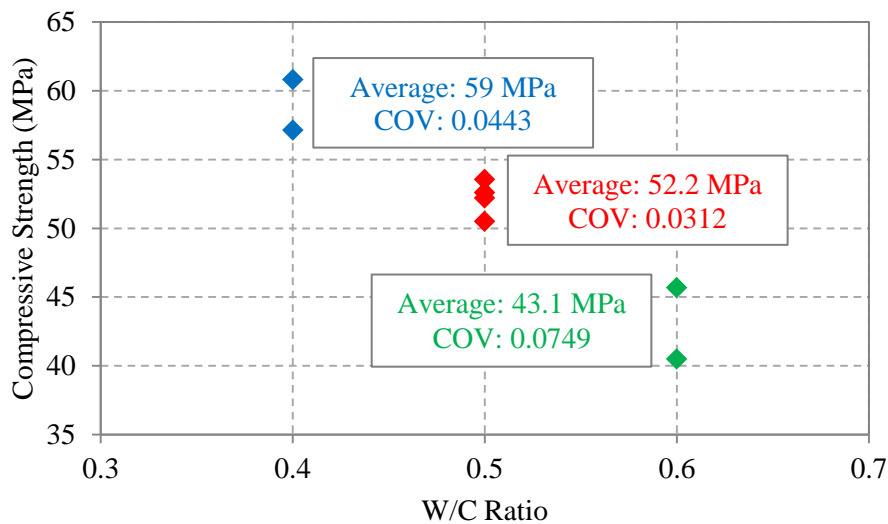
Figure 23: Single fibre pull-out tests compressive strength results

Slump tests were performed according to SANS 5862-1 (2006) to ascertain the fresh concrete's consistence and workability. Table 5 shows the slump test readings (±10 mm) for the various W/C ratios. None of the mixes exhibited segregation.

Table 5: Single fibre pull-out mixes average slumps

W/C ratio	0.4	0.5	0.6
Slump (mm)	70	150	200

3.5.2. Typical output

Figure 24 shows typical fibre pull-out result for one of each of the four fibres. The embedment lengths shown are 25 mm for the Geotex 500 series, Geotex 600 series and Chryso Structural fibre, and 30

mm for the Rocstay fibre. It should be noted that the responses of Figure 24 are in terms of the load resisted and not the interfacial bond stress.
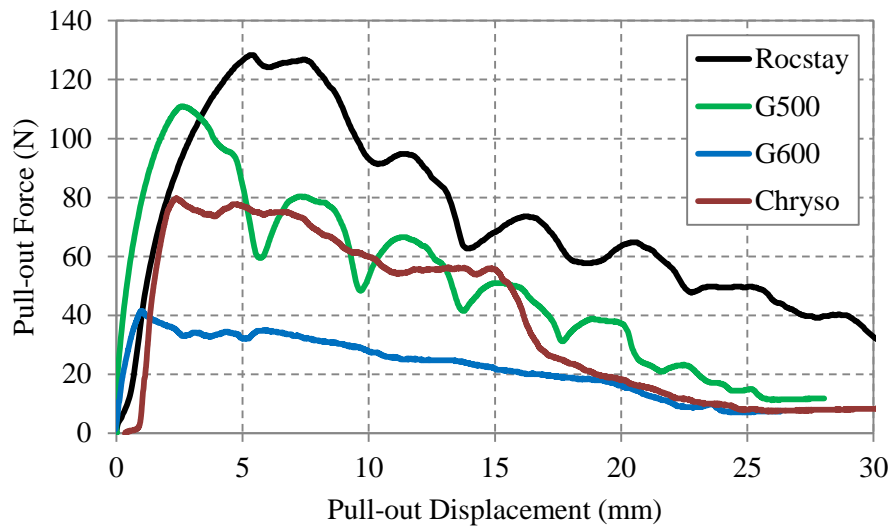
Figure 24: Typical single fibre pull-out graphs obtained

In Figure 24, the fibres all pulled out completely and did not fracture. When complete fibre pull-out occurs, the resisting force offered by the average bond stress over the embedded fibre length ($F_{r,bond}$, Equation [1]) is less than that of the force required for fibre fracture ($F_{fracture}$, Equation [2]). A maximum pull-out force equal to $F_{r,bond}$ is reached, after which the resisting force decreases with the decrease in embedded fibre length.

The bumps in the Rocstay and Geotex 500 series fibre graphs can be attributed to the crimped shape of the fibres. As the fibre pulls out, it catches onto the cement-based matrix, until the force straightens the top part of the fibre and it pulls out, only to be caught again. This could potentially provide an enhanced energy absorption capacity per fibre at a specific embedment length.

A typical single fibre pull-out test fibre fracture graph is shown in Figure 25. In this case, $F_{r,bond}$ exceeds $F_{fracture}$, resulting in the sharp drop in pull-out force as the fibre tensile strength is exceeded and the fibre fractures.

In all cases, the test was deemed finished once the force reading remained constant for 5 mm or it could be clearly seen that the fibre was completely pulled out.

3.5.3. Outlier selection

Various pre-determined criterion were used for initial data exclusion, which resulted in nine results being removed. If the fibre slipped in the clamp while being pulled out, the sample was rejected as this would lead to an unrepresentative low bond stress result. Samples with excessively poor bonding (for example, samples where the fibre could be easily removed by hand) were also rejected.
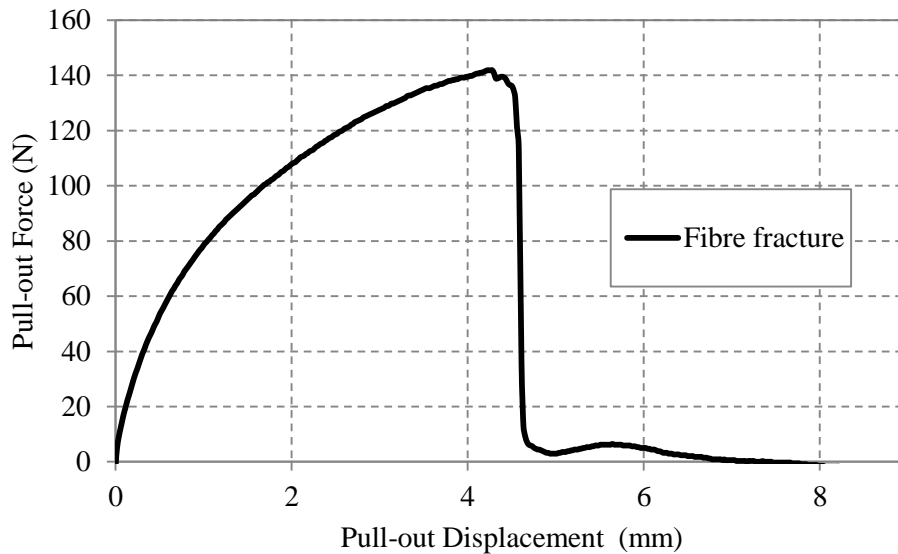
Figure 25: Typical single fibre fracture

Further outlier selection was based on the bond stress, as this is theoretically constant regardless of embedment length whereas the pull-out force varies with embedment length, if the uniform bond stress model described in Section 2.2.2 is assumed.

Various methods of outlier selection were considered. The first outlier selection method considered was visual inspection. However, this method is subjective and what may appear to be an outlier from visual inspection may simply be an indication of the variable nature of the test, or may not appear to be an outlier to another researcher.

The second outlier method selection considered and further used was exclusion based on a standard deviation analysis. Outliers were classified as data points which were not within three standard deviations of the data set average. This method of outlier selection retains the inherent variable nature of single fibre pull-out tests while remaining objective. No results were removed due to the standard deviation analysis.

3.5.4. General comments on single fibre pull-out results

In the following sections, pull-out forces, bond stresses and COVs (based on the bond stress) are presented for each fibre. The pull-out forces are plotted against the intended embedment length (i.e. the assumed embedment lengths of 10 mm, 20 mm, 30 mm and 40 mm for the Rocstay fibres and 12.5 mm, 25 mm, 37.5 mm and 50 mm for the other fibres). The bond stresses were calculated using the embedment length as determined by measuring the length of fibre protruding from the concrete, and subtracting this from the cut fibre length to obtain the actual embedment length. The bond stress results are plotted against the intended embedment length in the following sections. For all of the samples, the actual embedment length was always within 2 mm of the intended embedment length.

The bond stress (τ) for each sample was determined by using the maximum force (P) from the force-pull-out displacement output and a re-arranged Equation [1]:

$$\tau = \frac{P}{\pi \times d_e \times l_e}$$ [13]

3.5.5. Rocstay fibre results

The Rocstay single fibre pull-out test results are split into two sets. The first set of results was obtained before it was noted that the two batches of Rocstay fibres had different equivalent diameters, as noted in Section 3.1.1. The first set of single fibre pull-out tests utilised the fibres with an equivalent diameter equal to 0.998 mm for the L1 (10 mm), L2 (20 mm) and L3 (30 mm) embedment lengths, and fibres with an equivalent diameter equal to 0.703 mm for the 40 mm (L4) embedment length. Figure 26 and Figure 27 depict the first set's average pull-out forces and bond stresses at various W/C ratios and embedment lengths. Table 6 indicates the number of usable results (i.e. no fibre slippage in the clamp, excessively poor bonding and after any other outlier exclusion as described in Section 3.5.2) and fibre fractures per sample set.
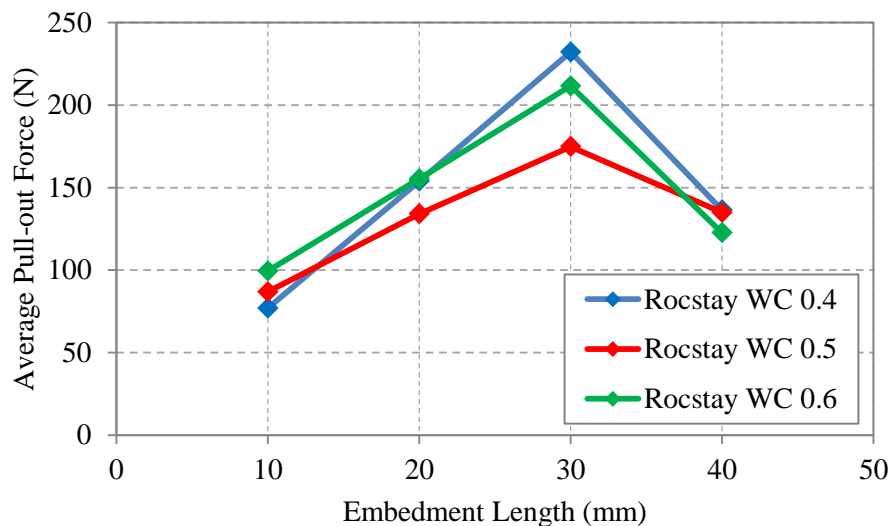
Figure 26: Rocstay fibre Set 1 average pull-out forces at various W/C ratios and embedment lengths

Note that the maximum average pull-out force obtained from Figure 26 is 232 N, which is approximately the same as the theoretical maximum value of 235 N as in Table 2. This indicates that the full capacity of the fibre has been utilised.

The drop in pull-out force at 40 mm (Figure 26) is due to the fibres used for the longer embedment length (L4) having a smaller fibre cross section (d_e = 0.7 mm), than the fibres used for the L1, L2 and L3 embedment lengths (d_e = 0.998 mm), although the cross sectional geometry was identical to the fibres used for the shorter embedment lengths.

31
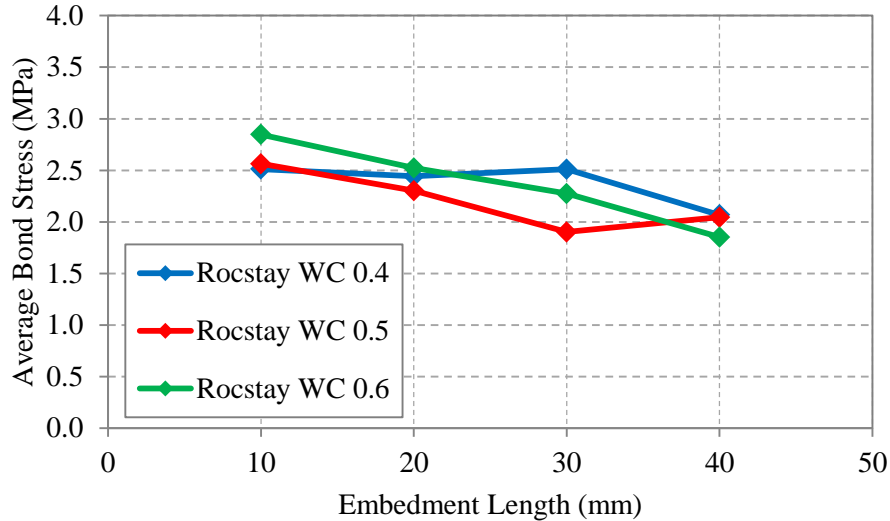
Figure 27: Rocstay fibre Set 1 average bond stresses at various W/C ratios and embedment lengths

Table 6: Rocstay fibre Set 1 number of usable results and fibre fractures per set

Embedment length (mm)	10			20			30			40		
W/C ratio	0.4	0.5	0.6	0.4	0.5	0.6	0.4	0.5	0.6	0.4	0.5	0.6
Number of usable results	8	8	8	6	8	8	8	8	8	8	7	7
Number of fibre fractures	0	0	0	2	0	0	5	2	6	5	5	1

As the W/C ratio appeared to have no significant effect on the results, a second set (Set 2) of Rocstay single fibre samples were cast at only the midway W/C ratio of 0.5, using fibres with an equivalent diameter equal to 0.7 mm for all four embedment lengths. The results are shown below in Figure 28, Figure 29, and Table 7.

Note that the maximum average pull-out force obtained from Figure 28 is 134 N, which is marginally higher than the theoretical maximum breaking force of 116 N as in Table 2. This indicates that the theoretical maximum fibre strength has been exceeded.

Table 8 indicates the bond stress COVs for the Rocstay single fibre pull-out tests at each embedment length and W/C ratio for both sets. The average COV was determined over all of the results.
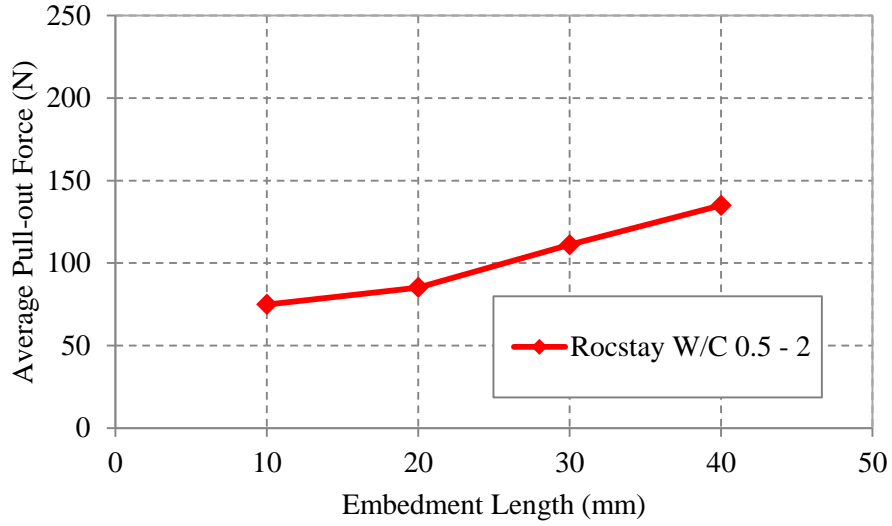
Figure 28: Rocstay fibre Set 2 average pull-out forces at 0.5 W/C ratio and various embedment lengths
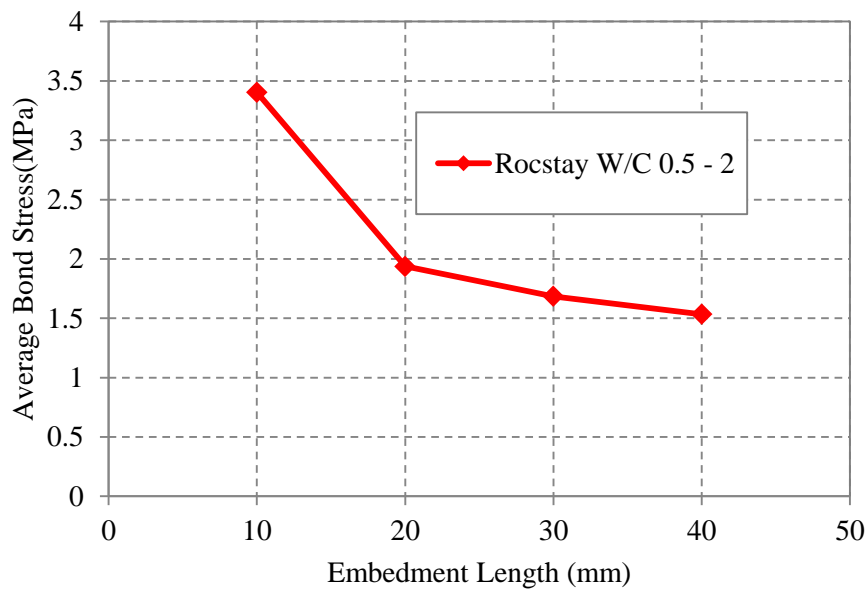
Figure 29: Rocstay fibre Set 2 average bond stresses at 0.5 W/C ratio and various embedment lengths

Table 7: Rocstay fibre Set 2 number of usable results and fibre fractures per set

Embedment length (mm)	10	20	30	40		
W/C ratio	0.5	0.5	0.5	0.4	0.5	0.6
Number of usable results	8	7	8	8	7	7
Number of fibre fractures	0	0	0	5	5	1

33

Table 8: Rocstay single fibre pull-out COVs

W/C ratio	Embedment length (mm)			
	10	**20**	**30**	**40**
0.4 – Set 1	0.3158	0.1357	0.1724	0.1686
0.5 – Set 1	0.2353	0.1884	0.1848	0.1774
0.5 – Set 2	0.2653	0.2486	0.1171	0.1774
0.6 – Set 1	0.1602	0.1792	0.0785	0.1681
Average	0.2441	0.1880	0.1382	0.1729

3.5.6. Geotex 500 series fibre results

Figure 30 depicts the average pull-out for the Geotex 500 series fibres at various W/C ratios and embedment lengths. The drop in pull-out force is due to the longer length fibres' crimping not being as pronounced as for the shorter length fibres.
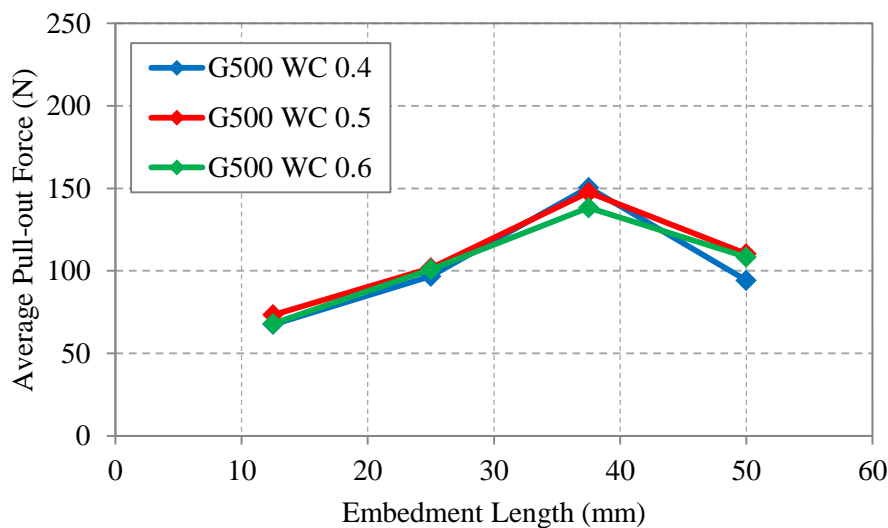
Figure 30: Geotex 500 series average pull-out forces at various W/C ratios and embedment lengths

Note that the maximum average pull-out force obtained from Figure 30 is150 N, which is marginally higher than the theoretical maximum breaking force of 134 N as in Table 2, indicating that the theoretical maximum fibre strength has been reached.

Figure 31 depicts the average bond stresses for the Geotex 500 series fibres at various W/C ratios and embedment lengths. Note once again that the crimping of the fibres used for the 50 mm (L4) embedment length was noticeably less than the crimping of the fibres used for the shorter embedment

lengths, thus resulting in the steep drop in bond stress at the 50 mm embedment length. Table 9 indicates the number of usable results and fibre fractures per sample set, and Table 10 the COVs for all the sample sets.
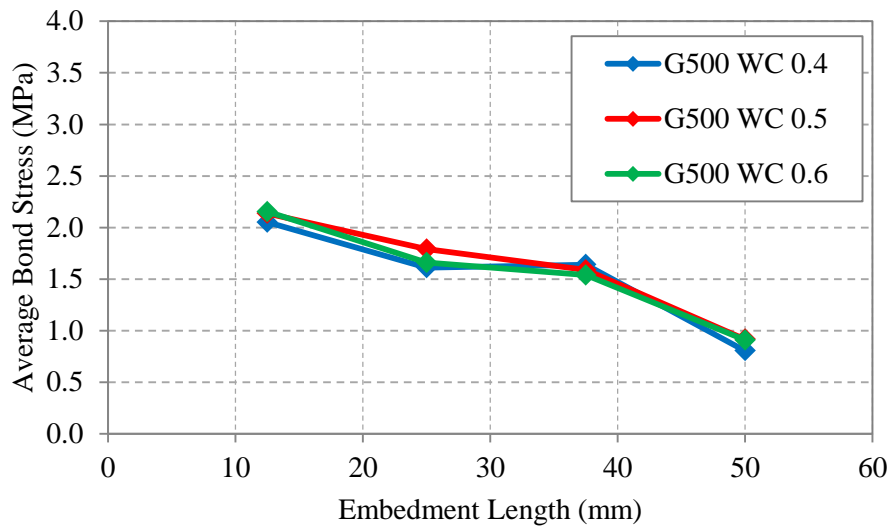
Figure 31: Geotex 500 series average bond stresses at various W/C ratios and embedment lengths

Table 9: Geotex 500 series fibre number of usable results and fibre fractures per set

Embedment length (mm)	12.5			25			37.5			50		
W/C ratio	0.4	0.5	0.6	0.4	0.5	0.6	0.4	0.5	0.6	0.4	0.5	0.6
Number of usable results	8	8	8	8	8	8	8	8	8	8	7	7
Number of fibre fractures	0	0	0	0	0	0	5	2	1	1	4	0

Table 10: Geotex 500 series single fibre pull-out COVs

W/C ratio	Embedment length (mm)			
	12.5	25	37.5	50
0.4	0.2539	0.1109	0.1595	0.1515
0.5	0.1250	0.2891	0.1766	0.2523
0.6	0.1953	0.1958	0.2078	0.2958
Average	0.1914	0.1986	0.1813	0.2332

35

3.5.7. Geotex 600 series fibre results

Figure 32 and Figure 33 depict the average pull-out forces and bond stresses for the Geotex 600 series fibres at various embedment lengths and W/C ratios. Table 11 indicates the number of usable results and fibre fractures per sample set and Table 12 the COVs for the tests.
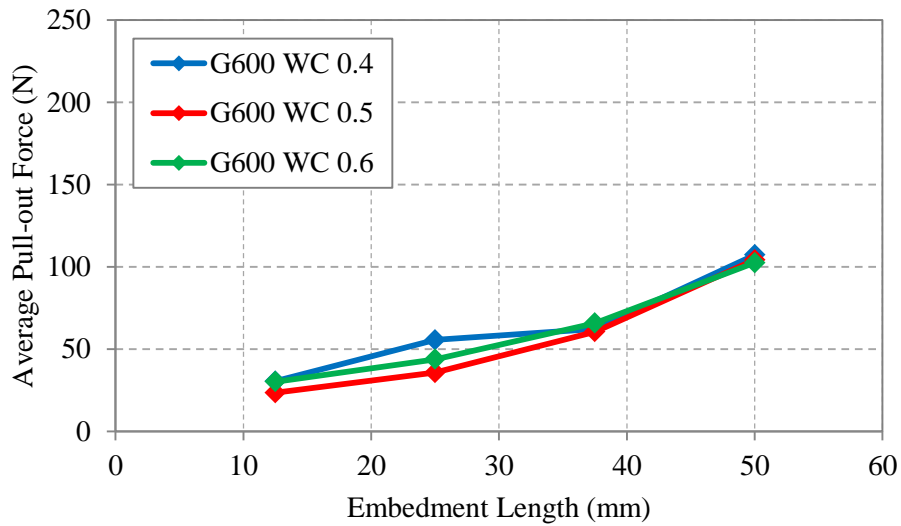
Figure 32: Geotex 600 series average pull-out forces at various W/C ratios and embedment lengths

Note that the maximum average pull-out force obtained from Figure 32 is107 N, which is still lower than the theoretical maximum pull-out force of 178 N as in Table 2.
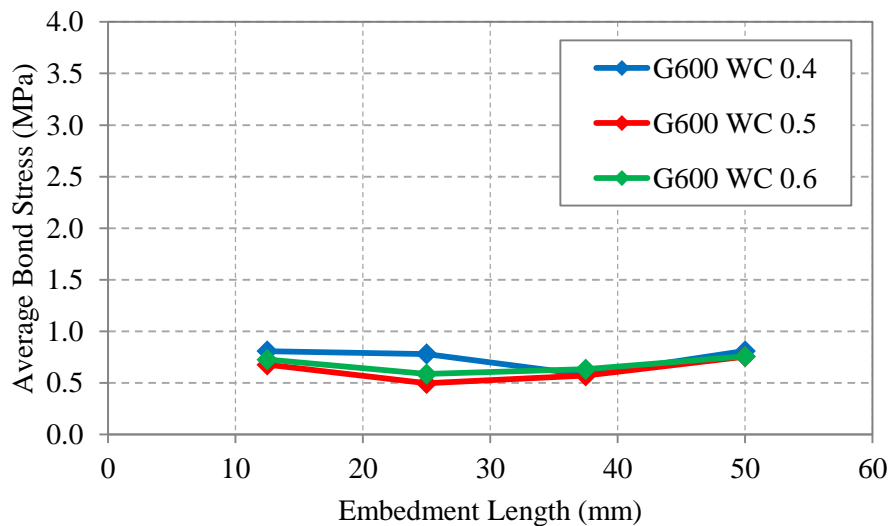
Figure 33: Geotex 600 series average bond stresses at various W/C ratios and embedment lengths

36

Table 11: Geotex 600 series fibre number of usable results and fractures per sample set

Embedment length (mm)	12.5			25			37.5			50		
W/C ratio	0.4	0.5	0.6	0.4	0.5	0.6	0.4	0.5	0.6	0.4	0.5	0.6
Number of usable results	8	8	8	8	8	8	8	8	8	8	7	7
Number of fibre fractures	0	0	0	0	0	0	1	0	1	1	1	0

Table 12: Geotex 600 series single fibre pull-out COVs

W/C ratio	Embedment length (mm)			
	12.5	25	37.5	50
0.4	0.2898	0.3512	0.0578	0.0866
0.5	0.2307	0.2637	0.1846	0.1193
0.6	0.1746	0.1530	0.2390	0.0704
Average	0.1746	0.1530	0.2390	0.0704

3.5.8. Chryso Structural fibre results

Figure 34 and Figure 35 depict the average pull-out forces and bond stresses for the Chryso Structural fibres at various embedment lengths and W/C ratios. Note the L4 embedment length is 45 mm and not 50 mm. Table 13 indicates the number of usable results and fibre fractures per sample set, and Table 14 the COVs.
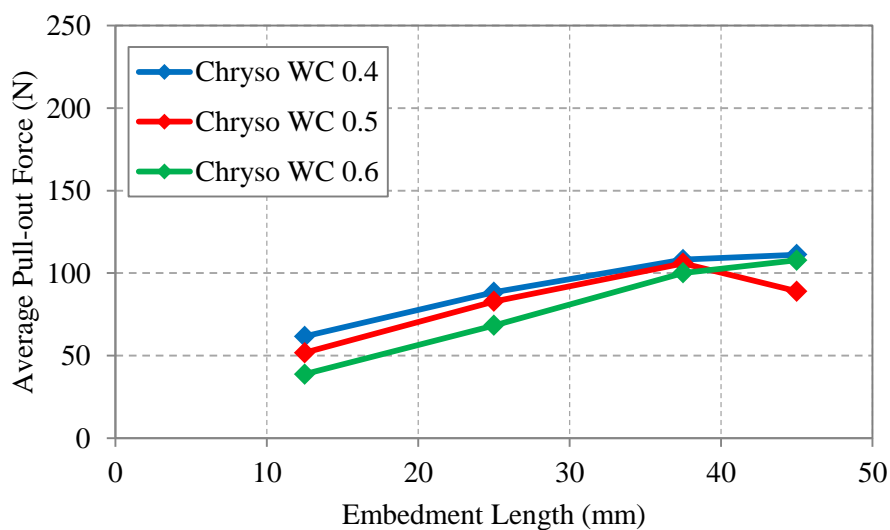
Figure 34: Chryso Structural fibre average pull-out forces at various W/C ratios and embedment lengths

37

Note that the maximum average pull-out force obtained from Figure 34 is111 N, which is slightly higher than the theoretical maximum breaking force of 100 N as in Table 2.
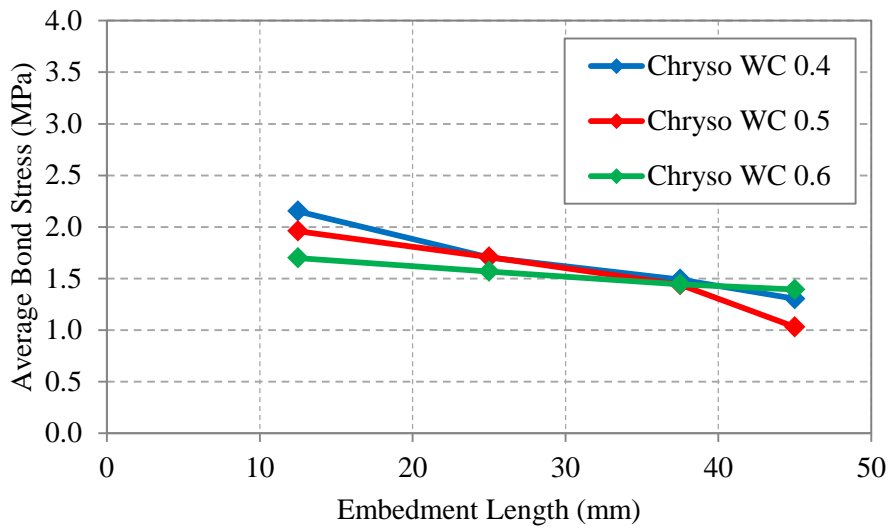
Figure 35: Chryso Structural fibre average bond stresses at various W/C ratios and embedment lengths

Table 13: Chryso Structural fibre number of usable results and fibre fractures per sample set

Embedment length (mm)	12.5			25			37.5			45		
W/C ratio	0.4	0.5	0.6	0.4	0.5	0.6	0.4	0.5	0.6	0.4	0.5	0.6
Number of usable results	8	7	7	8	8	8	8	7	8	4	6	7
Number of fibre fractures	1	0	0	2	0	1	8	5	8	3	6	6

Table 14: Chryso Structural fibre single fibre pull-out COVs

W/C ratio	Embedment length (mm)			
	12.5	25	37.5	45
0.4	0.1681	0.1343	0.1066	0.0519
0.5	0.1221	0.1820	0.1366	0.1973
0.6	0.2236	0.1421	0.1072	0.0955
Average	0.1713	0.1528	0.1168	0.1149

38

3.5.9. Fibre snubbing angle results

The effect of increasing the fibre snubbing angle (φ) was observed by plotting the average bond stresses against snubbing angle, at a constant embedment length of 20 mm for the Rocstay fibres (Figure 36), and 25 mm for the other three fibres (Figure 37, Figure 38 and Figure 39). The bond stresses are determined from the maximum pull-out force, and as the embedment lengths are all within a 2 mm tolerance the pull-out forces would typically follow a similar pattern to the bond stresses. The number of fibre fractures for each set is summarised in Table 15. Each set consisted of eight samples.
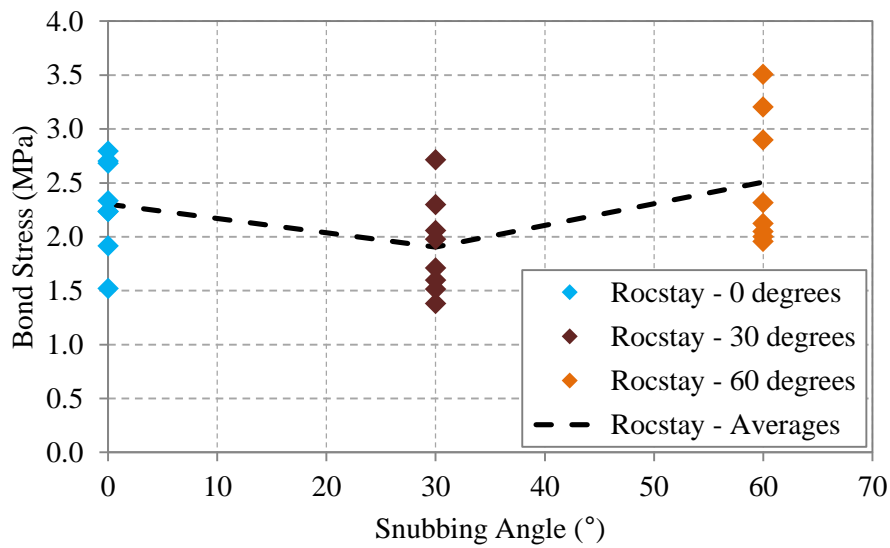
Figure 36: Rocstay fibre snubbing
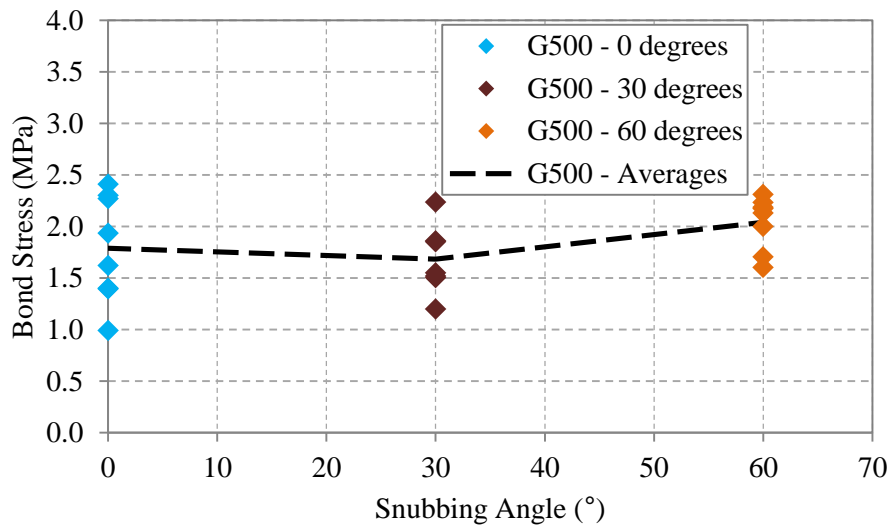
Figure 37: Geotex 500 series fibre snubbing

39
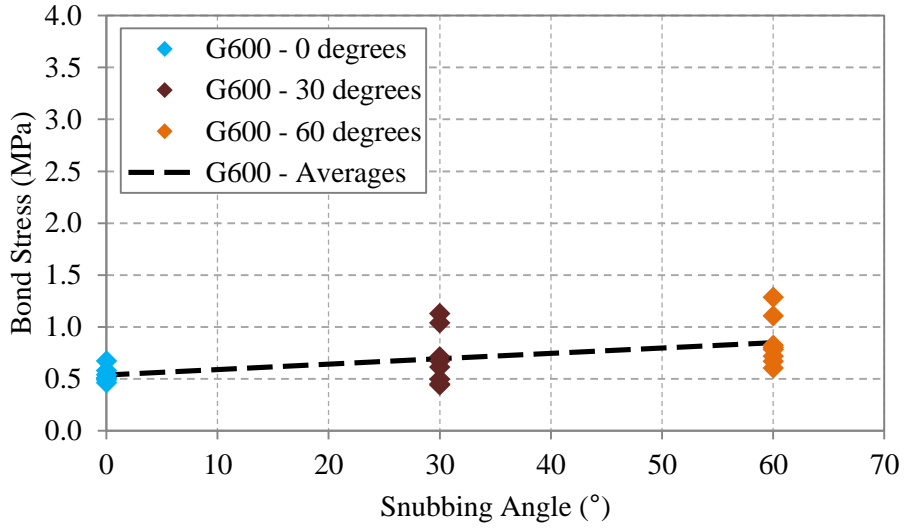
Figure 38: Geotex 600 series fibre snubbing
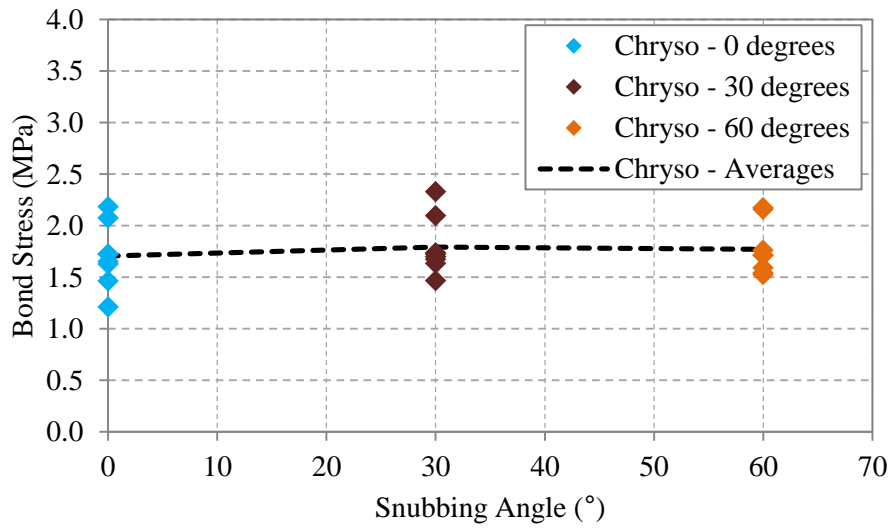
Figure 39: Chryso Structural fibre snubbing

Table 15: Fibre fractures per set for various snubbing angles

φ	Fibre			
	Rocstay	Geotex 500 series	Geotex 600 series	Chryso Structural
0°	0	0	0	0
30°	0	0	1	4
60°	4	5	1	7

Figure 40 provides a summary of all the fibre snubbing bond stress results in the form of a normalised graph. The average bond stresses, excluding visual outliers, were normalised by dividing the average bond stress at each snubbing angle by the average bond stress value at zero snubbing.
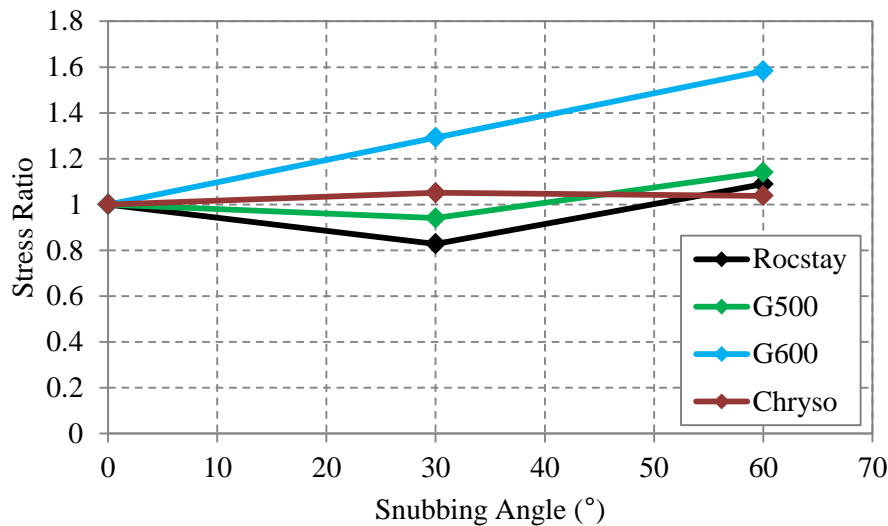
Figure 40: Normalised average snubbing bond stresses for all four fibres

The differences in normalised bond stresses from the 0° values can be attributed to the additional frictional resistance provided by the snubbing effect.

3.6. Discussion

3.6.1. Compressive strength and workability

The compressive strength decreased with an increasing W/C ratio, as expected. Concrete with a lower W/C ratio is typically less porous and has fewer weak zones for cracks to propagate.

The COVs of the compressive strength results were 0.0443, 0.0312 and 0.0749 for the 0.4, 0.5 and 0.6 W/C ratios respectively. The possibility of inconsistent compaction was considered. The cube densities were determined and can be viewed in Appendix C. The difference in densities for the same W/C ratio mixes was at most 26 kg.m^{-3}, which approximates to 1 % excess air voids (Kellerman, 2009). However, for a decrease in density in the 0.4 and 0.5 W/C ratio mixes, an increase in strength was experienced, while only the 0.6 W/C ratio mixes exhibited the expected decrease in strength with a decrease in density. The result variation can thus be attributed to typical experimental variation.

The fresh concrete workability increased with increasing W/C ratio. This was as expected.

3.6.2. Effect of W/C ratio on single fibre results

The W/C ratio had no obvious effect on the two crimped non-flat fibres' (Rocstay and Geotex 500 series) maximum pull-out forces and thus bond stresses. This was not entirely unexpected (Li et al.,

41

1994), but it stood to reason that the maximum pull-out force and bond stress would increase with a decrease in W/C ratio, as the cement matrix surrounding the fibre would be more densely packed with solid cement hydration products, which would increase the mechanical interlock between the fibre and surrounding matrix. The lack of impact of the W/C ratio could be due to the surface area of the fibre being so small that it is unaffected by the change in cement matrix density brought on by increased cement content, as well as the polypropylene fibres being hydrophilic.

Table 16 summarises the performance difference in bond stress values between the 0.4 W/C ratio values, and the 0.5 and 0.6 W/C ratio values at the first two different embedment lengths for the two flat fibres, Geotex 600 series and Chryso Structural. Only the first two embedment lengths were used to compare bond stress improvements as fibres began fracturing at the L3 embedment length, and the fibres' tensile strength would thus start becoming predominant as opposed to the resisting force offered by the bond stress. The differences were determined by subtracting the 0.5 or 0.6 W/C ratio value from the 0.4 W/C ratio value and dividing this difference by the 0.4 W/C ratio value. Thus, for example, the bond stress value at L1 for the Geotex 600 series fibres was 16.27 % higher at the 0.4 W/C ratio than at the 0.5 W/C ratio, and 10.20 % higher for the 0.4 W/C ratio when compared to the 0.6 W/C ratio.

Table 16: Percentage improvements of 0.4 W/C ratio bond stress values over 0.5 and 0.6 W/C ratios

W/C ratio	L1		L2		Average	
	G600	Chryso	G600	Chryso	G600	Chryso
0.5	16.27	8.90	36.46	-0.18	26.37	4.36
0.6	10.20	21.06	24.83	7.97	17.52	14.52

From Table 16 it can be seen that the Geotex 600 series fibres were influenced by the W/C ratio. The 0.4 W/C ratio displayed the highest pull-out forces and bond stresses for both embedment lengths. The effect of bond stress decreasing with increasing W/C ratio did not extend to the 0.5 and 0.6 W/C ratios, as the 0.6 W/C ratio pull-out force and bond stress values were consistently higher than those of the 0.5 W/C ratio (Figure 32 and Figure 33).

The W/C ratio also influenced the Chryso Structural fibres' performance, with the 0.4 W/C ratio bond stress results being an average of 4% and 14% higher than the 0.5 and 0.6 W/C ratios. The Chryso Structural fibre also performed better at the 0.5 W/C ratio than at the 0.6 W/C ratio. This could indicate that the surface treatment applied to the Chryso Structural fibre enhances the effect of a changing W/C ratio.

The influence of the W/C ratio is limited to the flat fibres, and is on average less than 16% over the embedment lengths. The influence is also not consistent over the W/C ratios for untreated fibres. The general lack of influence of the W/C ratio could be due to the chemical inertness of polypropylene fibres. This is supported by the Chryso Structural fibre exhibiting a consistent increase in bond stress with decreasing W/C ratio.

It can thus be said, according to the single fibre pull-out tests that the fibre performance is typically the same in a 59 MPa (0.4 W/C ratio) and 43 MPa (0.6 W/C ratio) cement-based matrix for untreated flat and non-flat fibres, and possibly influenced by surface treatment.

3.6.3. Pull-out force and bond stress variation with embedment length

The first set of Rocstay fibres displayed a linear increase in pull-out force with increasing embedment length (Figure 26), to a peak at an embedment length of 30 mm. At the 30 mm embedment length, fibre fracture occurred for more than half the samples, indicating that 30 mm is nearing the critical length. The drop in pull-out force at 40 mm can be attributed to the smaller equivalent diameter of 0.703 mm, as noted in Sections 3.1.1 and 3.5.5.

The second set of Rocstay fibres displayed a linear increase in pull-out force with embedment length. The increase in pull-out force from 10 mm to 20 mm (13.7 %) was not as pronounced as the increase in pull-out force from 20 mm to 30 mm (30.5 %) and 30 mm to 40 mm (21.4 %).

The first set of Rocstay fibres had decreasing bond stresses with increasing embedment lengths at the 0.5 and 0.6 W/C ratios. The 0.4 W/C ratio exhibited a constant bond stress over the 10 mm, 20 mm and 30 mm embedment lengths, indicating that for those sets the bond stress model was adequate. The second set of Rocstay fibres (Figure 29) had a sharp 43 % decrease in bond stress from the 10 mm to 20 mm embedment lengths, after which the bond stress decreases were much more gradual at 13 % and 9 %, indicating a near uniform bond stress over the embedded length. The initial sharp decrease in bond stress can be linked to the higher than expected pull-out force at 10 mm. The unexpectedly high value at 10 mm can possibly be attributed to experimental variation, as the COV for this sample set was high (0.2653).

The difference in maximum pull-out forces for the two sets of Rocstay fibres can be attributed to the smaller equivalent diameter resulting in less surface area available for fibre-matrix bonding, which in turn results in a lower resisting force offered by the bond stress and thus a larger critical length. The amount of fibre fractures at the 40 mm embedment length (5 out of 8 for two of the W/C ratio sample sets) indicates that the critical fibre length for the smaller cross sectional fibre was approximately 40 mm, which is longer than the 30 mm for the larger diameter fibres in the first set.

The Geotex 500 series fibre exhibited similar behaviour to the Rocstay fibres, with a linear increase in pull-out force with embedment length between 12.5 mm and 37.5 mm and fibre fractures occurring at 37.5 mm, followed by an unexpected drop in pull-out force at the 50 mm embedment length. The equivalent diameter of the longer length fibres was found to be the same as that of the regular length fibres, thus excluding the smaller equivalent diameter explanation as for the Rocstay fibres. The longitudinal geometry of the longer length fibres was inspected, and it was noted that the crimps in the longer length fibres were not as pronounced as for the regular length fibres. This resulted in a lower mechanical bond stress and thus a lower pull-out force at a higher embedment length.

The Geotex 500 series fibres also displayed a downwards trend in bond stress, with an average decrease of 20 % in bond stress between 12.5 mm and 25 mm, and a smaller decrease of less than 6 % on average over the 25 mm to 37.5 mm embedment lengths, indicating again a near constant bond stress over these embedment lengths. The drop in bond stress at 50 mm can be attributed to the lower mechanical bond as for the drop in pull-out force at 50 mm. If the longer length fibre had the same geometry as the regular length fibres, it is likely that the decrease in bond stress would have been significantly less, as for the decrease between the 25 mm and 37.5 mm embedment lengths.

The sudden drop in pull-out force for the two crimped fibres at the longer L4 embedment lengths is probably due to the cross-sectional (Rocstay Set 1) and longitudinal (Geotex 500 series) fibre geometries of the longer length (L4) fibres differing from the typical length fibres used for the shorter embedment length (L1, L2 and L3) tests, and not due to the shared crimping feature.

However, the similarity in the bond stress behaviour can possibly be attributed to a similar bond stress mechanism, as shown in Figure 41.
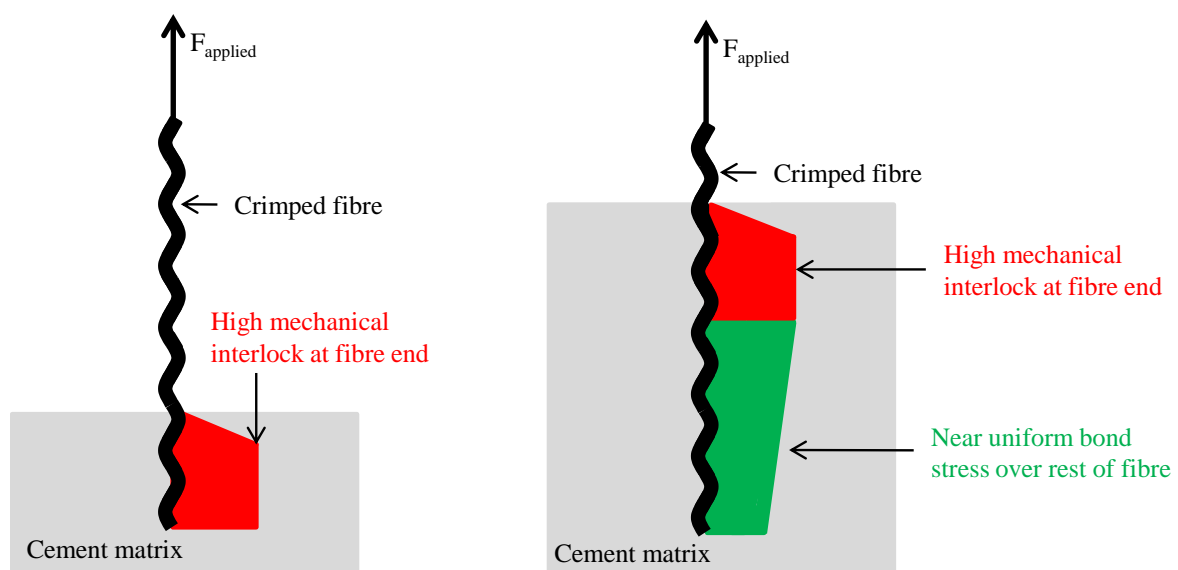
Figure 41: Possible crimped fibre bond stress mechanism

In Figure 41, the bond stress near the surface end of the fibre is extremely high, as this is where the fibre will begin debonding. After a certain distance, this enhanced mechanical interlock is no longer effective, and a near uniform but slightly decreasing bond stress takes over, resulting in a slowly decreasing bond stress at deeper embedment lengths.

The Geotex 600 series fibres displayed a linear pull-out force embedment length relationship. This indicates that the critical fibre length was never embedded in the concrete. This is confirmed by the fact that the few fractures which did occur were partial fractures.

The Geotex 600 series fibres initially displayed an average decrease in bond stress of 11.6 %, followed by a 1 % decrease and then a 30 % increase. Although these values may seem large, the actual bond stress increases never exceed 0.23 MPa, nor do the decreases exceed 0.20 MPa. Thus, the Geotex 600 series fibres appear to have an almost constant bond stress over the embedment length.

The Chryso Structural fibres exhibited the expected pull-out behaviour of a linear increase in pull-out force with increasing embedment length up until the majority of the fibres fractured at the 37.5 mm embedment length. At the 45 mm embedment length, all but two of the fibres fractured across the W/C ratios. The pull-out forces appeared to be plateauing at 110 N, as the pull-out force increases only slightly for the 0.4 and 0.6 W/C ratios, and drops slightly for the 0.5 W/C ratio.

The Chryso Structural fibres displayed a generally low rate of bond stress decrease, averaging below 15 % over the W/C ratios for each embedment length step. The slow decrease of bond stress over all embedment length steps indicates a more uniform, but still decreasing bond stress mechanism is acting over the fibre, much like for the Geotex 600 series fibres.

3.6.4. Bond stress and critical length comparisons

From Figure 27, Figure 29, Figure 31, Figure 33 and Figure 35 the bond stress is shown to have a generally downward trend with an increasing embedment length. This indicates that the uniform bond stress model chosen to represent the bond stress (Equations [1] and [13]) is too simplistic. The non-constant bond stress can be attributed to the factors mentioned in Section 2.2.3.

The fibre critical embedded length is defined as the length at which fibre fracture occurs as opposed to fibre pull-out. Thus, if a significant portion of fibres fracture at a particular embedment length, it indicates that the critical embedded length was reached between the previous embedment length and the current embedment length. Figure 42 shows the percentage of fibre fractures which occurred at each embedment length over all three W/C ratios.
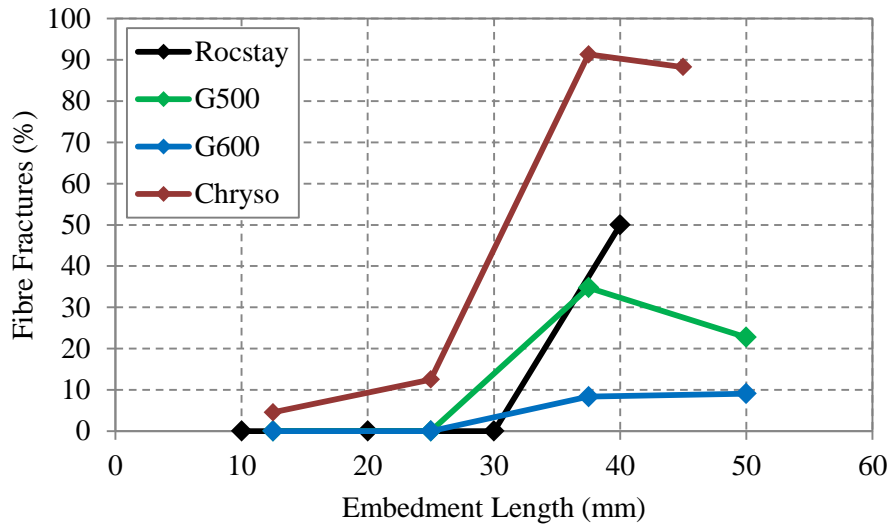
Figure 42: Percentage of fibres ruptured at various embedment lengths

The Rocstay fibres displayed 50 % fibre fractures at 40 mm embedment length. The Geotex 500 series fibre fractures peaked at 35 % at the 37.5 mm embedment length. It is likely that the Geotex 500 series fibres would have had more than 50 % fibre fractures at 50 mm if the longitudinal fibre crimping had not been less pronounced for the longer embedment length fibres. The less pronounced crimping of the longer length fibres resulted in a lower bond stress and thus a longer critical length for the longer length Geotex 500 series fibres.

The Geotex 600 series fibres displayed less than 10 % fibre fractures at the 50 mm embedment length, indicating that the critical length was not close to being reached. The Chryso Structural fibres displayed 91 % and 88 % fibre fractures at 37.5 mm and 45 mm respectively, indicating that the critical length had been reached at 37.5 mm.

The bond stress value was decided to be the average value over the three W/C ratios at the second embedment length. The first shortest embedment length was not used as the values could be unrealistically high for the crimped Rocstay and Geotex 500 series fibres, and fibre fracture occurred at the L3 embedment lengths. Using the values at the second embedment length, the critical fibre length was determined using the tensile strength as per the information sheets and Equation [3]. These bond stress values and corresponding critical lengths are presented in Table 17, along with the critical lengths based on the percentage of fibre fractures.

Note that the fracture based critical length for the Geotex 500 series fibre is taken as between the length at which 35 % fracture occurred (37.5 mm), and the next embedment length. If the longitudinal fibre geometry (i.e. the level of crimping) had been similar, then it is likely that close to 100 % fibre fractures would have occurred at 50 mm.

46

Table 17: Calculated embedded fibre critical lengths

Fibre	Rocstay	Geotex 500 series	Geotex 600 series	Chryso Structural
τ_{ave} (MPa)	1.94	1.69	0.62	1.66
l_c (mm) – Model based	27	33	99	31
l_c (mm) – Fracture based	40	45	Unknown	37.5

The embedment lengths at which the peak percentage of fractures occurs is a true indication of the critical length. The difference in critical lengths as determined by the uniform bond stress model and the actual fibre fractures again highlights the inadequacy of the uniform bond stress model used to determine the bond stresses of crimped fibres. For the flat Chryso Structural fibres, the critical length value calculated using the uniform bond stress model, 31 mm, only underestimates the fracture based critical length by 6.5 mm. This indicates that the uniform bond stress model, although not perfectly suited to flat fibres, is better for flat fibres than for crimped fibres, and only requires slight adjustments.

In terms of performance comparison, the Rocstay fibre exhibited the highest bond stress, followed by the Geotex 500 series, Chryso Structural and Geotex 600 series fibres. The Geotex 600 series fibres could possibly increase their bond stress by means of a surface treatment. As described in Section 2.2.2, fibres should ideally be cut to a maximum of twice their critical length . Bearing this in mind, the fibres can all be cut to longer lengths. However, this could negatively affect fresh concrete workability, as well as cause fibre balling during mixing.

3.6.5. Effect of fibre geometry on bond stresses

The X-shaped cross section of the Rocstay fibre produced the highest bond stress of the fibres tested. This can be attributed to the comparatively large surface area available for bonding as well as the crimped fibre shape. The SEM photographs of the Rocstay fibre pull-out (Section 3.7) show damage occurring on all surfaces of the fibre, indicating the cement matrix encompassed the entire fibre and utilised the entire surface area, as opposed to the initial concern that the cement matrix might not extend to all the fibre surface area due to the cement matrix simply settling around the fibre, and air and water voids forming around the fibre. This initial concern is shown in Figure 43, with the areas of concern highlighted in red.

The flat fibres have vastly different bond stresses. The Chryso Structural fibre has a bond stress two and a half times greater than the Geotex 600 series fibre. This could possibly be attributed to the Chryso Structural fibre's surface treatment, which would attract the surrounding particles to the fibre and thus increase the calcium silicate hydrate (CSH) concentration around the fibre.

47
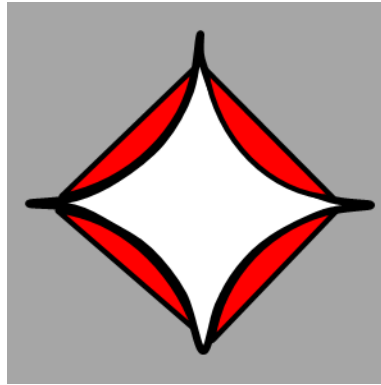
Figure 43: Diagrammatic representation of initial concern for Rocstay fibre

The flat surface-treated Chryso Structural and oval crimped Geotex 500 series fibres have similar bond stresses (1.66 MPa and 1.69 MPa) despite having completely different cross-sectional and longitudinal geometry.

It appears that untreated flat fibres have the lowest bond stress, while untreated crimped oval/circular fibres will exhibit similar bond stresses to treated flat fibres. The fibre with the most effective geometry is the Rocstay fibre with its irregular cross section and crimping. Should the Rocstay fibre have also been provided with a surface treatment, its bond stress would probably increase, leading to a lower value for the critical fibre length.

3.6.6. Effect of equivalent diameter on average bond stresses

Figure 44 shows the effect of the equivalent diameter on the bond stress. All of the results were used to construct Figure 44 including the first set of Rocstay fibres.
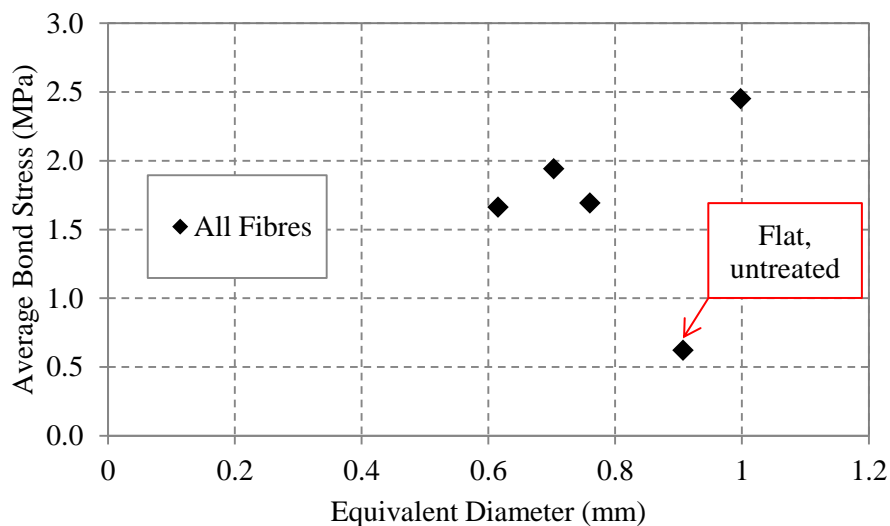
Figure 44: Effect of equivalent diameter on bond stress

Figure 44 appears to show an increasing trend of average bond stresses with equivalent diameter. The flat, untreated Geotex 600 series did not fit the same pattern as that of the flat treated Chryso Structural fibres and the crimped non-flat fibres. Excluding the Geotex 600 series fibre, it appears that the average bond stress increases by 0.08 MPa with every 0.01 mm equivalent diameter increase.

3.6.7. Results variability

The bond stress COVs at each embedment length, averaged over the W/C ratios are graphically summarised Figure 45.
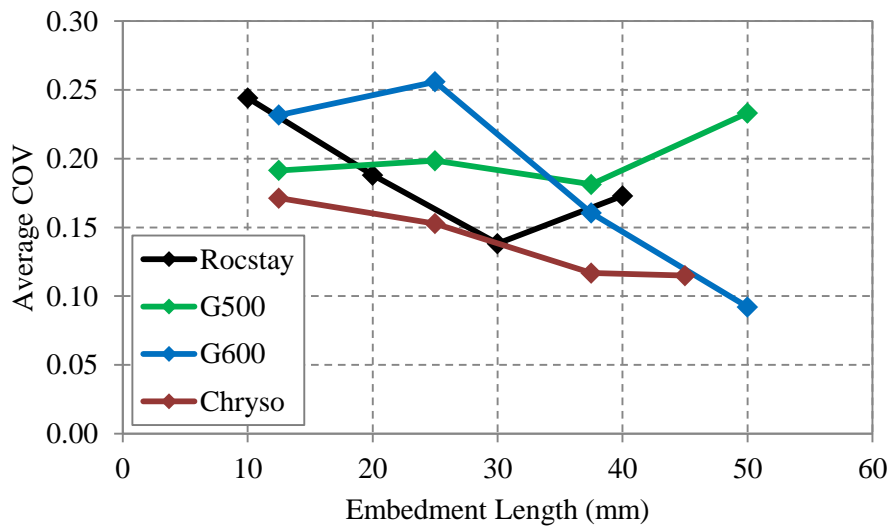
Figure 45: Average COVs for single fibre pull-out tests

The Rocstay fibres had a decreasing COV from the 10 mm to 30 mm embedment lengths. This can be attributed to an increase in surface area over which the bond stress is acting, resulting in more uniformity. The increase in COV at 40 mm can be attributed to the smaller surface area of the longer length fibres as a result of the smaller equivalent diameter.

The Geotex 500 series fibres had a relatively constant COV of approximately 0.2 across the embedment lengths. The lack of decrease in COV with an increase in bond length can possibly be attributed to the variable nature of the single fibre pull-out tests.

The flat Geotex 600 series and Chryso Structural fibres displayed a general decrease in COV with increasing embedment lengths. The Chryso Structural fibres had the lowest average COVs across all the embedment lengths, possibly due to more uniformity in the bond stress resulting from the surface treatment providing a more uniform cement matrix particle attraction to the fibre surface. The Geotex 600 series general decrease in variation with increasing embedment length can be attributed to the increase in surface area which will allow for more uniformity.

49

Although the COVs presented in Figure 45 and Table 8, Table 10, Table 12 and Table 14 are relatively high, the single fibre pull-out test procedure is variable by nature due to its small surface area. In addition, values tended to be gathered around the average. Result sets with COVs higher than 0.2 were individually inspected and found to be the result of two or less samples which deviated from the rest of the samples. As previously mentioned, detailed results including characteristic values, and minimum and maximum values are available in Appendix B.

3.6.8. Fibre snubbing angle effect

The percentage increases discussed in this section are with reference to the bond stress values which experience no fibre snubbing ($\varphi = 0°$). The total bond stress refers to the frictional bond stress caused by the snubbing angle, in addition to the customary bond stress which the fibres experience with no snubbing.

The flat Geotex 600 series and Chryso Structural fibres were inserted at a consistent orientation, for bending about their strong axes. If the fibre is considered as a beam subjected to flexural bending, bending the fibre about its strong axis requires a larger force than for bending it to the same rotation about the weak axis. This will subsequently lead to a larger frictional bond stress for a constant area for strong axis bending as opposed to weak axis bending. In addition strong axis bending is exerted over a smaller area, again leading to a larger frictional bond stress.

The Geotex 600 series fibres experienced a 29 % and 58 % increase in average bond stress at 30° and 60°. This is expected, as the increase in snubbing angle will cause an increase in the frictional force over a constant surface area, and thus a larger increase in the overall bond stress contribution.

The Chryso Structural fibres experienced a 5 % and 4 % bond stress increase at 30° and 60°. The plateau can be attributed to the fibre's tensile strength being exceeded by the additional resisting force offered by the frictional snubbing resistance. This is confirmed by six of the eight fibres fracturing at the cement-matrix surface at the 60° snubbing angle.

The Rocstay fibres experienced a 17 % decrease in average bond stress at 30°, and a 9 % increase in average bond stress at 60°. There is no obvious trend, although an increase in the total bond stress was expected due to the increase in frictional resistance with increasing snubbing angle. A possible reason for this could be that it was not possible to insert the fibres at a consistent orientation due to their irregular cross-section. It is therefore possible that some of the fibres were bent about their weak axes while others were bent about their strong axes, as it was not possible to discern between the two axes when the fibres were embedded.

The Geotex 500 series experienced a 6 % decrease in bond stress at 30°, and an increase of 14 % at 60°. Again, no consistent trend was evident. This was again probably due to the irregular elliptical cross-sectional fibre shape, as for the Rocstay fibres, and the lack of control over the axis of bending.

At the 30° and 60° snubbing angles, 50 % and 88 % of the Chryso Structural fibres fractured, indicating that the friction generated by the snubbing effect significantly increased the total bond stress. At the 60° snubbing angle, more than 50 % of the Rocstay and Geotex 500 series fibres fractured, which implies that at any snubbing angle higher than 60°, the total bond stress would have exceeded the fibres' tensile strength and more fibre fracture would have occurred, which would lead to a plateau in the increase in bond stress with snubbing angle.

3.7. SEM Photographs

Scanning Electron Microscope (SEM) images were taken of the single fibres to confirm various findings. Table 18, Table 19, Table 20 and Table 21 show relevant SEM images for all of the fibre types.

The damage on the Rocstay fibres (Table 18) is pronounced for the fibre pull-out. It can clearly be seen that there is damage all around the fibre, indicating that there was mechanical adhesion on all fibre surfaces. The Rocstay fibre fracture appears to be a combination of clean breakage and tearing.

The Geotex 500 series fibres (Table 19) show severe fibre damage caused by the scraping of the cement matrix against the fibre during pull-out. From the image of the pull-out damage at the interface or surface, it can be seen that there is significantly less damage as opposed to the images of the pull-out damage at the middle of the fibre and at the embedded ends. The increased damage could be due to the embedded end having to travel further to exit the cement matrix, resulting in more scrapings. The fracture mode for the Geotex 500 series fibres appears to be fibre splitting.

The Geotex 600 series fibres (Table 20), which had the lowest bond stress, had minimal surface damage. This is due to the flat geometry and lack of surface treatment.

The Chryso Structural fibres (Table 21) also indicate severe scrapings. The damage is significantly more than that of the Geotex 600 series fibre, which indicates that the surface treatment definitely has an effect on attracting the cement matrix particles to the fibre. The Chryso Structural fibre also tended to fibrillate as the fracture mode.

Table 18: Rocstay fibre SEM images

Description	Image(s)
Undamaged	
Pull-out damage	
Fracture damage	

Table 19: Geotex 500 series fibre SEM images
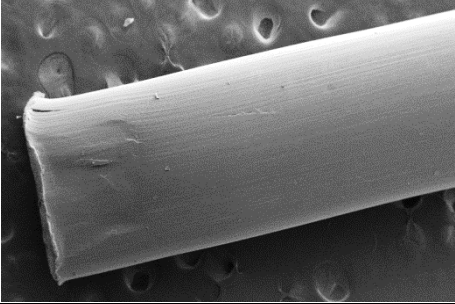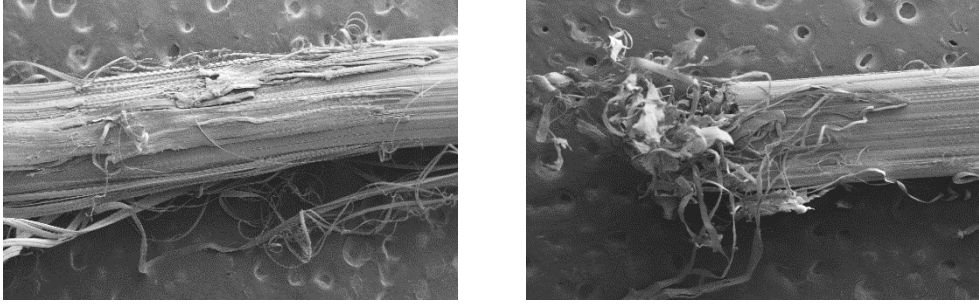
Description	Image(s)
Undamaged	
Pull-out damage (middle and end)	
Pull-out damage (interface)	
Fracture damage	
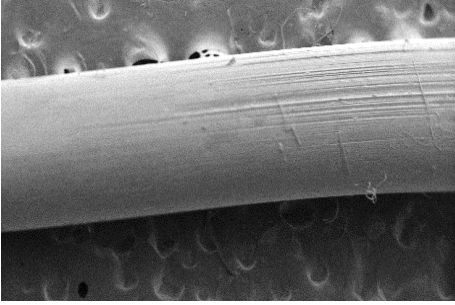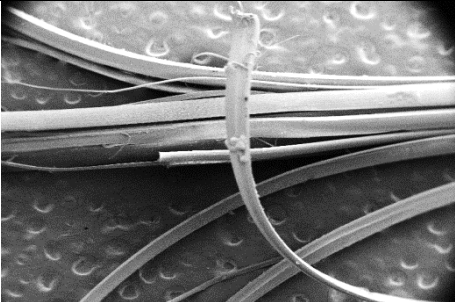
Table 20: Geotex 600 series fibre SEM images
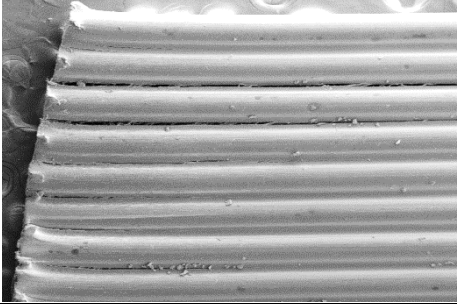
Description	Image(s)
Undamaged	
Pull-out damage (middle and end)	
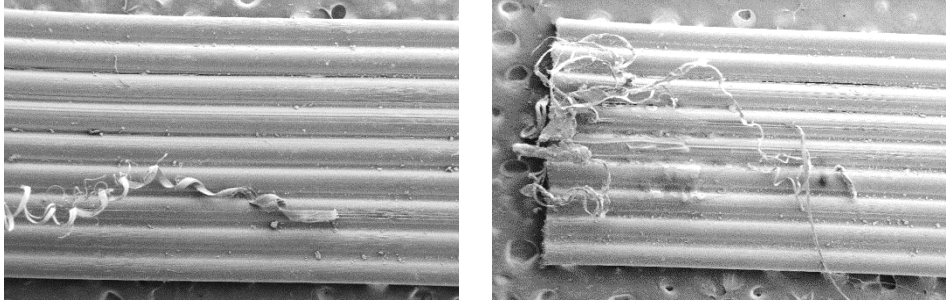
Table 21: Chryso Structural fibre SEM images
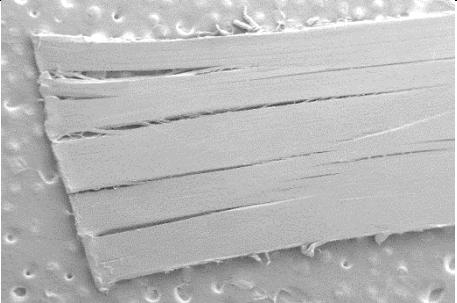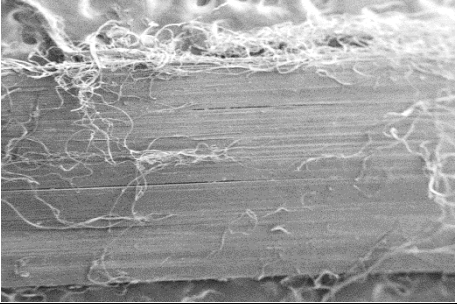
Description	Image(s)
Undamaged	
Pull-out damage	
Fracture damage (in concrete and in clamp)	

54
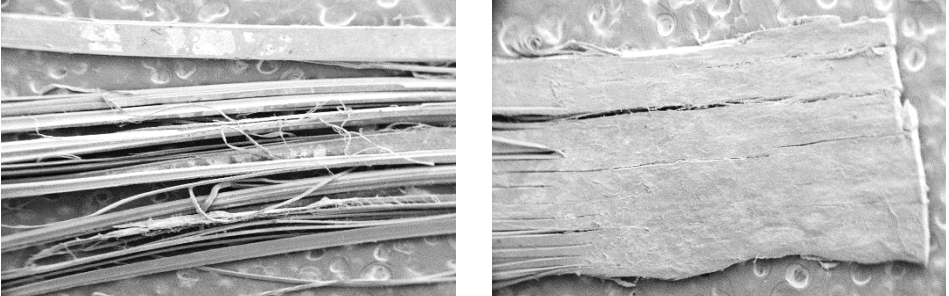
3.8. Concluding Summary

The W/C ratio does not appear to have any significant effect on the pull-out resistance and bond stress of non-flat fibres. The untreated flat fibres appear to be slightly affected by the W/C ratio. The 0.4 W/C ratio showed enhanced performance over both the 0.5 and 0.6 W/C ratios for all of the Geotex 600 series comparisons, with an average improvement of 26.37 % and 17.52 % at the 0.5 and 0.6 W/C ratios respectively. The 0.5 W/C ratio samples did not consistently perform better than the 0.6 W/C ratio samples, and the performance improvement of the 0.4 W/C ratio over the 0.5 and 0.6 W/C ratios had an extremely wide range, from 10 % to 36 %. The treated Chryso Structural fibre bond stresses were generally higher at the 0.4 W/C ratio than at the 0.5 W/C ratio, and also higher at the 0.5 W/C ratio than at the 0.6 W/C ratio. This indicates that the surface treatment of the Chryso Structural fibre possibly influences the bond stress of flat fibres by attracting the cement matrix to the fibre surface for a higher bond stress.

The fibre geometry and surface treatment have a large influence on the single fibre performance. From the results the crimped, irregular cross-section fibre had the highest bond stress, while the flat, untreated fibre had the lowest bond stress. The treated flat Chryso Structural fibre had a bond stress two and a half times higher than the untreated flat Geotex 600 series fibre (1.66 MPa versus 0.62 MPa). From this, it appears that for the highest possible bond stress, fibres should be crimped, with an irregular cross section and surface treatment.

The effect of the equivalent fibre diameter cannot be ascertained for certain, as there is one severe outlier in the form of the untreated flat Geotex 600 series fibre. If the outlier is excluded, the effect of equivalent diameter on bond stress for crimped and flat treated fibres is approximately an increase of 0.08 MPa in bond stress for each 0.01 mm increase in equivalent diameter.

The results variation generally decreases with an increase in embedment length, due to increased surface area allowing for more uniformity.

The consistency of the fibre snubbing angle effect appears to be dependent on the axis of bending. The fibres whose orientation could be controlled exhibited the expected increase in total bond stress with an increase in snubbing angle. The snubbing effect was significant for the flat Geotex 600 series fibres, with total bond stress increases exceeding 29 % and 58 % at the 30° and 60° snubbing angles. In addition, the additional resistance offered by the snubbing friction can also be enough to cause fibre fracture, even if the increase in total bond stress is minimal, as for the Chryso Structural fibres. The non-flat Rocstay and Geotex 500 series fibres, whose axis of orientation could not be controlled, did not display a consistent snubbing effect over the increase in snubbing angle, but did exhibit more than 50 % fibre fractures at the 60° snubbing angle, indicating that the snubbing effect does exist for non-flat fibres.

55

The uniform bond stress model used to determine the critical lengths is inadequate. It appears that different bond stress mechanisms exist for the flat fibres than for the crimped fibres, with the flat fibres experiencing a more uniform bond stress while the crimped fibres experience a high bond stress at the fibre end near the surface, and then a decreasing bond stress towards the embedded end.

The Rocstay fibres had the highest bond stress (1.94 MPa), while the Geotex 500 series and Chryso Structural fibres had bond stresses of 1.69 MPa and 1.66 MPa, and the Geotex 600 series fibre a bond stress of 0.62 MPa. All of the fibres can be cut to longer lengths, as explained in Section 2.2.2, as they are currently cut to below twice their critical lengths. However, negative effects such as loss of workability may be encountered.

CHAPTER 4

Macro-Mechanical

Behaviour

One of the objectives of this research is to establish a suitable test method for performance specification of SynFRC from existing international test methods. The three point beam bending as detailed in BS EN 14651 (2007) and Section 2.3, and RDPT as detailed in ASTM C1550 (2012) and Section 2.5 were selected for comparison based on literature.

Various mix designs were tested using the three point beam bending test and RDPT to determine the effects of various W/C ratios, coarse aggregate sizes, fibre types and fibre volume dosages on performance and result scatter.

4.1. Materials

The same materials were used as in the single fibre pull-out experiments. Additional materials included 13 mm and 19 mm Greywacke coarse aggregate.

4.2. Test Program

The test program included mix variations (fully detailed in Appendix D) as described in the following sections to ascertain the effect of the W/C ratio, coarse aggregate size, fibre dosage and fibre type on the performance parameters and result scatter. Each mix, unless otherwise stated consisted of two 115 litre batches. The first batch consisted of two beams and two panels, while the second batch consisted of four beams and one panel. Mix control was exercised in the form of slump tests and compressive strength tests according to SANS 5862-1 (2006) and SANS 5863 (2012) respectively. The mix designs are detailed in the following sections.

57

4.2.1. Reference mixes

Three fibre-less reference mixes were cast (Table 22, values in kg.m^{-3}). These mixes are the same as the single fibre pull-out mixes. Only beams were cast for these mixes as round panel tests cannot be performed on specimens without fibres.

Table 22: Macro-mechanical reference mixes, all values in kg.m^{-3}

Mix number	Water	Cement	W/C ratio	6 mm Aggregate	Sand
R1	240	400	0.6	781.5	926.2
R2	240	480	0.5	781.5	859.4
R3	240	600	0.4	781.5	759.3

4.2.2. Fibre dosage and type effect mixes

All four macro-synthetic fibres described in Section 3.1.1 were used to determine the effect of fibre dosage and type. The W/C ratio, aggregate size and content, as well as the fine aggregate content were kept constant, while the fibre types and dosages were varied. The fibre dosages for the Rocstay, Geotex 500 series, Geotex 600 series were varied at 0.5 %, 0.6 % and 0.7 % by volume. The Chryso Structural fibres could only be used to cast a 0.6 % dosage sample set for RDPT testing. The Geotex 600 series fibre was used to test two extreme dosages of 0.3 % and 0.9 % by volume. These mix designs are given in kg.m^{-3} in Table 23.

Table 23: Macro-mechanical fibre type and dosage effect mixes, all values in kg.m^{-3}

Water	Cement	W/C ratio	6 mm Aggregate	Sand	Fibre dosage
240	400	0.6	781.5	926.2	3.33 / 5.56 / 6.67 / 7.78 / 10

4.2.3. Coarse aggregate size effect mixes

The coarse aggregate size was varied between 6 mm, 13 mm and 19 mm, while the aggregate mass content and all other contents kept constant in order to determine the effect of coarse aggregate size on fibre distribution and thus performance and result variation. The aggregate size was varied with all three W/C ratios, with a constant Geotex 600 series fibre dosage of 0.6 %. The mix variations are shown in kg.m^{-3} in Table 24.

4.2.4. W/C ratio effect mixes

The effect of varying the W/C ratio between 0.4, 0.5 and 0.6 was observed by altering the cement content and keeping the water content constant at 240 kg.m^{-3}. The coarse aggregate content remained

Table 24: Macro-mechanical aggregate size mix variations, all values in kg.m^{-3}

Water	Cement	W/C ratio	6 mm / 13 mm / 19 mm Aggregate	Sand	Fibre dosage
240	400	0.6	781.5	926.2	6.67
240	480	0.5	781.5	859.4	6.67
240	600	0.4	781.5	759.3	6.67

constant, while the fine aggregate content decreased to account for the increase in cement content, i.e. a reduction in W/C ratio. These mixes are the same as in Table 24.

4.3. Sample Preparation and Curing

As discussed previously two 115 litre batches were mixed per mix design, using a 120 litre mixer. The dry constituents were mixed for 60 seconds before the mix water was added and allowed to mix in for 120 seconds. The fibres were then uniformly added by hand. Once all the fibres had been added, the materials were allowed to mix for a further two minutes. Slump tests were performed and the results recorded according to SANS 5862-1 (2006). Cubes were cast according to SANS 5863 (2012) to ascertain the compressive strength. The moulds were filled and vibrated using a poker vibrator until air bubbles no longer appeared, and then trowelled off. Once demoulded the beams were submerged in water at 23°C, while the panels were placed under wet blankets.

4.4. Test Setups

The three point beam bending test was performed according BS EN 14651 (2007). In total, six beams measuring 150 x 150 x 700 mm were cast for each mix variation. The RDPT was performed according to ASTM C1550 (2012), with three panels of 800 mm diameter and 75 mm height cast per mix variation.

4.4.1. Three point beam bending test setup

The three point beam bending test setup is shown in Figure 46. Prior to testing a notch measuring 25 mm was sawn into the beam on a side 90° from the casting surface. The loading roller was manufactured with springs so that the roller could rest evenly on the surface and thus apply the load uniformly. The beams were marked with chalk to ensure that the frame was consistently placed at mid-height and that the beam was centred over the 500 mm wide supports.

The test was conducted at a rate of 0.2 mm.min^{-1} up to a deflection of 3.65 mm using a 2 MN Instron Materials Testing Machine, with all data being recorded at a rate of 5 Hz. A sample was considered invalid if the crack occurred outside the notch. 10 mm LVDTs were used to measure the beam deflection at mid-span, mid-height on either side of the beam. The LVDTs measured the deflection by

pressing against thin metal plates which were glued onto the beam sample prior to testing. The plates did not affect crack formation as shown in Figure 47.

Figure 46: Three point beam bending test setup

Figure 47: Metal plate for LVDT to press against not affecting crack formation

4.4.2. RDPT setup

The RDPT setup is shown in Figure 48. A 100 mm LVDT was used to measure the central deflection to 45 mm. The load was applied at a rate of 5 mm.min^{-1} with a hemispherical load applicator conforming to the dimensions specified in ASTM C1550 (2012). A metal plate (Figure 49) was used to prevent the LVDT from slipping into the cracks.

ASTM C1550 (2012) requires two panels to crack with three cracks between supports of roughly equal sizes, as shown in Figure 50. Panels which cracked in a beam like fashion (Figure 51), either with only one crack or two large cracks and one small crack, were considered invalid.

60

Figure 48: RDPT setup

Figure 49: Metal plate preventing LVDT from slipping into cracks

Figure 50: Valid RDPT sample

Figure 51: Invalid RDPT sample exhibiting beam like-failure

4.5. Results

Compressive strength results, and results of the two types of tests are given in the following sections. The three point beam bending test results are presented as the average MOR, average third equivalent post peak flexural strengths ($f_{eq,3}$) and average third equivalent flexural strength ratios ($R_{e,3}$ values), as

described in Section 2.3.4. The MOR and the LOP were equivalent for every sample, as no samples experienced a peak load past a deflection of 0.077 mm (equivalent to a CMOD of 0.05 mm). The LOP is thus referred to as the better known MOR. The third equivalent post peak flexural strength was determined as described in Section 2.3.4, up to a deflection of 2.65 mm past the deflection at which the first crack and peak strength occurred. The $R_{e,3}$ values, as described in Section 2.3.4, were calculated as the ratio between the third equivalent post peak flexural strength and the MOR.

The RDPT results are presented as the average peak force obtained (at the first crack) and average energy absorbed up to a deflection at 40 mm. No adjustments were required for the load-deflection graph as the deflection was measured on the tensile surface of the panel.

Detailed results can be viewed in Appendix E.

4.5.1. Effect of fibre dosage on compressive strength and workability

Figure 52 shows the effect of the fibre dosage on compressive strength for all four fibre types.
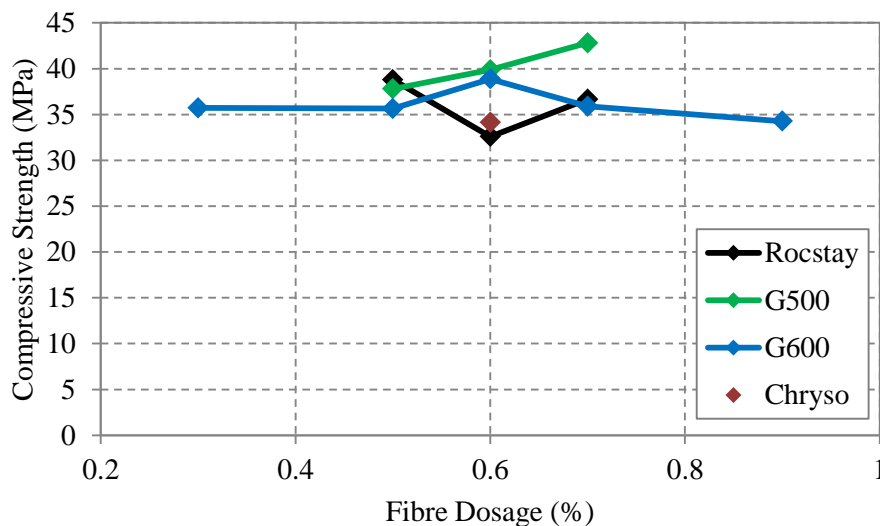
Figure 52: Effect of fibre dosage and type on compressive strength

The workability of the concrete was determined for each mix by a slump test (SANS 5862-1, 2006). None of the mixes exhibited segregation. The mix workability was largely unaffected at these fibre dosages, with a maximum difference of 40 mm in slump for a zero percent mix and a mix with fibres over the various W/C ratios.

4.5.2. Typical output and exclusion examples

An example of a typical three point beam bending result set where all of the results are valid is shown in Figure 53.

63
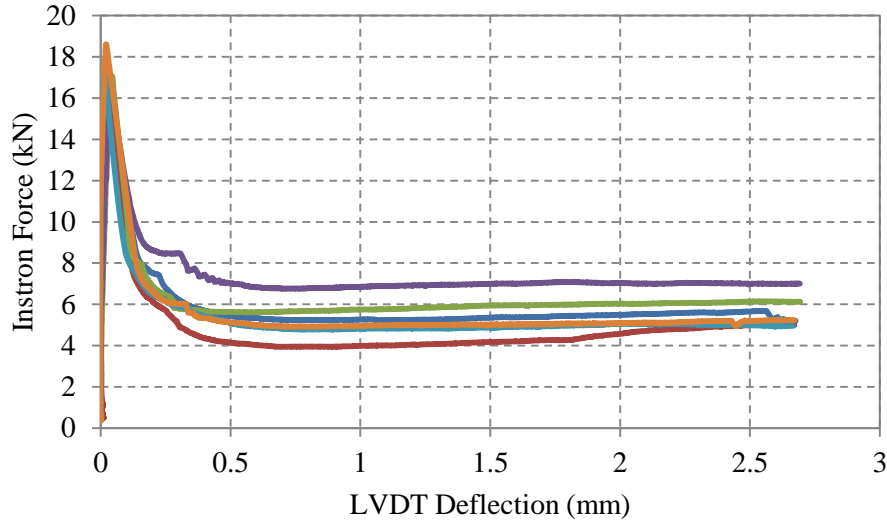
Figure 53: First type of typical three point beam bending result set

All of the results in Figure 53 are evenly dispersed within a relatively narrow band, with no obvious outliers.

Figure 54 shows an example of a three point beam result set which requires further consideration.
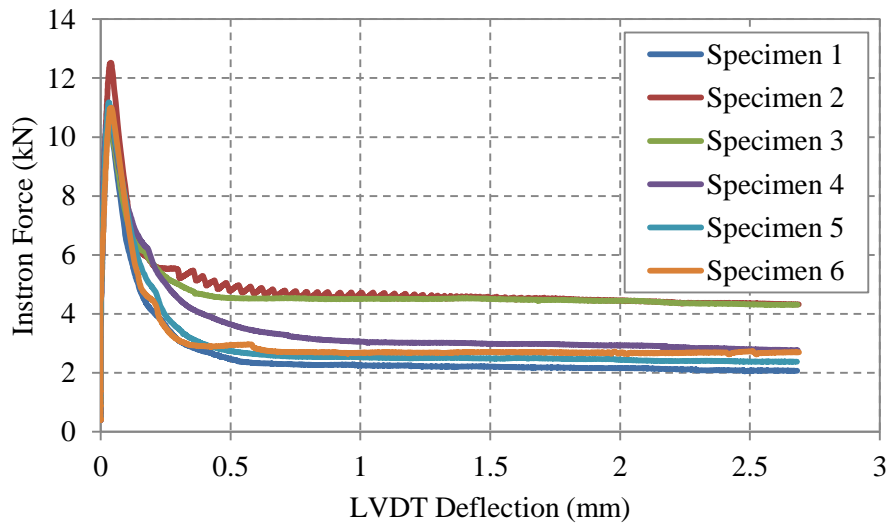
Figure 54: Second type of typical three point beam bending result set

Two of the results (Specimens 2 and 3) are distinctly higher than the rest. This can be accepted as part of the test variation as the two samples come from two different batches for the same mix design. However, if both samples had been from the first batch in which only two beams were cast, these would have been disregarded, provided the remaining four results corroborated with results from other sample sets. For example, if a higher fibre dosage (say 0.7 %) was used, and the lower four

64

results were worse compared to a 0.5 % and 0.6 % fibre dosages, then the lower results would have been disregarded and the two higher ones considered valid.

Figure 55 shows a typical valid set of RDPT results, with an explanation analogous to that of Figure 54.
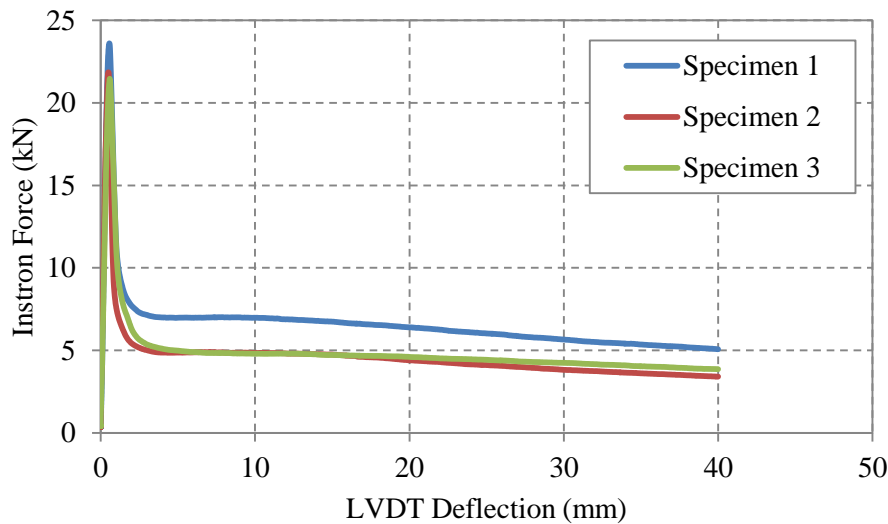
Figure 55: Valid RDPT result set

In total, only four beam results were excluded due to the values being unusually high. These values are highlighted in red in Appendix E. RDPT results which were excluded were due to the crack pattern being invalid according to ASTM C1550 (2012) and are not shown at all in the results in Appendix E.

4.5.3. Reference mix results

As stated previously, only reference beams were cast as reference round panels would have caused damage to the LVDTs. Figure 56 shows a typical output of a mix with no fibre reinforcement, with the full typical FRC beam deflection on the horizontal scale to demonstrate the minimal post-cracking capacity of fibre-less beams.

The average peak forces and MORs are given in Table 25 for the reference beams cast at 0.4, 0.5 and 0.6 W/C ratios.

The flexural strengths in terms of MOR can be classified into various strength classes, such as those found in the 2010 Model Code. Although the 2010 Model Code does not explicitly use flexural strength for strength classification, it provides a relationship between the axial tensile strength (f_{ctm}) and the flexural tensile strength (MOR) in the 2010 Model Code:

$$MOR = f_{ctm} \frac{1+0.06h_b^{0.7}}{0.06h_b^{0.7}}$$
[14]

65

which can be re-arranged to determine an axial tensile strength to be compared with the classes found in the 2010 Model Code. For example, the corresponding axial tensile strengths according to Equation [14] would be 3.42 MPa, 2.88 MPa and 2.39 MPa for the 0.4, 0.5 and 0.6 W/C ratios, which would correspond to the C35/45, C25/30 and C20/25 strength classes.
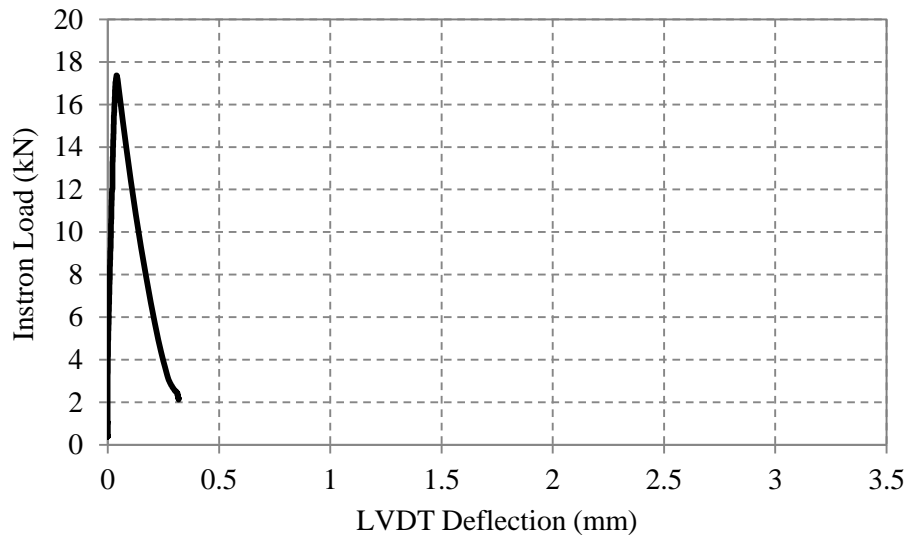
Figure 56: Example of macro-mechanical reference mix three point beam bending test output

Table 25: Macro-mechanical behaviour reference mix results

W/C Ratio	Peak Force (kN)	MOR (MPa)	COV (MOR)
0.4	16.49	5.13	0.1073
0.5	13.70	4.32	0.0355
0.6	10.78	3.58	0.0966

4.5.4. Effect of fibre type and dosage on post-cracking performance

Figure 57 and Figure 58 show the effects of fibre dosage on the RDPT average peak load and average energy absorbed for the four fibre types. The energy absorption was calculated up to a deflection of 40 mm. There were only enough Chryso Structural fibres for one set of round panels at a fibre dosage of 0.6 %.

The average peak RDPT force is unaffected by fibre dosage. The average RDPT energy absorption increases with increasing fibre dosage. The Geotex 600 series fibre performance increases at a faster rate than the Rocstay and Geotex 500 series fibres. This is evident from the slightly steeper gradient of the Geotex 600 series plot.
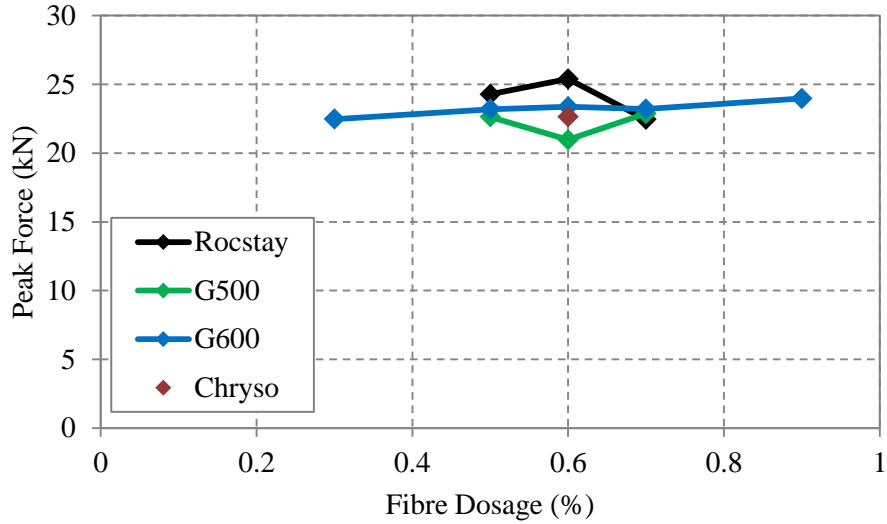
Figure 57: RDPT peak forces for various fibre types and dosages
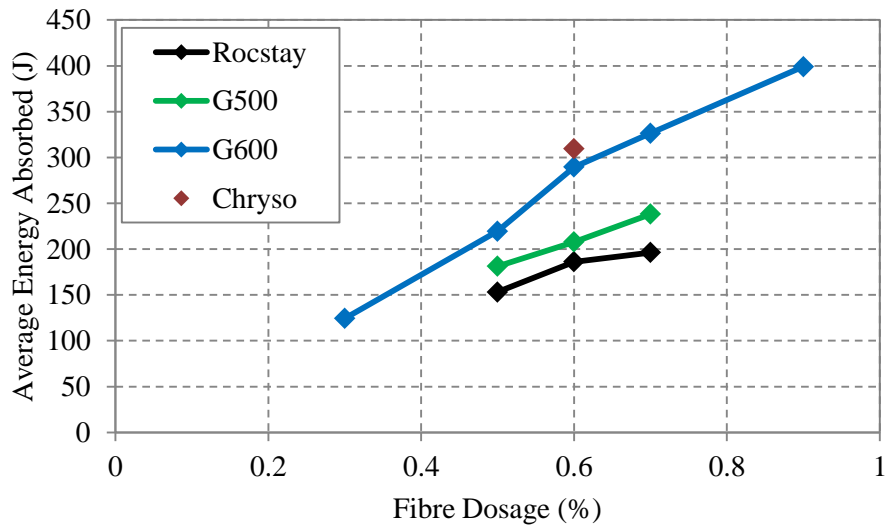
Figure 58: RDPT average energy absorbed for various fibre types and dosages

Figure 59, Figure 60 and Figure 61 show the effects of fibre dosage on the three point beam bending tests' average MOR, equivalent flexural tensile strength ($f_{eq,3}$) and $R_{e,3}$ values. Note the Chryso Structural fibre was not tested at all on the three point beam bending test setup.

The MOR appears to be unaffected by changing the fibre type and dosage. The third equivalent flexural tensile strength shows an upward trend with increasing fibre dosage. The beams containing Geotex 500 series fibre only showed slightly increasing performance with increasing fibre dosage when compared to the Rocstay and Geotex 600 series fibres. The $R_{e,3}$ value increased with increasing fibre dosage for the Rocstay and Geotex 600 series fibres. However, it remained relatively constant for the Geotex 500 series fibres.

The values obtained can be compared to, for example, the EFNARC (1996) standard. The panel test classification is based on a square panel test, which would require converting the values of the RDPT to square panel values, as described in Section 2.8.1. According to the EFNARC square panel values, the best performing fibre (Geotex 600 series at 0.9 % dosage) would have an equivalent energy absorption value of 1000 J and would have a toughness classification of "c". The RDPT results can also be compared with those of other studies, such as the one conducted by Bernard (2002). Similar results to Bernard's study were obtained for polypropylene fibres.
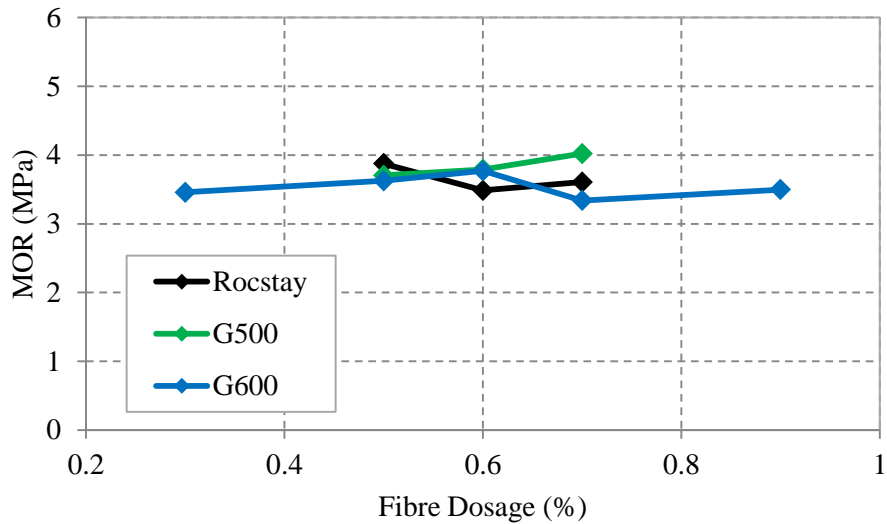
Figure 59: Three point beam bending test MOR for various fibre types and dosages
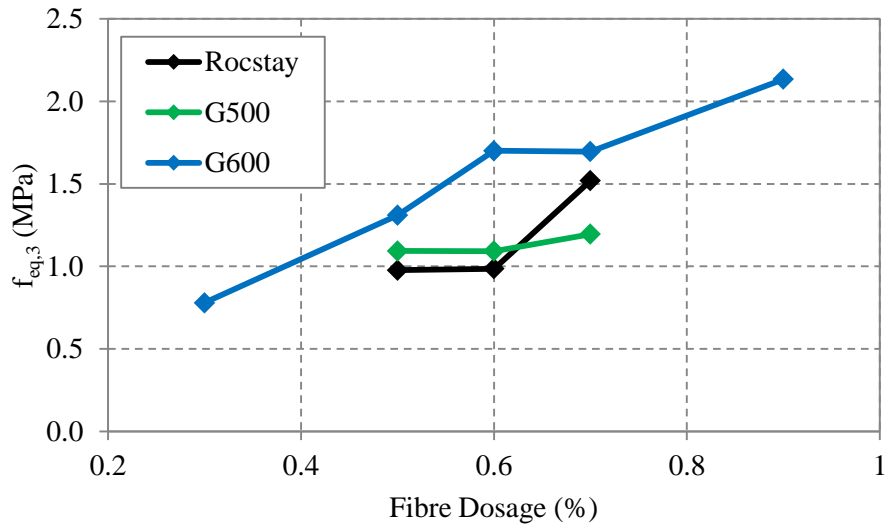
Figure 60: Three point beam bending test third equivalent flexural tensile strengths for various fibre types and dosages

68
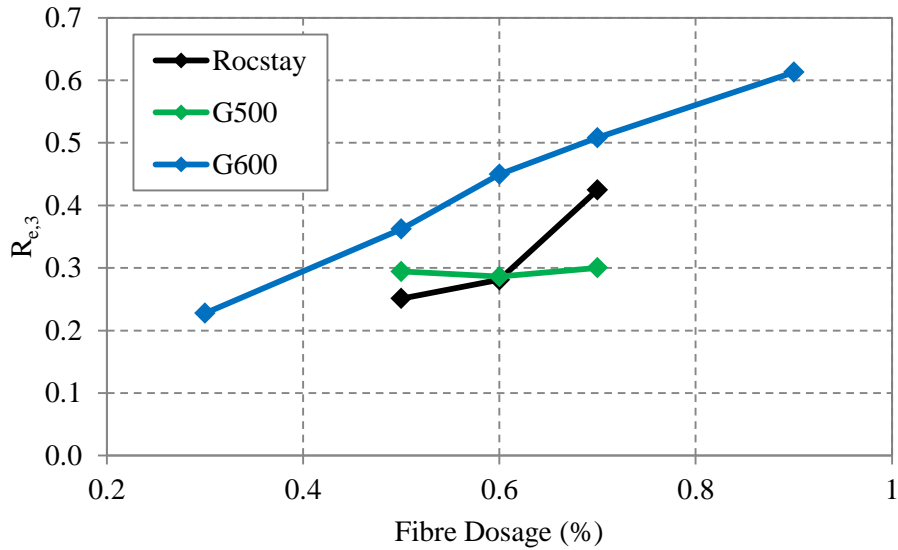
Figure 61: Three point beam bending test $R_{e,3}$ value for various fibre types and dosages

4.5.5. Effect of aggregate size on post-cracking performance

Figure 62 and Figure 63 show the effects of the aggregate size on the RDPT peak load and average energy absorbed.

It is clear from the RDPT results that the aggregate size has an effect on the peak cracking strength of the concrete, as well as the energy absorption, regardless of W/C ratio. The peak force drops an average of 17 % from 6 mm to 19 mm aggregate size. It can be further seen that the aggregate size also has an effect on the average energy absorbed, with an average decrease of 35 % from 6 mm to 19 mm stone size. Note the averages are taken over all three W/C ratios.
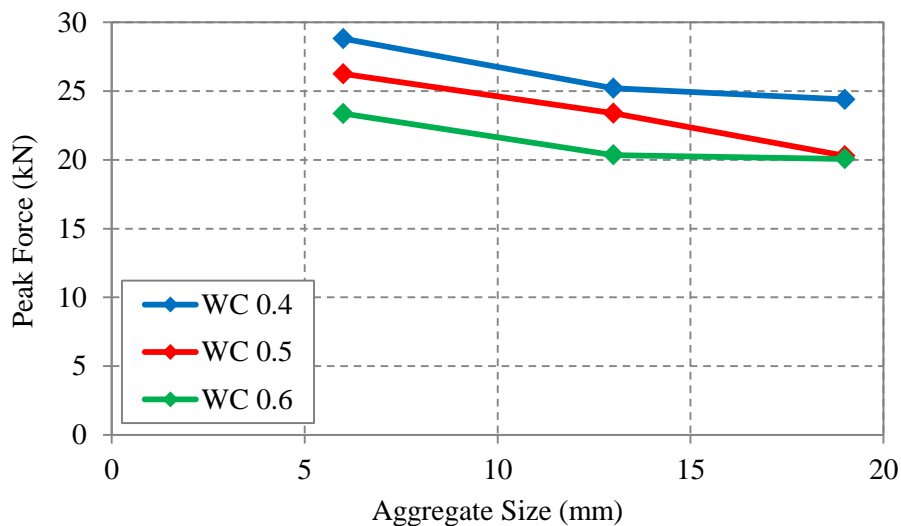
Figure 62: RDPT peak forces for various aggregate sizes at various W/C ratios

69
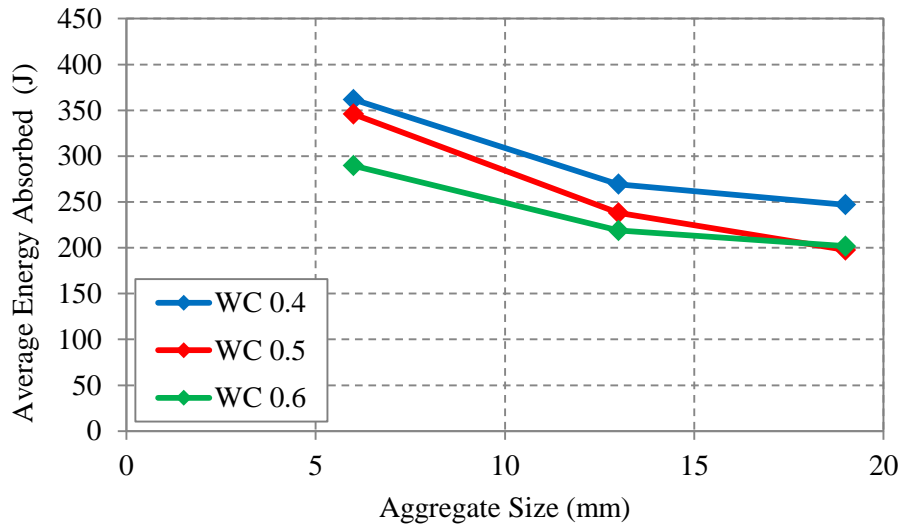
Figure 63: RDPT average energy absorbed for various aggregate sizes at various W/C ratios

Figure 64, Figure 65 and Figure 66 show the effects of aggregate size on the three point beam bending tests' MOR, third equivalent flexural tensile strength and $R_{e,3}$ values.
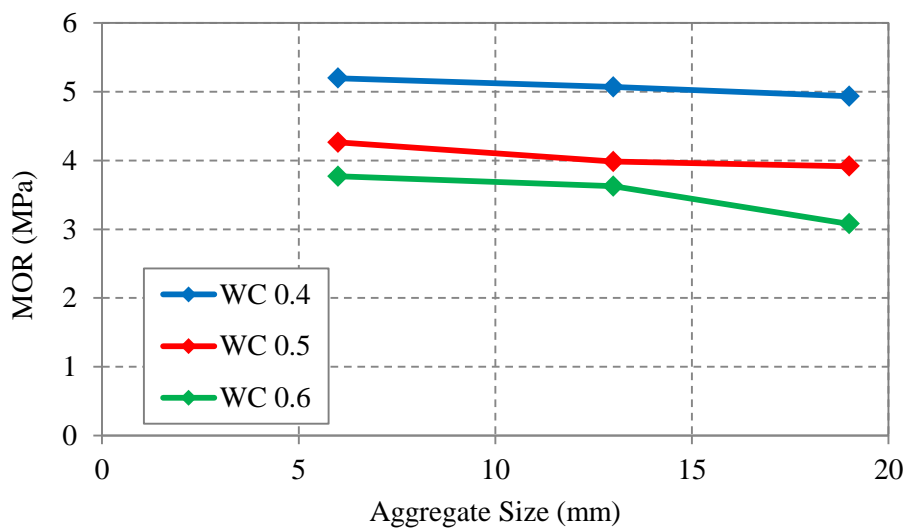
Figure 64: Three point beam bending test MOR for various aggregate sizes at various W/C ratios

Looking at Figure 64, the MOR decreases with increasing aggregate size, as with the peak force of the RDPT tests. The MOR decreases on average 11 % from the 6 mm to the 19 mm aggregate size.

70
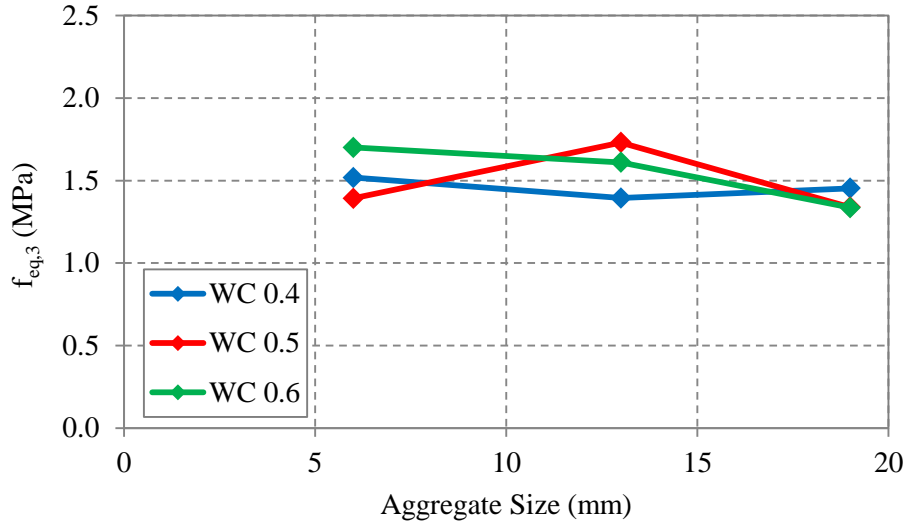
Figure 65: Three point beam bending test third equivalent flexural tensile strengths for various aggregate sizes at various W/C ratios
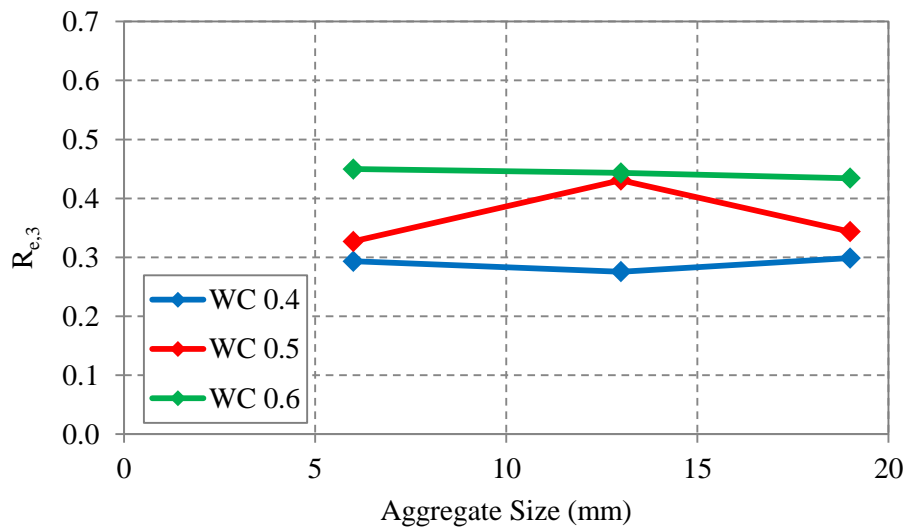
Figure 66: Three point beam bending test $R_{e,3}$ value for various aggregate sizes at various W/C ratios

The equivalent flexural tensile strengths generally decrease with increasing aggregate size, but have anomalies at the 0.5 W/C ratio 13 mm aggregate size, and 0.4 W/C ratio 19 mm aggregate size. The anomaly at the 0.5 W/C ratio 13 mm aggregate size is due to the result set having a high dispersion (a maximum value (2.33 MPa) more than 95 % higher than the lowest value (1.2 MPa). The remaining results were evenly dispersed between these values, thus not warranting exclusion of any results. The slight increase of the 0.4 W/C ratio 19 mm aggregate size is due to two values which were significantly higher than the rest. The $R_{e,3}$ values follow the same trend as the third equivalent flexural tensile strengths values, thus the anomalies can be explained in the same way.

71

Figure 67 shows the effect of aggregate size on the equivalent flexural tensile strength with the anomalies removed, and Figure 68 the effect of aggregate size on the $R_{e,3}$ value with the anomalies removed.

Figure 68 shows a slight increase in $R_{e,3}$ value from 6 mm to 19 mm for the 0.5 W/C ratio. This is due to the MOR decreasing at a faster rate than the equivalent flexural tensile strength.
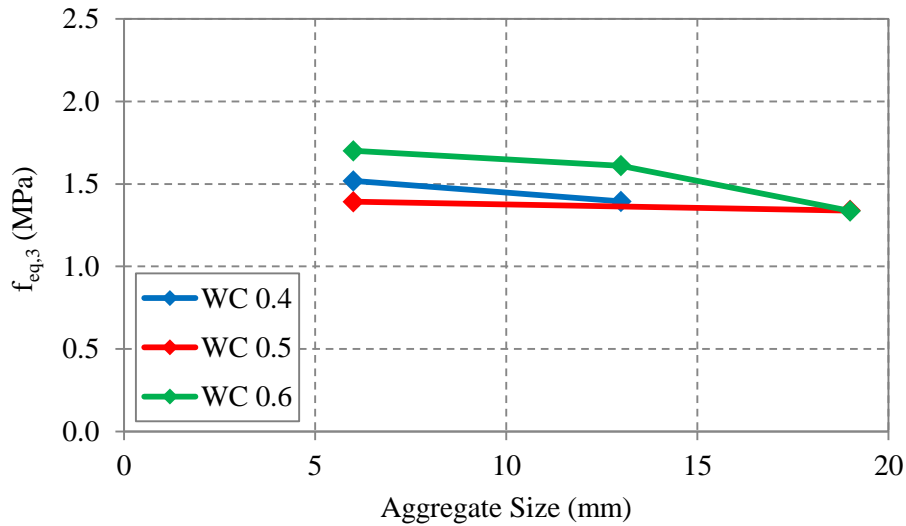
Figure 67: Effect of aggregate size on third equivalent flexural tensile strengths without anomalies
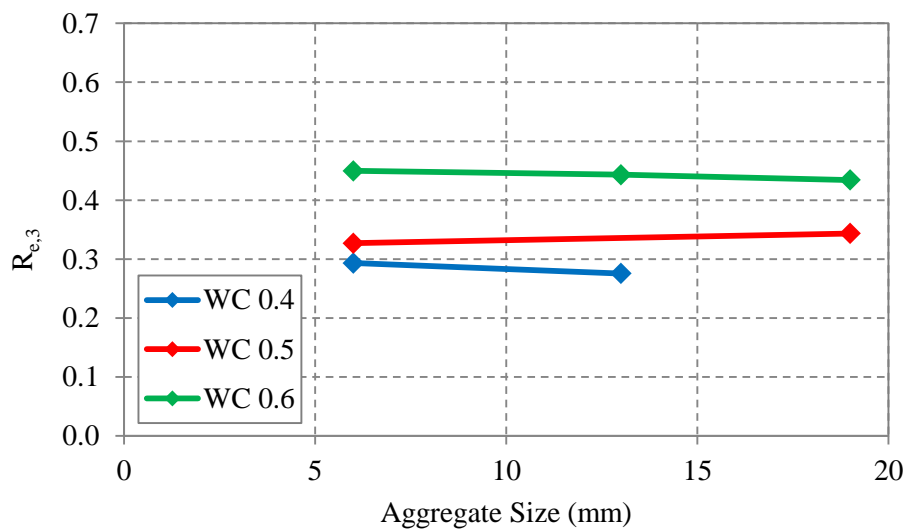
Figure 68: Effect of aggregate size on $R_{e,3}$ values without anomalies

4.5.6. Effect of W/C ratio on post-cracking performance

Figure 69 and Figure 70 show the effects of the W/C ratio on the RDPT peak load and average energy absorbed.

72
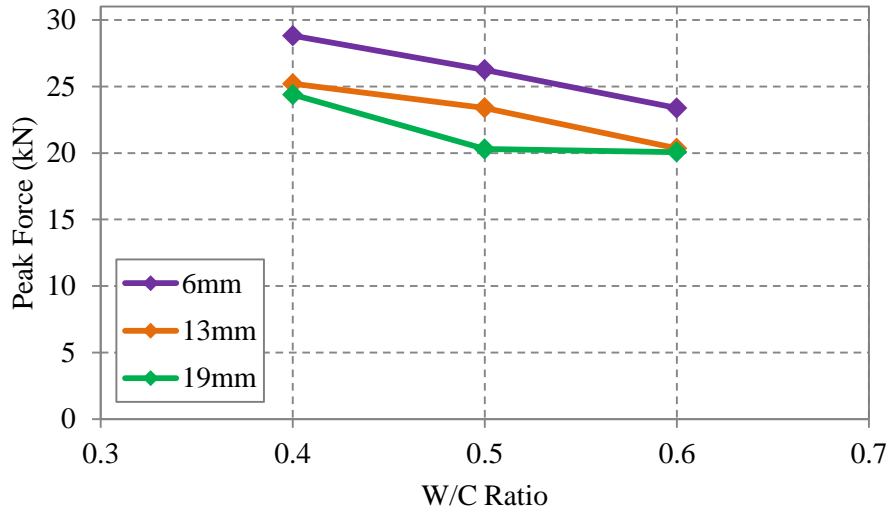
Figure 69: RDPT peak forces for various W/C ratios at various aggregate sizes
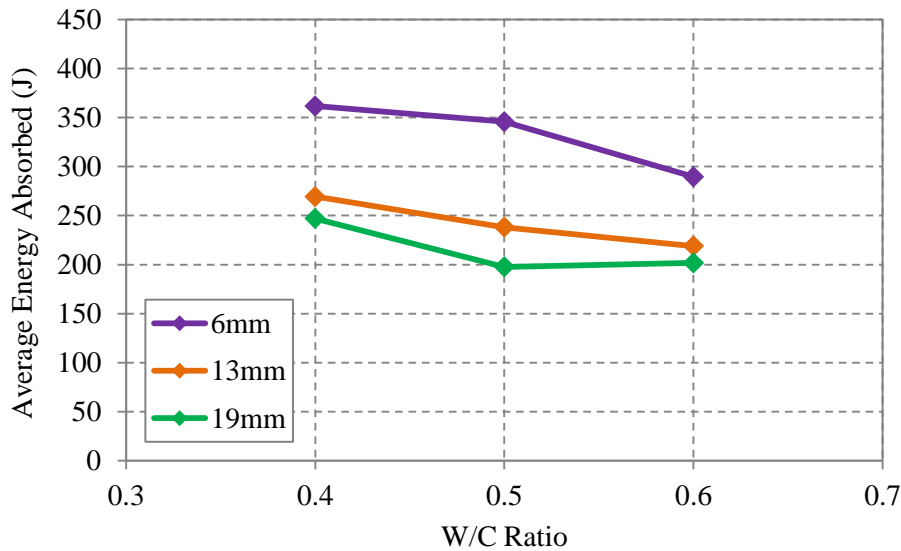
Figure 70: RDPT average energy absorbed for various W/C ratios at various aggregate sizes

The peak cracking values and the average energy absorbed both decrease with increasing W/C ratio. The peak load and average energy absorbed of the 6 mm aggregate both decrease by 19 % over from the 0.4 W/C ratio to the 0.6 W/C ratio while the values decrease by 18 % for the 19 mm aggregate. The 13 mm aggregate peak load and energy absorbed decreased by 7 % and 18 % respectively over the W/C ratios respectively.

Figure 71, Figure 72 and Figure 73 show the effects of the W/C on the three point beam bending tests' MOR, third equivalent flexural tensile strength and $R_{e,3}$ values.
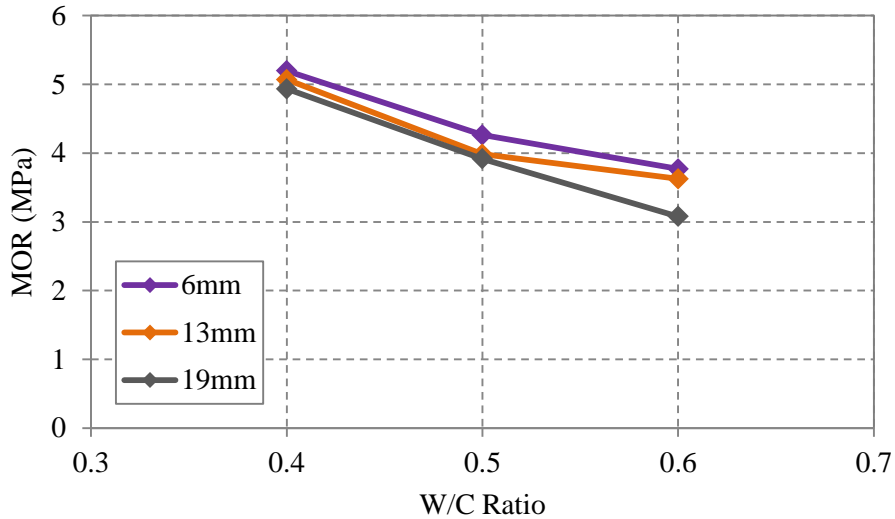
Figure 71: Three point beam bending test MOR for various W/C ratios at various aggregate sizes
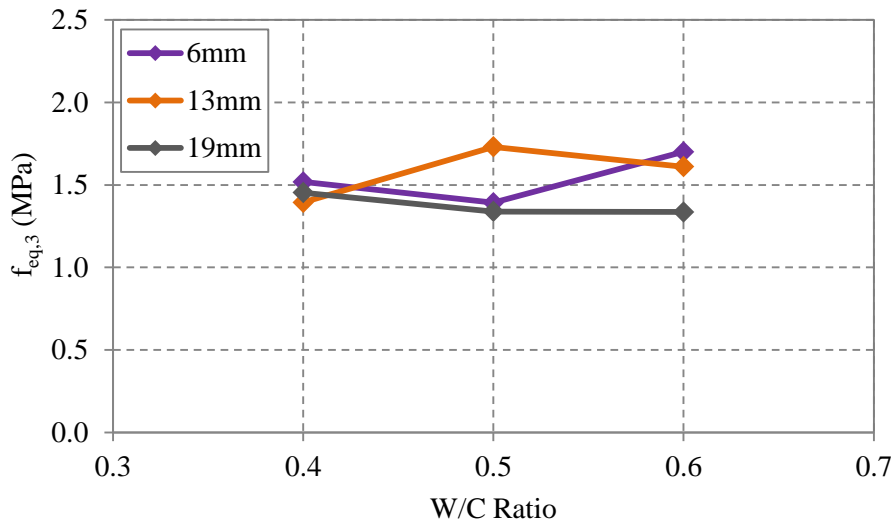
Figure 72: Three point beam bending test third equivalent flexural tensile strengths for various W/C ratios at various aggregate sizes

The MOR decreased with increasing W/C ratio, as expected. The 6 mm and 13 mm equivalent flexural tensile strength values did not consistently decrease with increasing W/C ratio as the MOR and average energy absorption did.

The $R_{e,3}$ value increases with increasing W/C ratio. This is due to the MOR having a wide range from 5.2 MPa to 3.08 MPa from the 0.4 to 0.6 W/C ratios, while the equivalent flexural tensile stresses vary minimally within a range of 1.34 MPa to 1.73 MPa from the 0.4 to 0.6 W/C ratios.
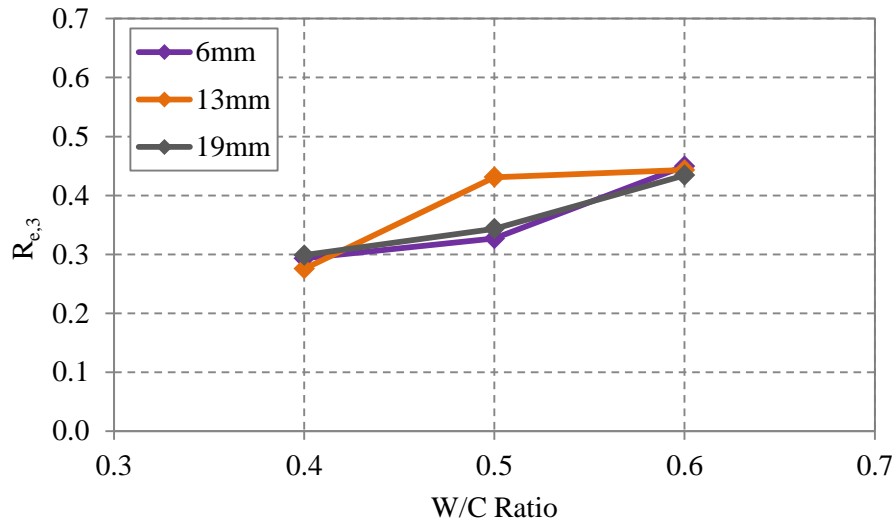
Figure 73: Three point beam bending test $R_{e,3}$ values for various W/C ratios at various aggregate sizes

4.5.7. Result scatter

For each set of beam samples, the COV was determined based on the $R_{e,3}$ value and on the energy absorbed up to 40 mm central deflection for the RDPT sample sets. Table 26, Table 27 and Table 28 detail the COVs for the fibre dosage effect, aggregate size effect and W/C ratio effect tests respectively. COVs less than 0.15 are highlighted in green.

Table 28 indicates that the average COV increases with increasing aggregate size for the RDPT, as expected. However, the three point beam bending test only showed a higher COV for the 19 mm aggregate.

The three point beam bending test COVs, ranging from 0.0692 to 0.3792 and averaging 0.2052 and the RDPT COVs ranging from 0.0147 to 0.2889 and averaging 0.1030, are in line with those generally found in literature (Vandewalle et al.,2008; Parmentier et al., 2008 and Bernard, 2002).

4.6. Discussion on Choice of Test

One of the research objectives was to determine which test would be preferable for performance specifications. This is discussed here, followed by a discussion of the performance test results in terms of fibre dosage and effect type, aggregate size and W/C ratio in Section 4.7. The choice of test is based on three factors: the ease of the tests and quality control, result utility and result consistency.

4.6.1. Ease of tests and quality control

The three point beam bending test required six beams and a minimum of 80 litres (100 litres with the available moulds) of concrete, while the RDPT required three panels and 115 litres of concrete. It was less strenuous to cast the round panels than the beams. With regards to actual testing, the beams proved easier to pick up and place in a testing machine, but took longer per sample and required

75

Table 26: COVs for the fibre dosage effect tests

Fibre type	Fibre dosage (%)	Beams			Panels		
		Average $R_{e,3}$	Standard deviation	COV	Average energy absorbed (J)	Standard deviation	COV
Rocstay	0.5	0.25	0.08	0.3000	153.17	6.37	0.0416
	0.6	0.28	0.08	0.2997	186.17	26.21	0.1408
	0.7	0.42	0.09	0.2141	196.37	10.17	0.0518
G500	0.5	0.29	0.02	0.0697	181.32	2.67	0.0147
	0.6	0.29	0.04	0.1233	207.82	18.55	0.0893
	0.7	0.30	0.06	0.2140	238.21	15.88	0.0667
G600	0.3	0.23	0.04	0.1773	124.26	20.86	0.1678
	0.5	0.36	0.12	0.3255	219.50	45.85	0.2089
	0.6	0.45	0.08	0.1837	289.53	23.74	0.0820
	0.7	0.51	0.11	0.2193	326.49	32.09	0.0983
	0.9	0.61	0.12	0.1896	399.10	46.16	0.1157
Chryso	0.6	-	-	-	309.67	21.84	0.0705

testing more samples than the panels. The beams also require notching, which is a time consuming and labour intensive process. In addition, processing the data for the RDPT was less time-consuming than for the three point beam bending tests.

In terms of quality control, the three point beam bending test are easier to exercise control over in terms of compaction as there is a smaller surface area over which compaction occurs. Sample hydration is also important. Obtaining curing tanks large enough to house the round panels during the curing period can present a problem. If a curing tank is not large enough, the panels could potentially be cured in an uncontrolled environment. For example the blankets covering the panels may be shifted and expose the panel, or the blankets covering the panels may not be evenly saturated. Samples not placed in curing tanks are also at risk of not being in a temperature controlled environment, which could affect the rate of strength gain.

Table 27: COVs for W/C ratio and aggregate size effect tests

W/C ratio	Aggregate size (mm)	Beams			Panels		
		Average $R_{e,3}$	Standard deviation	COV	Average energy absorbed (J)	Standard deviation	COV
0.4	6	0.29	0.0718	0.2448	361.72	43.99	0.1216
	13	0.28	0.0500	0.1816	269.24	24.50	0.0910
	19	0.30	0.1132	0.3792	247.00	18.14	0.0734
0.5	6	0.33	0.0470	0.1437	345.77	8.87	0.0257
	13	0.43	0.0607	0.1409	238.09	37.16	0.1561
	19	0.34	0.0864	0.2518	197.56	14.84	0.0751
0.6	6	0.45	0.0826	0.1837	289.53	23.74	0.0820
	13	0.44	0.0634	0.1430	218.82	17.49	0.0799
	19	0.43	0.0583	0.1344	201.78	58.30	0.2889

Table 28: Average COVs based on aggregate sizes

Aggregate size	6 mm	13 mm	19 mm
Beams	0.1907	0.1552	0.2551
Panels	0.0764	0.1090	0.1458

Thus, both tests have advantages and disadvantages in terms of quality control and ease. If the main concern is time, the round panel test is favourable. Both test methods are disadvantageous in terms of man power, as the RDPT is large and awkward to move, while the three point beam bending test requires notching. The three point beam bending test is advantageous in terms of quality control of the actual sample preparation and hydration.

4.6.2. Utility of results

The $R_{e,3}$ value and equivalent flexural strengths which can be obtained from the three point beam bending tests is of much more use in terms of design than the average energy absorbed. If the compressive strength of concrete is known, the required flexural tensile strength can be determined. Using this and the ultimate moment, the $R_{e,3}$ value can be determined for a required post-cracking load carrying capacity, or the post-cracking moment can be determined from a known $R_{e,3}$ value. A specific fibre type and dosage can be recommended to obtain the required $R_{e,3}$ value or post cracking

moment capacity. Various publications such as the Concrete Society (2003) Technical Report 34 (TR34) detail the use of the $R_{e,3}$ value in structural design.

A relation exists between the $R_{e,3}$ values and the average energy absorbed, as presented in Section 2.8.2. However, the $R_{e,3}$ value increases with decreasing W/C ratio (Figure 73) as it includes the MOR which decreases with increasing W/C ratio, while the average energy absorbed decreases with increasing W/C ratio (Figure 70). Thus, in order to relate the average energy absorbed to a parameter which may be used in design, the average energy absorbed and another parameter, such as the equivalent flexural tensile strength could be related.

4.6.3. Result consistency

In Table 26, Table 27 and Table 28 the COVs less than 0.15 are highlighted in green. It is clear from the highlighted cells and the COV averages (0.2179 and 0.2012 for the three point beam bending test and 0.0980 and 0.1104 for the RDPT) that the RDPT is more consistent than the three point beam bending test.

Of the RDPTs, thirteen had COVs less than 0.1 and five had COVs between 0.1 and 0.2. The two RDPT COVs exceeding 0.2 are easily explained - the highest COV, 0.2889, is due to the larger aggregate size, which lessens fibre dispersion and thus increases the result variation. The other COV above 0.2 (only marginally), can be attributed to one value being significantly higher than the others. The possibility of acceptable panel thickness variation was considered. However, the panel thicknesses did not deviate by more than 1.85 mm from 75 mm, thus this could not be the reason.

The generally higher COV for the beam tests can be attributed to the significantly smaller beam bending test crack area than the crack area offered by the RDPT. The beam tests have a crack area of only 22500 mm^2, while the panels have a crack area of 90000 mm^2. Thus a crack area four times higher results in approximately twice as consistent results.

The increase in beam bending test variability with an increase in aggregate size (Table 28) was not as pronounced as expected. Although the averages of the COV increases with an increase in aggregate size for RDPT, the three point beam bending test only shows a higher COV for the largest aggregate size, with the COV of the 6 mm aggregate (0.1907) slightly higher than that of the 13 mm aggregate (0.1508). In addition, the highest RDPT COV (0.1458) is also lower than the lowest three point beam bending COV (0.1552) across the three aggregate sizes. Thus, the RDPT is significantly more consistent than the three point beam bending test.

4.6.4. Test method recommendation

The RDPT, in addition to having less variation, also identifies trends such as the effect of aggregate size and W/C ratio which the three point beam bending test doesn't identify due to test variation or the manner in which the results are determined.

Although the beam test results can be used directly in structural design calculations, it may be possible to incorporate the energy absorption into calculations once the RDPT becomes more well-known and energy absorption classes become more common-place. Taking these aspects – ease of tests and quality control, the result utility and result consistency, the ASTM C1550 (2012) RDPT is better suited for testing SynFRC than the three point beam bending test.

4.7. Results Discussion

4.7.1. Compressive strength and workability

It is clear from Figure 52 that the fibre dosage does not have an effect on the compressive strength of the concrete. This is due to the low fibre dosages used, which do not occupy a significant enough volume of the concrete. The difference in workability was also largely unaffected at these fibre dosages, with the maximum difference in 6 mm aggregate size at 0.6 W/C ratio going from 200 mm with no fibres to a minimum of 145 mm with a 0.6 % fibre dosage.

4.7.2. Peak forces and MOR

The RDPT standard (ASTM C1550 (2012)) only allows for a peak force, while the three point beam bending test has a peak force which is resolved into the MOR by means of Equation [4].

From Figure 57 and Figure 59, it can be seen that the fibre type and dosage has no effect on the maximum force which the concrete can withstand. At these low dosages, the cement matrix's tensile strength still constitutes an overwhelming majority of the pre-cracking strength, and thus at the same aggregate size and W/C ratio, the peak forces should remain constant.

The RDPT peak force exhibits a decrease with an increase in aggregate size. The three point beam bending test also showed a decrease in MOR with increasing aggregate size, averaging an 11 % decrease over the aggregate sizes, while the RDPT peak forces averaged a decrease of 17 % over the aggregate sizes. This is due to the smaller aggregate being more closely packed than the larger aggregate, resulting in more aggregate interlock and thus slower crack propagation at smaller aggregate sizes.

An increase in W/C ratio results in a decrease in the RDPT peak force and MOR (Figure 69 and Figure 71). This is due to there being less solid cement hydration products and more free water in the cement matrix, resulting in a more porous and thus weaker matrix.

4.7.3. Effect of fibre type and dosage on post-cracking performance parameters

Figure 58 shows the expected linear increase in RDPT average energy absorbed for an increase in fibre dosage for all fibre types. This was expected, as a higher fibre dosage will provide more fibres bridging the cracks to provide residual load carrying capacity.

Figure 60 and Figure 61 showed the expected increase in performance (equivalent flexural tensile strengths and $R_{e,3}$ values) for the Rocstay and Geotex 600 series fibres, but no noteworthy effect for the Geotex 500 series fibre. This could possibly be due to the Geotex fibres being longer than the Rocstay fibres and stiffer than the Geotex 600 series and thus not mixing throughout the matrix as well.

The fibre shape also appears to affect the post-cracking performance. The flat fibres with rectangular cross section performed better than the non-flat crimped fibres, even though the bond stress of the crimped Geotex 500 series fibres is similar to that of the flat Chryso Structural fibres. Although only three panels were cast containing Chryso Structural fibres, from that result it can be expected that the behaviour would be similar to that of the Geotex 600 series fibres. This can potentially be attributed to a similar fibre shape and fibre tensile strength, although their bond stresses are significantly different. From Figure 58, it appears that the Chryso Structural fibre has the potential to be the best-performing fibre.

4.7.4. Effect of aggregate size on post-cracking performance parameters

The three point beam bending test (Figure 66) did not show any particular trend for the effect of aggregate size on the $R_{e,3}$ value. However, the third equivalent flexural tensile strength (Figure 65) does show a downward trend for the 0.4 and 0.6 W/C ratios. The 0.5 W/C ratio had a significant increase in equivalent flexural tensile strength at the 13 mm stone. This increase can be attributed to the small crack area and aggregate size, which did not allow for uniform fibre distribution and thus caused high result variation.

The RDPT showed a decrease in energy absorbed for an increase in aggregate size (Figure 63). The larger aggregate will occupy more crack area and distribute the fibres unevenly resulting in weak areas with few or no fibres, as opposed to smaller aggregate which would allow more uniform fibre distribution across the crack area and thus better performance.

4.7.5. Effect of W/C ratio on post-cracking performance parameters

The three point beam bending test shows that an increase in W/C ratio causes an increase in $R_{e,3}$ value. This is misleading, as the equivalent flexural strength stays relatively constant (Figure 72) for an increase in W/C ratio, and the MOR decreases (Figure 71) due to the cement matrix being weakened by the additional free water in the cement matrix at higher W/C ratios. The decreasing

MOR causes the $R_{e,3}$ value to increase (Figure 73), but this does not necessarily mean that the post-cracking performance is improved.

However, the RDPT shows a decrease in energy absorbed if the W/C ratio is increased (Figure 70). This could possibly be due to the fibre bond stress decreasing with increasing W/C ratio, which although perhaps not noticeable on a single fibre level (Section 3.6.2), may be noticeable on a cumulative effect.

4.8. Macro-Mechanical and Single Fibre Parameter Comparison

The macro-mechanical performance parameters and single fibre pull-out tests results were expected to correlate, in the sense that the fibre with the highest bond stress (Rocstay) would also perform the best on a macro-mechanical level. This was not true, as can be seen from Figure 58 and Figure 60, where the Rocstay fibres display the poorest macro-mechanical performance, and the fibre with the poorest single fibre performance (Geotex 600 series) displays close to the best performance. Figure 74 shows the relation between the bond stress and average energy absorbed at the 0.6 W/C ratio and 6 mm coarse aggregate size, with 0.6 % fibre dosage. Figure 75 shows the relation between the bond stress and the equivalent flexural tensile strength at the 0.6 W/C ratio and 6 mm coarse aggregate size, with 0.6 % fibre dosage. Note the treated Chryso Structural fibre is not included in the data of Figure 75 due to supply issues.
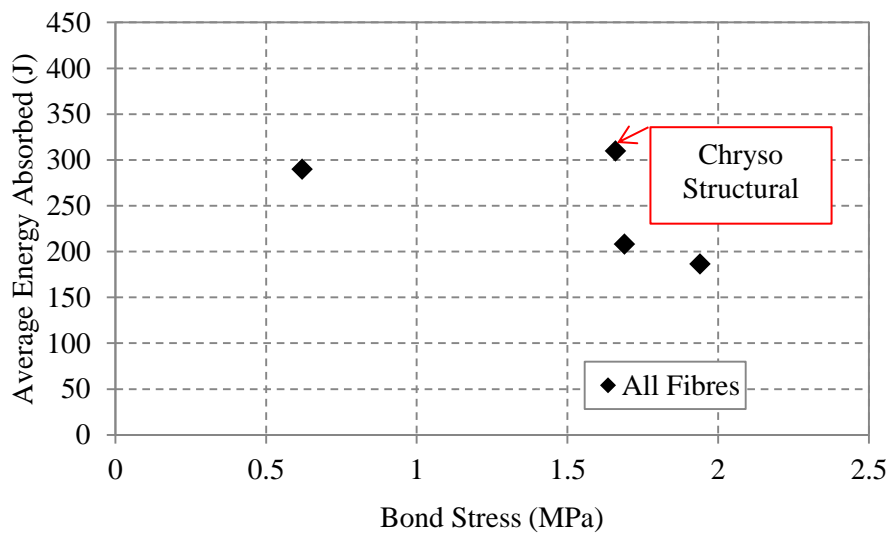
Figure 74: Bond stress versus average energy absorbed

81
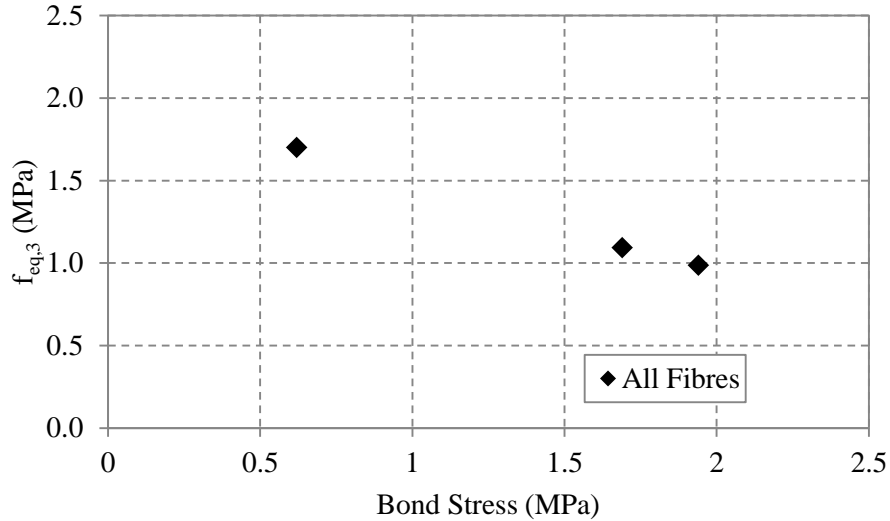
Figure 75: Equivalent flexural tensile strength relationship with bond stress

Figure 74 and Figure 75 show a decreasing macro-mechanical performance (in terms of average energy absorbed and third equivalent flexural tensile strength) with increasing bond stress, except for the Chryso Structural fibre in Figure 74. The outlier can perhaps be ascribed to the surface treatment of the Chryso Structural fibre. If there was no surface treatment present, the bond stress would have been less, perhaps even less than that of the Geoetx 600 series fibre, in which case it would have fitted the decreasing trend.

The macro-mechanical performance was also compared with the measured equivalent diameters, as shown in Figure 76 (average energy absorbed) and Figure 77 (equivalent flexural tensile strengths).
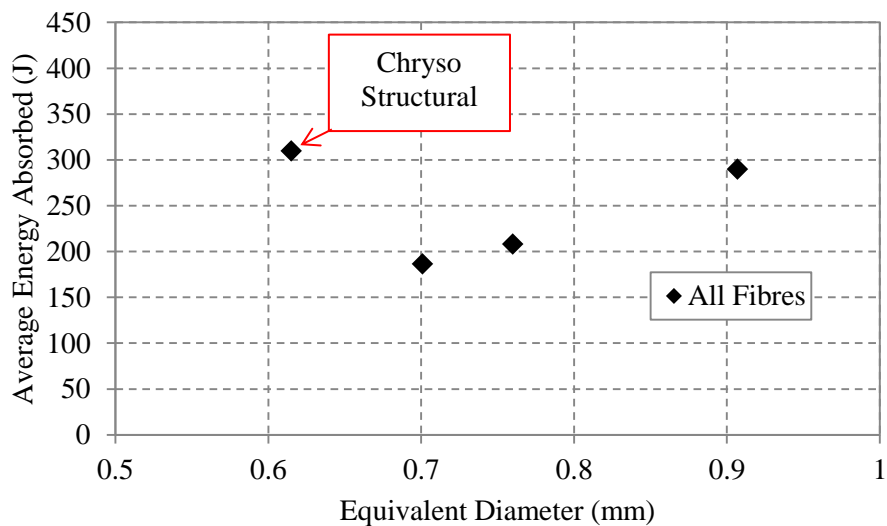
Figure 76: Equivalent diameters versus average energy absorbed
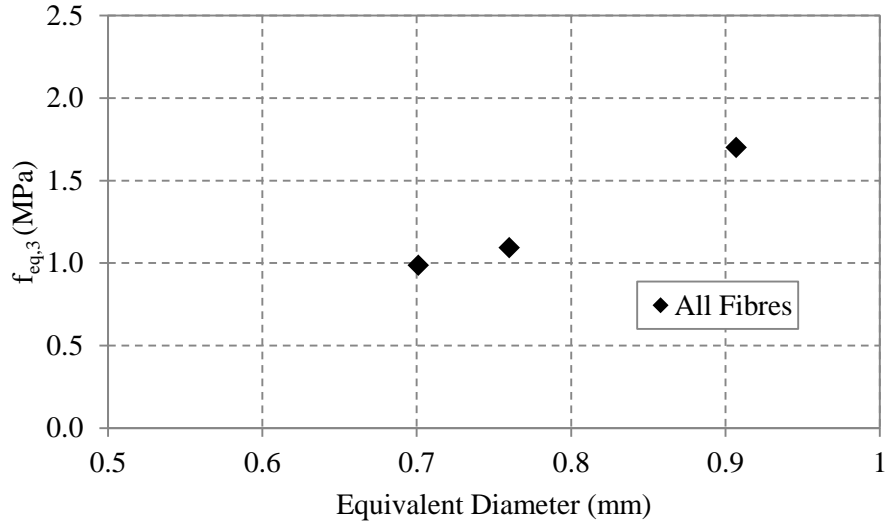
Figure 77: Equivalent diameters versus equivalent flexural tensile strengths

From Figure 76 and Figure 77, the macro-mechanical performance increases with increasing equivalent diameter for all of the fibres except for the surface treated Chryso Structural fibre.

A possible explanation for the relationships between the macro-performance parameters and the bond stress and equivalent diameter could be due to:

$$F_{r,bond} = \tau \times \pi \times d_e \times l_e = \tau \times Surface\ Area \qquad [15]$$

Fibres with a higher bond stress will have a higher maximum force which must be applied before fibre pull-out begins. Thus, at the same force, a fibre with a lower bond stress will have pulled out more than a fibre with a higher bond stress as the force which a higher bond stress fibre would be able to resist would be higher. The amount of fibre elongation (i.e. the energy absorbed or work done) in a longer length of fibre will be higher for a fibre with a lower bond stress, as more of the fibre will be available for elongating and thus for work (Figure 78)
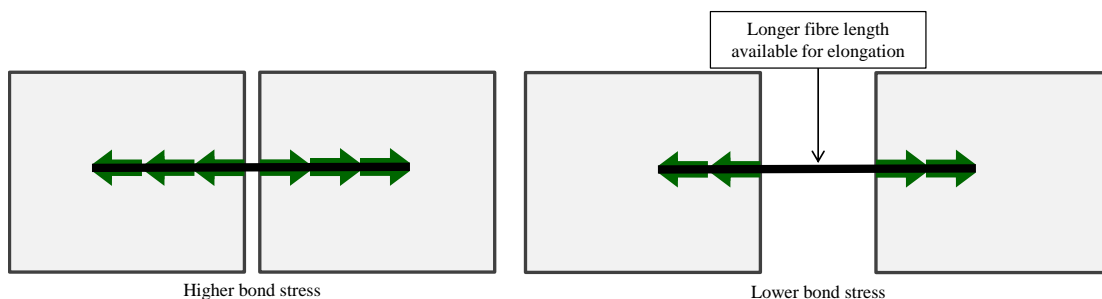
Figure 78: Higher energy absorption for lower bond stresses

If the equivalent diameter of a fibre is increased, then for a set volume of fibres, the equivalent surface area will decrease due to volumetric considerations. Figure 76 and Figure 77 show that for an increase

83

in equivalent diameter, implying a decrease in total surface area for a set volume of fibres the macro-performance increases. Thus, as for a lower bond stress, the total surface area will decrease, and a similar scenario as in Figure 78 occurs.

Finally, the average energy absorbed (Figure 79) and equivalent flexural tensile strengths (Figure 80) were plotted against the fibre aspect ratio, separated for flat and non-flat fibres. The Chryso Structural fibre third equivalent flexural tensile strength could not be computed as no beams were cast with the Chryso Structural fibres. The Chryso Structural fibre data point in Figure 80 was determined by using the gradients from Figure 79 and the non-flat fibres in Figure 80.
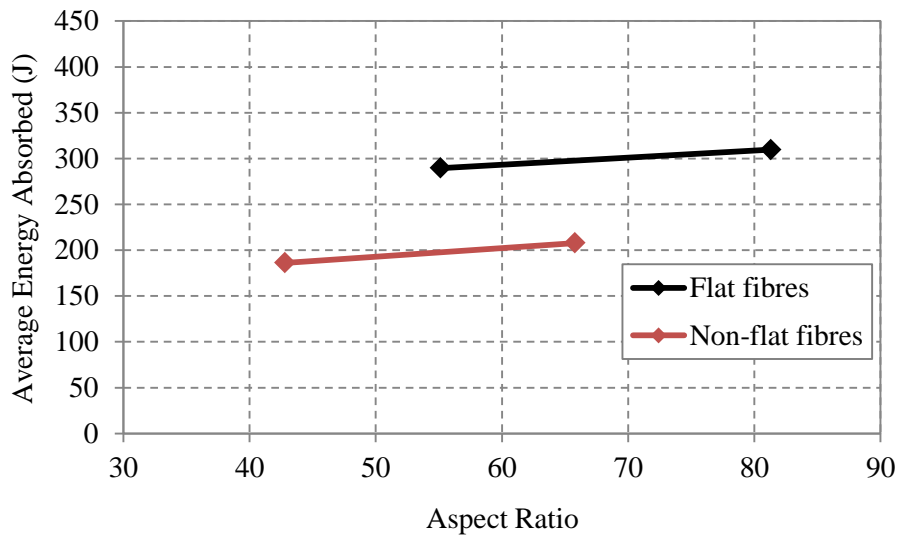
Figure 79: Fibre aspect ratios versus average energy absorbed
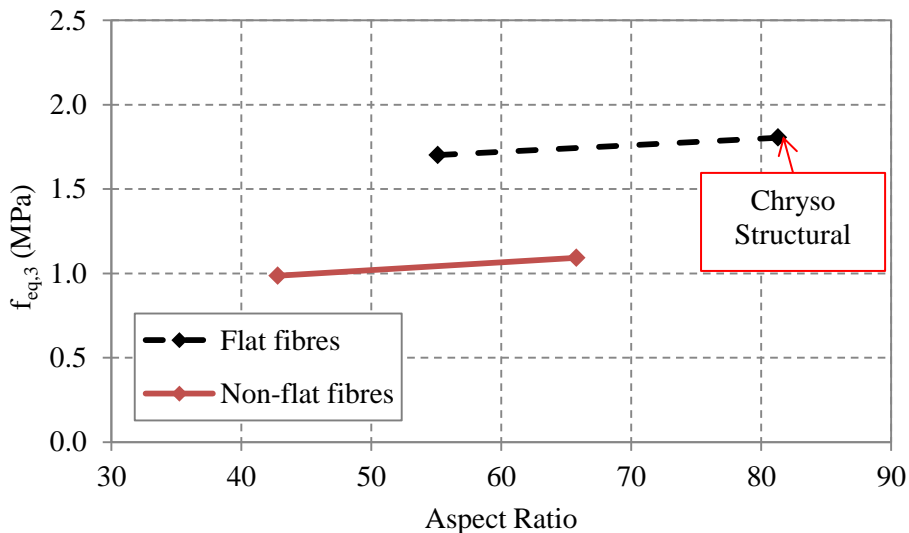
Figure 80: Fibre aspect ratios versus third equivalent flexural tensile strength

84

It can clearly be seen in Figure 79 and Figure 80 that although the actual values are different, the macro-mechanical performance increases with increasing aspect ratio at the same rate for non-flat fibres as for flat fibres. This indicates that it is possible that the fibre cross-sectional shape plays a role in macro-mechanical performance, as does the fibre aspect ratio.

4.9. Concluding Summary

The fibre dosage and type does not have an effect on the compressive strength of the concrete, possibly due to the low fibre dosages used.

The result variation is significantly less for the RDPT (on average 0.1) than for the three point beam bending test (on average 0.2). This can be attributed to the larger crack area of the RDPT. The result variation increases with increasing aggregate size. The RDPT notes this variation better than the three point beam bending test.

The macro-mechanical post-cracking performance parameters decrease with increasing aggregate size, due to non-uniform fibre dispersion resulting in weak zones for cracks to propagate.

The three point beam bending test indicated an increase in the $R_{e,3}$ value for an increase in W/C ratio, while the RDPT indicated a decrease in average energy absorption with an increase in W/C ratio. The increase in $R_{e,3}$ value can be attributed to the MOR decreasing significantly while the equivalent flexural tensile strength remains relatively constant. Thus, the $R_{e,3}$ value is not a good parameter with which to investigate the effect of the W/C ratio on SynFRC post-cracking performance.

The bond stress was unexpectedly inversely proportional to the macro-mechanical performance parameters. The controlling factors relating single fibre parameters to the macro-mechanical performance parameters appear to be the fibre shape (flat or non-flat) and the aspect ratio. Both of the flat fibres (Geotex 600 series and Chryso Structural) performed significantly better than the non-flat Rocstay and Geotex 500 series fibres.

The macro-mechanical test of choice is the RDPT, due to it being more consistent and identifying trends such as the effect of aggregate size on performance parameters which the three point beam bending test does not. In addition, the RDPT results are not misleading (such as for the three point beam bending test with increasing W/C ratios). If the three point beam bending test is to be used, then the $R_{e,3}$ value should perhaps be replaced by the third equivalent flexural tensile strength value if different W/C ratios are being considered, as the beam bending test post-cracking performance is not significantly and consistently affected by the changes in W/C ratio.

CHAPTER 5

Prediction Modelling

This chapter focuses on developing principles for the prediction of SynFRC performance parameters, from which a full guideline can be developed once a wider range of input parameters have been tested.

This is achieved by determining principles for how performance parameters, including compressive strength, first crack strengths and post-cracking load carrying ability and energy absorption are affected by the fibre dosage, single fibre properties, W/C ratio and aggregate size. These performance parameters are also correlated to each other.

For each principle, equations are developed based on the available data to demonstrate the use of the principle described.

5.1. Compressive Strength

Compressive strength is the most common concrete performance-based specification. Figure 52 shows the effect of fibre type and dosage on compressive strength. The crimped non-flat Geotex 500 series fibre displayed a slight increase in compressive strength with fibre dosage. However, the crimped non-flat Rocstay fibre did not display any consistent trend, nor did the flat fibrillated Geotex 600 series fibre. It can thus be said that for the fibres tested the fibre dosages, cross-sectional and longitudinal geometries did not affect the compressive strength.

Figure 81 shows the effect of aggregate size on compressive strength for the three W/C ratios which were tested.
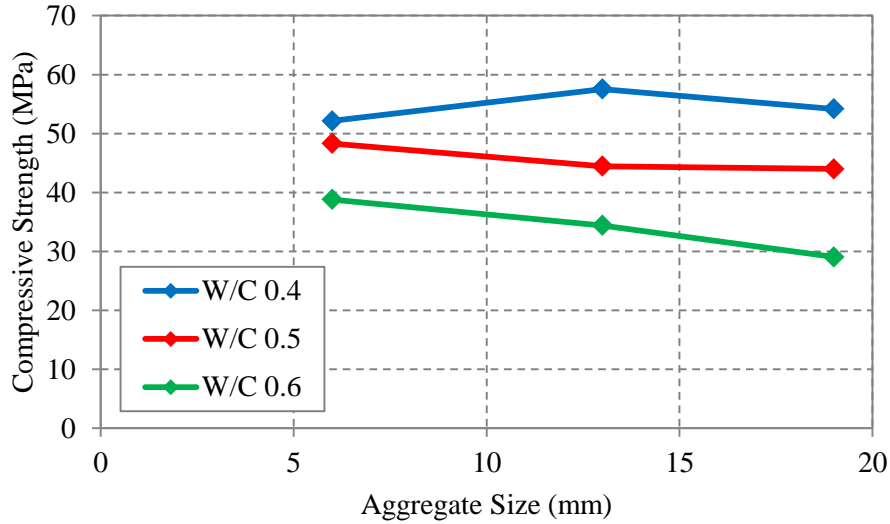
Figure 81: Effect of aggregate size on compressive strength for various W/C ratios

Figure 81 shows a general decrease in compressive strength with increasing aggregate size. The slight increase from 6 mm to 13 mm aggregate at the 0.4 W/C ratio can be attributed to experimental variation. The rate at which the compressive strength decreases with increasing aggregate size is indicated by the gradient of the lines between the data points. Table 29 details the average rate of decrease (A_1), measured in MPa per mm increase in aggregate size for each W/C ratio, as obtained from Figure 81. Note that the average rate of decrease for the 0.4 W/C ratio was determined between the 13 mm and 19 mm aggregate sizes.

Table 29: Rate of decrease of compressive strength according to W/C ratio

W/C ratio	0.4	0.5	0.6
A_1 (MPa per mm increase in aggregate size)	0.56	0.64	0.76

The rate of decrease A_1 can be described by a linear equation:

$$A_1 = 0.1528 + 1.0026 \times W/C \qquad [16]$$

The initial values for each W/C ratio at a 6 mm aggregate size can be determined from a second order polynomial as:

$$f_{cu,initial} = -283 \times (W/C)^2 + 216.4 \times (W/C) + 10.85 \qquad [17]$$

The compressive strength could then be predicted as:

$$f_{cu} = f_{cu,initial} - A_1 \times (Aggregate\ size - 6) \qquad [18]$$

87

Figure 82 shows the effect of W/C ratio on compressive strength for the three aggregate sizes which were tested. Figure 81 and Figure 82 were constructed from the same data, but in different contexts to demonstrate various methods of identifying trends.
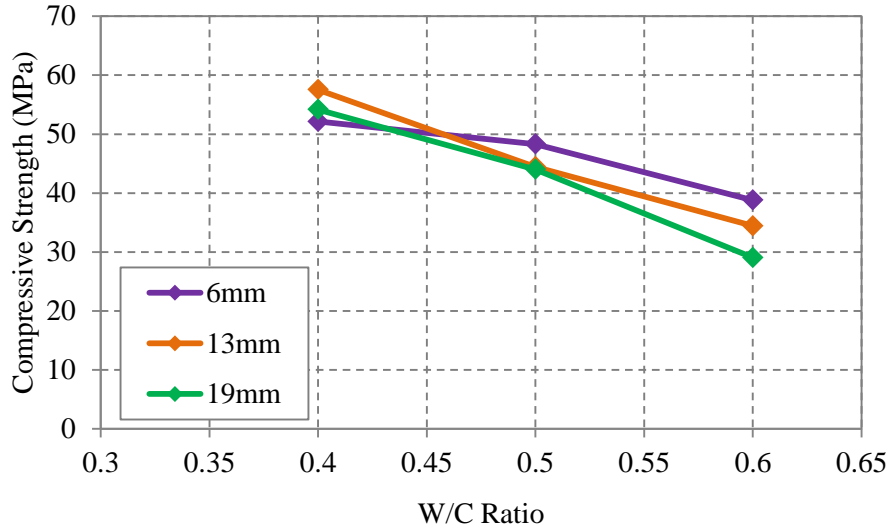
Figure 82: Effect of W/C ratio on compressive strength for various aggregate sizes

Figure 82 shows that the maximum compressive strength at the 0.4 W/C ratio over the three aggregate sizes has a range of less than 10 %, from 52 MPa (6 mm) to 57 MPa (13 mm), and shows no trend of increasing or decreasing with aggregate size. The compressive strength at a 0.4 W/C ratio can thus be conservatively said to be 53 MPa.

Figure 82 shows that the compressive strength decreases with increasing W/C ratio and that the average rate of compressive strength decrease increases with increasing aggregate size.

The average rate of compressive strength decrease (A_2), measured in MPa per 0.1 increase in W/C ratio is given in Table 30 for the three aggregate sizes.

Table 30: Rate of compressive strength decrease (A_2) per 0.1 increase in W/C ratio for various aggregate sizes

Aggregate Size (mm)	6	13	19
A_2 (MPa per 0.1 increase in W/C ratio)	6.66	11.56	12.56

Figure 83 shows the data of Table 30 graphically with a linear trend line describing the data.
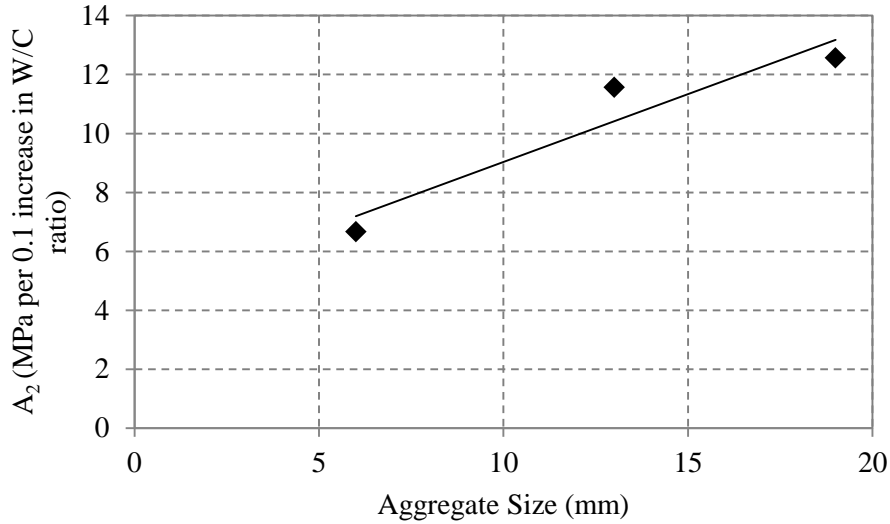
Figure 83: Rate of compressive strength decrease as a function of aggregate size

The rate of compressive strength decrease can be written as a function of aggregate size as:

$$A_2 = 0.4607 \times (Aggregate\ size) + 4.4275 \qquad [19]$$

The compressive strength can then be written as a function of aggregate size and W/C ratio as:

$$f_{cu} = 53 - 10 \times (W/C - 0.4) \times A_2 \qquad [20]$$

Both of the equations for compressive strength (Equations [18] and [20]) take into account that the compressive strength decreases with increasing W/C ratio. However, the second equation is more compact.

5.2. Compressive Strength and First Crack Strength Relations

The first crack strength is defined as the MOR (measured in MPa) for the three point beam bending test and as the peak load (measured in kN) for the RDPT.

Figure 57 and Figure 59 indicated that the fibre type and dosage had no effect on the first crack strengths at the fibre dosages tested.

5.2.1. MOR

The MOR was shown to decrease with increasing W/C ratio and aggregate size (Figure 64 and Figure 71), as did the compressive strength. Figure 84 plots the MOR as function of the compressive strength with a red line indicating a linear trend.

The red line of Figure 84 predicts the MOR as:

$$MOR = 0.0737 \times f_{cu} + 0.9051 \qquad [21]$$

with an R^2 value of 0.9217, indicating a strong correlation between the MOR and compressive strength over all aggregate sizes, W/C ratios and fibre types and dosages.
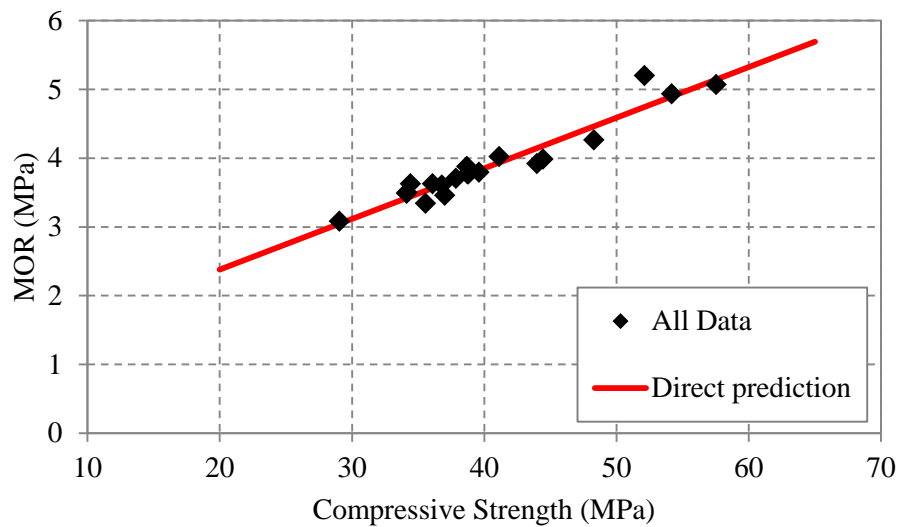
Figure 84: MOR and compressive strength relationship

5.2.2. Peak load

The RDPT peak load was shown to decrease with increasing aggregate size and W/C ratio (Figure 62 and Figure 69), as the compressive strength did.

Figure 85 shows that although the RDPT peak load increased with increasing compressive strength, the linear correlation was extremely poor with an R^2 value of 0.3293. In order to determine if particular factors were affecting the correlation between the peak load and compressive strength, the peak load was plotted against the compressive strength for each of the variable factors. Figure 86 shows the peak load as a function of compressive strength for the different fibres, without the W/C ratio and aggregate size variations.

Figure 86 shows a relatively horizontal spread of peak loads, ranging from 20.96 kN (Geotex 500 series fibres at a 0.6 % dosage) to 25.39 kN (Rocstay fibres at a 0.6 % dosage). The non-flat fibres (Rocstay and Geotex 500 series) occupy different ends of the spectrum, while the flat Chryso Structural and Geotex 600 series fibres are spread throughout the spectrum. The fibre dosage also has no influence on the spread of the data. As the peak load does not vary significantly or consistently with compressive strength, the fibre type does not affect the peak load-compressive strength relationship.

Figure 87 shows the relationship of compressive strength to peak load for various aggregate sizes.
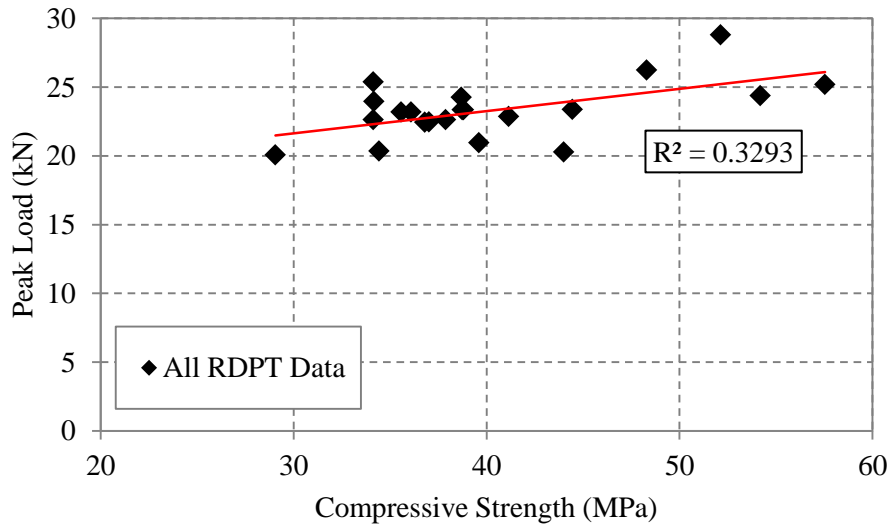
Figure 85: Peak load versus compressive strength for all RDPT data
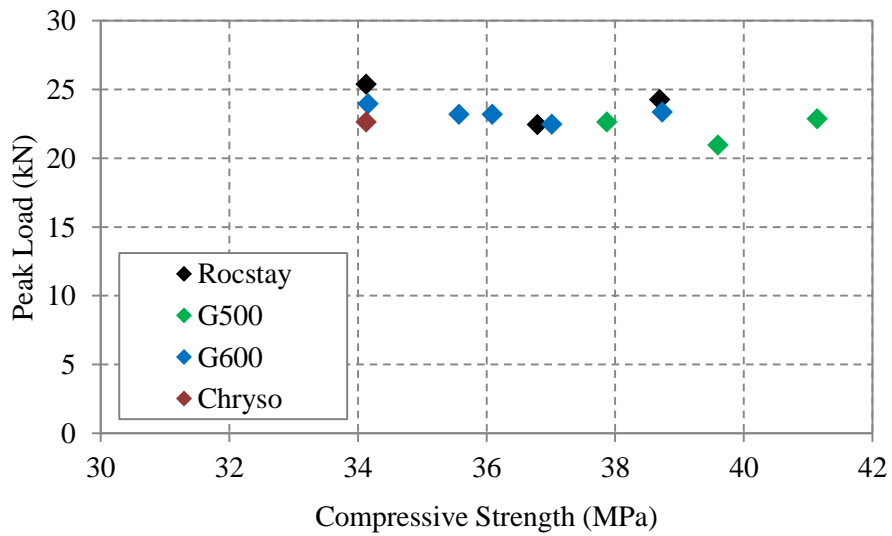
Figure 86: Peak load as a function of compressive strength for different fibres without the W/C ratio and aggregate size variations
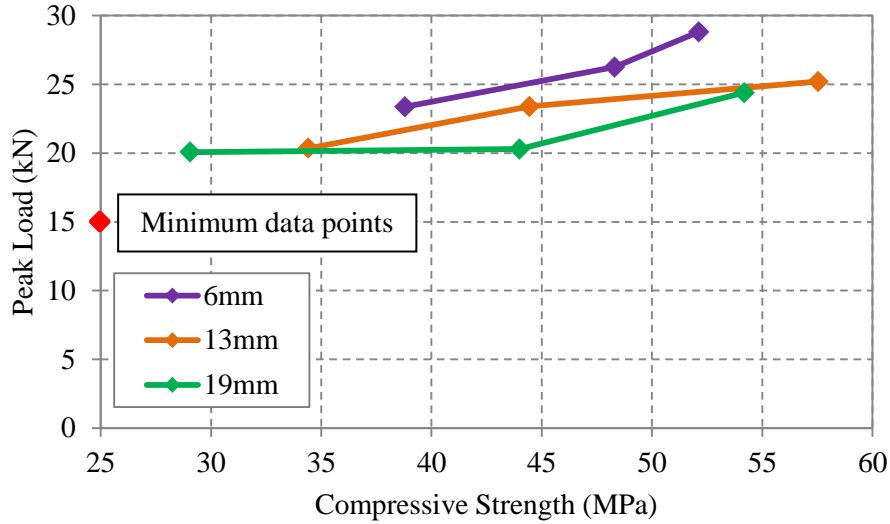
Figure 87: Peak load as a function of compressive strength for various aggregate sizes

The average rate of increase in peak load in relation to compressive strength (B), measured in $kN.MPa^{-1}$, is shown in Table 31 and Figure 88 for the various aggregate sizes. The average rate of increase of the peak load decreases with increasing aggregate size.

Table 31: Rate of increase in peak load for various aggregate sizes

Aggregate size (mm)	6	13	19
B $(kN.MPa^{-1})$	0.4082	0.2100	0.1718
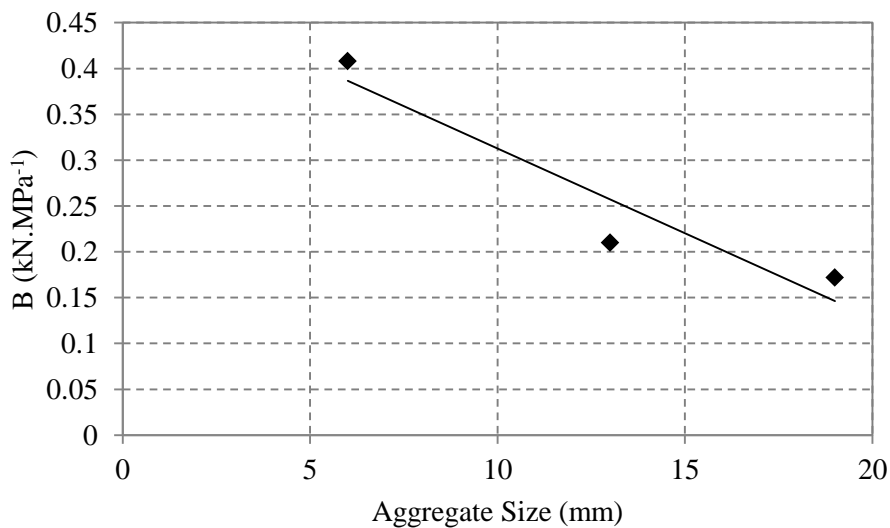
Figure 88: Rate of increase in peak load as a function of aggregate size

The rate of increase in peak load in relation to compressive strength, based on aggregate size, can be written as:

92

$$B = -0.0185 \times (Aggregate\ size) + 0.4972 \qquad\qquad [22]$$

Using the minimum data points of Figure 85, the peak load can be expressed as:

$$Peak\ Load = 18 + B \times (f_{cu} - 25) \qquad\qquad [23]$$

where the minimum compressive strength taken into consideration is 25 MPa.

5.3. Post-Cracking Performance Prediction

The post-cracking performance is measured by the average energy absorbed for the RDPT, and by the third equivalent flexural tensile strength ($f_{eq,3}$) and the third equivalent flexural tensile strength ratio ($R_{e,3}$ value) for the three point beam bending test.

5.3.1. Average energy absorbed prediction

Figure 58 shows the effect of fibre dosage on the average energy absorbed. The average energy absorbed increased with increasing fibre dosage, decreased with increasing bond stress (Figure 74), and increased with increasing equivalent diameter (Figure 76). In addition, the Geotex 600 series fibre energy absorption increases at a faster rate than both the Geotex 500 series and Rocstay fibres. Table 32 details the various fibres' rates of increase in energy absorbed (C), measured in Joules per 0.1 % increase in fibre dosage, along with various single fibre properties which could possibly affect the rate of energy absorption increase.

Table 32: Rate of increase in energy absorbed in comparison to single fibre parameters

Fibre	Rocstay	Geotex 500 series	Geotex 600 series
C (J per 0.1% increase in fibre dosage)	21.6	28.45	47.72
Bond stress (MPa)	1.94	1.69	0.62
Equivalent diameter (mm)	0.701	0.760	0.907
Aspect ratio	42.8	65.8	55.1

From Table 32 it can be seen that the rate of increase in energy absorption with increasing fibre dosage is inversely proportional to the bond stress (Figure 89) and directly proportional to the equivalent diameter (Figure 90). There is no relation between C and the aspect ratio.

The rate of increase in energy absorption is related to the bond stress by:

$$C = -17.71 \times \tau + 57.039 \qquad\qquad [24]$$
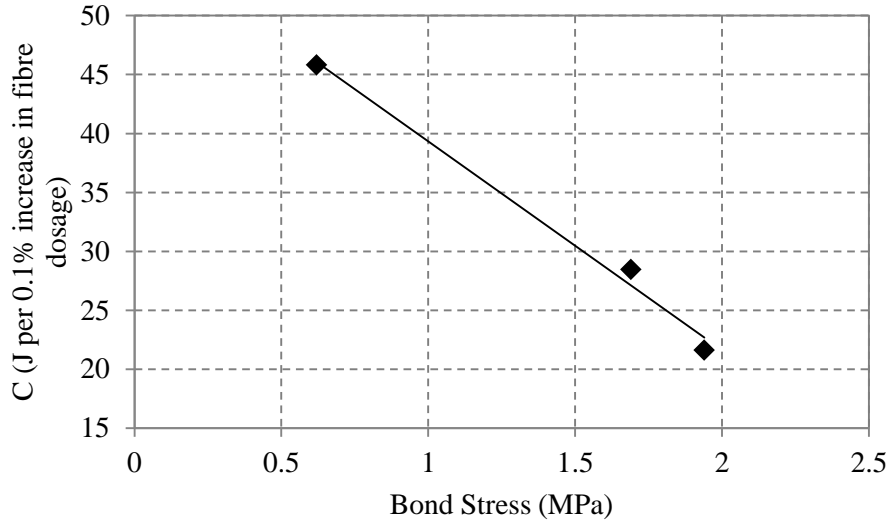
Figure 89: Rate of increase in energy absorption as a function of the bond stress
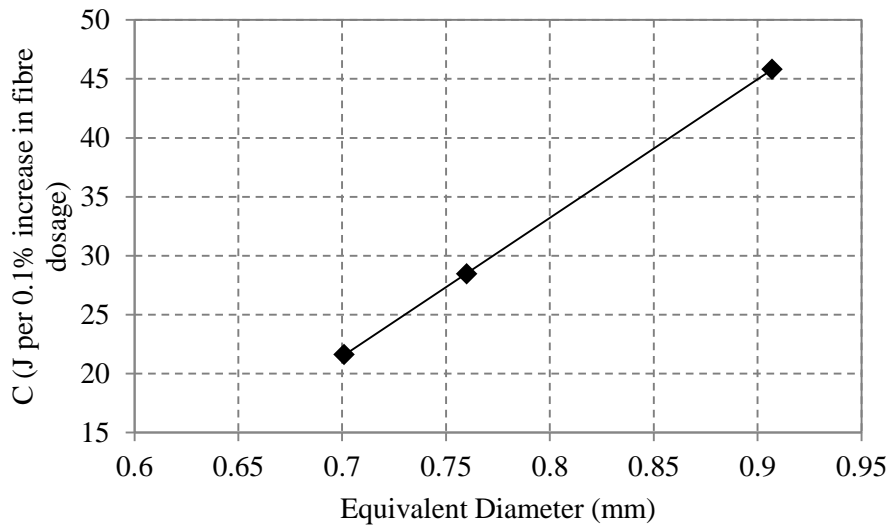
Figure 90: Rate of increase in energy absorption as a function of the equivalent diameter

The rate of energy absorption increase is related to the equivalent diameter by:

$$C = 117.62 \times d_e - 60.892 \qquad\qquad [25]$$

The effect of increasing the W/C ratio is shown in Figure 70 for each aggregate size. The average energy absorbed decreases with an increasing W/C ratio. The rate at which the energy absorption decreases from a W/C ratio of 0.4 to a W/C ratio of 0.6 (D), measured in Joules per 0.1 increase in W/C ratio, decreases with increasing aggregate size and is shown in Table 33 and graphically in Figure 91.

94

Table 33: Rate of decrease in energy absorbed per 0.1 increase in W/C ratio for various aggregate sizes

Aggregate size (mm)	6	13	19
D (J per 0.1 increase in W/C ratio)	36.09	25.21	22.61
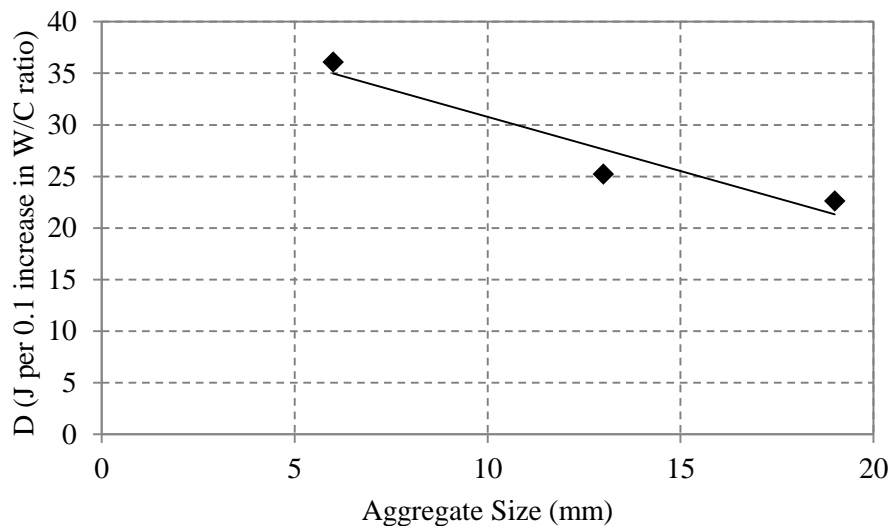
Figure 91: Rate of decrease in energy absorbed per 0.1 W/C ratio increase for various aggregate sizes

The adjustment factor can be quantified as D:

$$D = -1.0518 \times (Aggregate\ size) + 41.292 \qquad [26]$$

with a minimum aggregate size of 6 mm.

From Figure 58, with a minimum fibre dosage 0.3 % and energy absorption of 124 J, the energy absorption can then be predicted based on fibre dosage, single fibre properties (bond stress or equivalent diameter), aggregate size and W/C ratio as:

$$W = 124 + C \times (Fibre\ dosage\ \%) + D \times (0.6 - W/C) \times 10 \qquad [27]$$

5.3.2. Equivalent flexural tensile strength prediction

The equivalent tensile strength results tended to have a higher result scatter than the RDPT. Thus where there are uncertainties in the bending test results, RDPT results were used as reference. For example, if the RDPT test indicated a decreasing trend, and a beam bending test indicated a decrease and then a slight increase, then the decreasing trend was assumed to be the true trend, and the increase was assumed to be due to experimental variation.

95

Figure 60 shows that the equivalent flexural tensile strength generally increases with increasing fibre dosage. The Rocstay fibre initially increases gradually (0.0087 MPa from a 0.5 % dosage to 0.6 % dosage), and then increased sharply to 1.52 MPa. This large jump is unexpected and does not coincide with the gradual increase from the RDPT. The Geotex 500 series and Geotex 600 series fibres displayed similar behaviour to the RDPT in the sense that the Geotex 600 series fibres performance increased at a faster rate than the Geotex 500 series fibres.

The rate of equivalent flexural tensile strengths increases (E), measured in MPa per 0.1 % increase in fibre dosage is shown in Table 34.

Table 34: Rates of increase in equivalent flexural tensile strength per 0.1 % increase in fibre dosage

Fibre	Rocstay	Geotex 500 series	Geotex 600 series
E (MPa per 0.1% increase in fibre dosage)	0.00877	0.10275	0.22

The rate of equivalent flexural tensile strength increase decreases with increasing bond stress (Figure 92) and increases with increasing equivalent diameter (Figure 93).
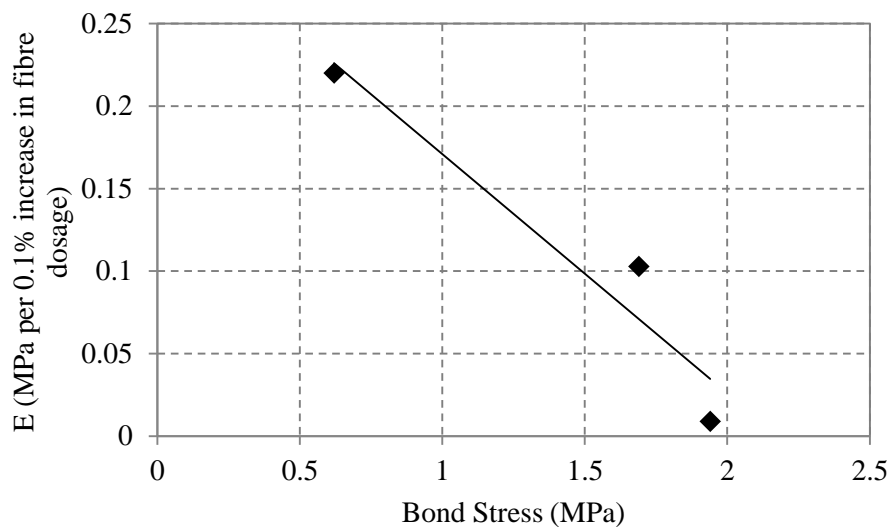
Figure 92: Rate of increase of equivalent flexural tensile strength in relation to bond stress

The rate of equivalent flexural tensile strength increase can be written as a function of the bond stress as:

$$E = -0.145 \times \tau + 0.3159 \qquad [28]$$

The rate of equivalent flexural tensile strength decrease is related to the equivalent diameter by:

$$E = 0.9818 \times d_e - 0.6644 \qquad [29]$$

96
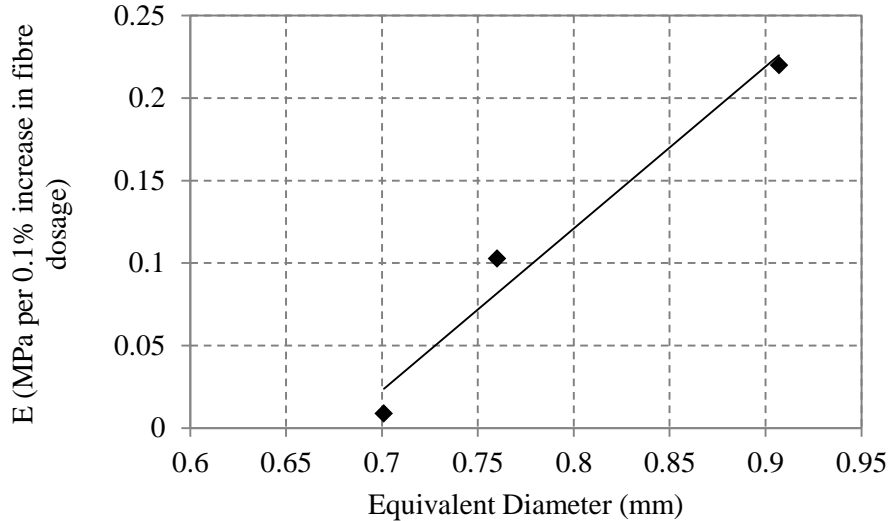
Figure 93: Rate of increase of equivalent flexural tensile strength in relation to equivalent diameter

The equivalent flexural tensile strength decreases with increasing W/C ratio (Figure 72). Although the equivalent flexural tensile strength increased between the 0.5 and 0.6 W/C ratios for the 6 mm aggregate, and also between the 0.4 and 0.5 W/C ratios for the 13 mm aggregate, the other four gradients indicated a decrease, as expected from the RDPT results. The average rate of decrease in equivalent flexural tensile strength per 0.1 increase in W/C ratio (F), measured in MPa per 0.1 increase in W/C ratio, was 0.12 MPa per 0.1 increase in W/C ratio, and can be written as:

$$F = 0.12 \times 10 \times (0.6 - W/C) = 0.72 - 1.2 \times W/C \qquad [30]$$

Using the data from Figure 60, and assuming a minimum equivalent flexural tensile strength of 0.75 MPa at a fibre dosage of 0.3 %, the equivalent flexural tensile strength can then be written as a function of fibre dosage, single fibre properties and W/C ratio as:

$$f_{eq,3} = 0.75 + E \times (Fibre\ dosage\ \%) + F \qquad [31]$$

Further testing may reveal a relation between aggregate size and the rate of the factor F.

5.3.3. $R_{e,3}$ value

The $R_{e,3}$ value decreases with lower W/C ratio. This is often misleading, as the MOR decreases significantly with an increase in W/C ratio, while the equivalent flexural tensile strength remains the relatively constant. The $R_{e,3}$ value is therefore not a useful parameter for comparing different W/C ratios, and if needed should simply be determined by dividing the equivalent flexural tensile strength by the MOR.

5.4. Relating RDPT and Three Point Beam Bending Test Parameters

The relationship between the MOR and the peak load is shown is Figure 94. The first crack strength

parameters are both related to the compressive strength. The peak load can thus be written as a function of the MOR by re-arranging Equations [21] and [23]:

$$Peak\ Load = 18 + B \times (13.57 \times MOR - 37.3)$$ [32]
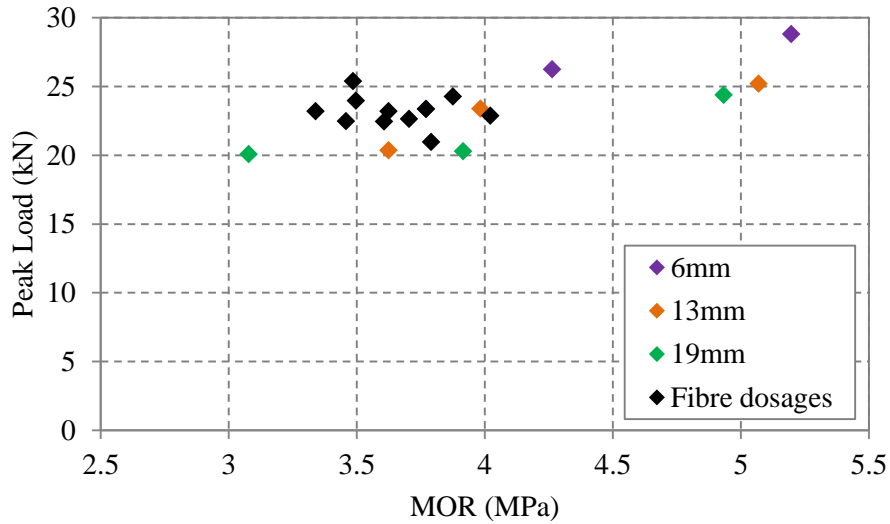
Figure 94: Peak load and MOR relation

The fibre dosage data of Figure 95 follows a linear pattern, but without strong correlation. The three point beam bending test's equivalent flexural tensile strength and RDPT's average energy absorbed both depend on fibre dosage, fibre bond stress and fibre equivalent diameter. The average energy absorbed depends on both aggregate size and W/C ratio, while the equivalent flexural tensile strength depends only on W/C ratio (from the available data).
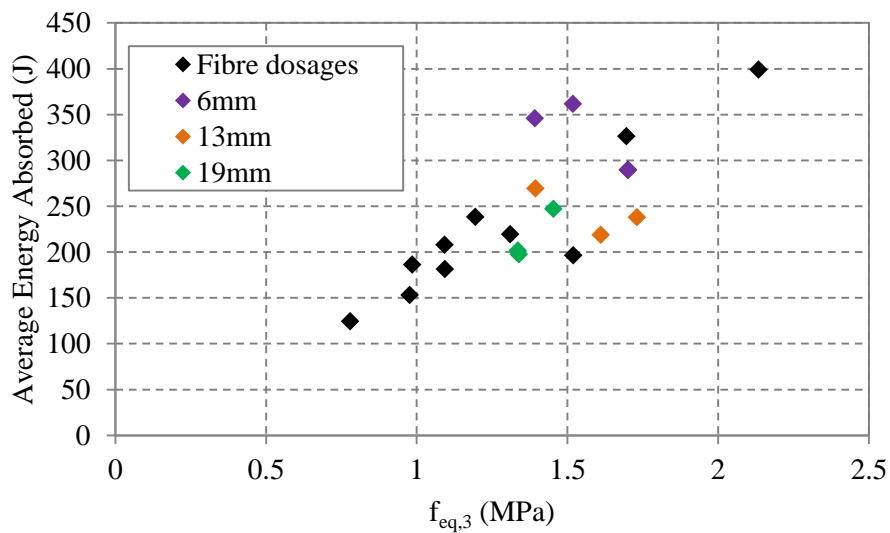
Figure 95: Equivalent flexural tensile strength and energy absorbed relation

5.5. Concluding Summary

The following sections summarise the observed trends in performance parameters, as well as the equations derived from the available data to describe the trends. Note that the equations developed are only for the fibres used, the fibre dosages used, the specific cement used, the W/C ratios and aggregate sizes tested.

5.5.1. Compressive strength

Compressive strength is unaffected by fibre properties, and is a function of only the W/C ratio and aggregate size. The rate at which compressive strength decreases with increasing W/C ratio is proportionate to the aggregate size.

5.5.2. First crack strength

The MOR was unaffected by the fibre properties, and affected by changes in W/C ratio and aggregate size in a manner similar to the compressive strength. The MOR was found to have a linear relation with the compressive strength.

The peak strength of the RDPT test was unaffected by the fibre properties. The RDPT peak strength increased with increasing compressive strength, but at a faster rate for the smaller aggregate sizes.

The MOR and RDPT peak strength can be related by:

$$Peak\ Load = 18 + B \times (13.57 \times MOR - 37.3) \tag{33}$$

The fibre content has no significant effect on the relationship between the peak load and the MOR. However, the relationship is affected by aggregate size. This is incorporated with the factor B, which indicates that the smaller aggregate sizes have a faster increase in peak load than larger aggregate sizes.

5.5.3. Average energy absorption

The average energy absorption of the RDPT increased with increasing fibre dosage. The rate of increase per 0.1 % increase in fibre dosage proved to be inversely proportional to the bond stress, and directly proportional to the equivalent diameter.

Average energy absorption also increases with decreasing W/C ratio. The rate of energy absorption increase is also proportional to the aggregate size.

5.5.4. Equivalent flexural tensile stress

The equivalent flexural tensile strength increased with increasing fibre dosage, and was found to also be inversely proportional to the bond stress and proportional to the equivalent diameter, as for the energy absorbed. An increase in W/C ratio resulted in a slight decrease in equivalent flexural tensile strength. The effect of aggregate size could not be determined.

99

5.5.5. Example guideline

Table 35, Table 36, Table 37 and Table 38 summarise the factors discussed in the previous sections, with values for typical input.

Table 35: Factors affected by W/C ratio

Factor	Equation	W/C = 0.4	W/C = 0.5	W/C = 0.6
A_1	[16]	0.554	0.654	0.754
$f_{cu,\ initial}$	[17]	52	48	39
F	[30]	0.24	0.12	0

Table 36: Factors affected by aggregate size

Factor	Equation	6 mm	13 mm	19 mm	26 mm
A_2	[19]	7.2	10.4	13.2	16.4
B	[22]	0.386	0.257	0.146	0.016
D	[26]	35.0	27.6	21.3	13.9

Table 37: Factors affected by bond stress

Factor	Equation	Bond stress (MPa)							
		0.5	0.6	0.7	0.8	0.9	1	1.1	1.2
C	[24]	48.184	46.413	44.642	42.871	41.1	39.329	37.558	35.787
E	[28]	0.2434	0.2289	0.2144	0.1999	0.1854	0.1709	0.1564	0.1419

Table 38: Factors affected by equivalent diameter

Factor	Equation	Equivalent diameter (mm)				
		0.6	0.7	0.8	0.9	1
C	[25]	9.68	21.44	33.20	44.97	56.73
E	[29]	0.2289	0.2144	0.1999	0.1854	0.1709

Table 39 summarises the equations developed in this chapter. The values in Table 35, Table 36, Table 37 and Table 38 can be used to predict fibre performance.

Table 39: Summary of equations for the prediction of SynFRC performance parameters

Performance parameter	Equation number	Equation
Compressive strength (MPa)	[18]	$f_{cu} = f_{cu,initial} - A_1 \times (Aggregate\ size - 6)$
Compressive strength (MPa)	[20]	$f_{cu} = 53 - A_2 \times 10 \times (W/C - 0.4)$
MOR (MPa)	[21]	$MOR = 0.0737 f_{cu} + 0.9051$
Peak load (kN)	[23]	$Peak\ Load = 18 + B \times (f_{cu} - 25)$
Average energy absorbed (J)	[27]	$W = 124 + C \times (Fibre\ dosage\ \%) + D \times (0.6 - W/C) \times 10$
Equivalent flexural tensile strength (MPa)	[31]	$f_{eq,3} = 0.75 + E \times (Fibre\ dosage\ \%) + F$

CHAPTER 6

Conclusions and Future Prospects

The purpose of this research was to increase the confidence in SynFRC in South Africa by testing locally available fibres on international test setups and quantifying the performance of the fibres and the reliability of the test setups. The fibre performance was first quantified on a single fibre level in terms of the bond stress using a single fibre pull-out test setup. The fibres were then tested on a macro-mechanical level using the BS EN 14651 (2007) three point beam bending test setup and the ASTM 1550 (2012) RDPT setup. The single fibre pull-out results and the macro-mechanical behaviour were then compared. The results did not link as expected, but were consistent for untreated fibres. The trends for the macro-mechanical tests with regards to fibre type and dosage, W/C ratio and aggregate size were then described in a guideline which can be further developed.

6.1. Single Fibre Behaviour

The single fibre behaviour was quantified by varying the W/C ratio between 0.4, 0.5 and 0.6 as well as the fibre embedment lengths. Varying the W/C ratio had no significant or consistent effect on the non-flat crimped fibres. The flat fibre without a surface treatment tended to perform slightly better at the 0.4 W/C ratio than at the 0.5 and 0.6 W/C ratios, although not in a consistent manner. The samples at the 0.5 W/C ratio did not consistently perform better than the samples at the 0.6 W/C ratio. The W/C ratio does therefore not significantly affect the fibre bond stress of untreated fibres at the W/C ratios tested. The surface treated flat fibre did however show consistent performance improvements at lower W/C ratios.

Fibre geometry and shape significantly affected the bond stress. The crimped, X-shaped fibre (Rocstay) had the highest bond stress of 1.94 MPa. The crimped oval shaped fibre (Geotex 500 series) had the second highest bond stress of 1.69 MPa. The flat surface treated fibre (Chryso Structural) had a bond stress of 1.66 MPa, while the flat untreated fibre (Geotex 600 series) had the lowest bond stress of 0.62 MPa. From the single fibre pull-out variations, the highest bond stress would be obtained with a crimped X-shaped fibre with a surface treatment. In addition, the fibre bond stress increases with increasing fibre diameter for non-surface treated fibres.

The fibre snubbing effect was noticeable for flat fibres, even causing majority fibre fracture for the flat surface treated fibre. The snubbing effect was evident but not consistent for the non-flat crimped fibres. This may be due to the axis of orientation not being controllable.

The results of the single fibre pull-out experiments showed that there appear to be different bonding mechanisms for flat fibres than for non-flat fibres. Flat fibres seem to have a more uniform bond stress, while crimped fibres seem to have a large interlock at the fibre end near the surface where debonding begins. As the fibre bond stress was not uniform, the bond stress was selected as the average value at the embedment length of half the fibre length. This value was used as majority fibre fracture occurred at the next embedment length, while the value at the first embedment length was uncharacteristically high for the crimped fibres.

6.2. Performance Measurement Test Choice

Two macro-mechanical tests were used during the experiments, the BS EN 14651 (2007) three point beam bending test setup and the ASTM C1550 (2012) RDPT setup.

The RDPT yields more consistent results than the three point beam bending test, with an average COV of 0.1 versus 0.2. This can be attributed to the significantly larger crack area of the RDPT. The COV also increases with increasing aggregate size due to less uniform fibre dispersion. In addition, the RDPT notes variation in performance with aggregate size, which the three point beam bending test does not.

The results of the three point beam bending test can also be misleading, as increasing the W/C ratio results in an increase in the $R_{e,3}$ value, even though the equivalent flexural tensile strength remains relatively constant. Thus, if the three point beam bending test must be used, the equivalent flexural tensile strength is a better performance parameter than the $R_{e,3}$ value.

6.3. Macro-Mechanical Performance

The macro-performance of SynFRC was determined by varying the fibre type and dosage, W/C ratio and aggregate size on the RDPT and three point beam bending test setup.

The fibre dosage does not have any effect on the compressive strength, MOR or RDPT peak load at the dosages used. The MOR and peak load decreased with increasing W/C ratio and increasing aggregate size.

The average energy absorbed decreased with increasing aggregate size and with increasing W/C ratio. Although the equivalent flexural tensile strength did generally decrease with increasing aggregate size and W/C ratio, the higher variability of the three point beam bending test resulted in anomalies.

The macro-performance was shown to decrease with increasing bond stress, and increase with increasing equivalent diameter and aspect ratio. However, for a set volume of fibres, a larger equivalent diameter implies fewer fibres. The decrease in performance with higher bond stress and fewer fibres was unexpected. The flat fibres had the best performance, while the crimped fibres were less impressive. This implies that the controlling factor in macro-performance may be fibre shape and the aspect ratio, as opposed to the fibre bond stress and equivalent diameter.

Overall, it was shown that the macro-synthetic fibres used in this study did increase the post-cracking performance with increases in fibre dosage. When compared to other studies which involved steel fibres and other synthetic fibres, such as Bernard (2002) and Buratti et al.(2011), it can be seen that the synthetic fibres used in this research do not necessarily perform on the same level as steel fibres from other research. However, the indication that certain single fibre properties may affect the macro-performance provides the stepping stone to adjust the single fibre parameters fibres in order to maximise the macro-performance.

6.4. Performance Based Specification for SynFRC

The effects of the fibre type, fibre dosage, W/C ratio and aggregate size on the pre-cracking performance parameters and post-cracking performance parameters were determined and compiled into basic principles.

The rate of macro-performance increase with fibre dosage was dependent on the bond stress and the fibre equivalent diameter, and the rates of performance decrease with increasing aggregate size and W/C ratio tend to depend on the aggregate size.

From the available data, the energy absorbed was expressed as:

$$W = 124 + C \times (Fibre\ dosage\ \%) + D \times (0.6 - W/C) \times 10 \hspace{3cm} [34]$$

and the equivalent flexural tensile strength as:

$$f_{eq,3} = 0.75 + E \times (Fibre\ dosage\ \%) + F \hspace{4cm} [35]$$

where C and E are factors depending on the fibre bond stress and equivalent diameter, D depends on the aggregate size and F on the W/C ratio.

6.5. Future Prospects

The following may be investigated further to expand the results obtained in this research:

- The model used to determine the bond stress in this study was for a uniform bond stress. It appeared that the bond stress distribution of flat fibres was different to that of crimped non-flat fibres, and neither of these was uniform. Thus, the bond stress distribution of flat versus non-flat fibres needs further investigation.

- The bond stress of the flat surface treated fibre was significantly higher than the bond stress of the flat non-treated fibre. The surface treatment appeared to make the flat fibre equivalent to crimped non-flat fibres in terms of bond stress. However, this could simply be an anomaly. The bond stresses of non-treated flat and non-flat fibres should be compared to that of the same fibres with surface treatment to determine the extent to which surface treatment affects bond stress.

- Further macro-mechanical tests should be performed at a wider range of W/C ratios, aggregate sizes, fibre dosages and types. This would provide more data to improve the prediction model, as well as a value of fibre dosage at which the performance no longer improves.

- The macro-mechanical tests showed that the flat surface treated fibre had the potential to be the best fibre. However, not enough tests could be performed. Macro-mechanical tests should be performed on surface treated flat and non-flat fibres with the same equivalent diameters and aspect ratios as untreated flat and non-flat fibres. This will aid in determining if the fibre shape is indeed the most important factor in macro-mechanical performance, and if the bond stress is actually inversely proportional to macro-mechanical performance.

- As indicated in Section 4.5.5 and Section 4.5.6, a higher post-cracking performance was obtained in the RDPT for the lower W/C ratios and smaller aggregate sizes at the same fibre dosages. An economic analysis should be performed to determine whether it is viable to use higher fibre dosages or to decrease the W/C ratio or aggregate size to improve post-cracking performance properties.

- Finally, the consistency of the fibres supplied should be investigated. A study in terms of quality assurance should be conducted where all of the fibres used in this study are tested in terms of strength, length and equivalent diameter to ascertain the level of variation, as this could affect future results.

105

CHAPTER 7
References

ACI Committee 544, 1996. *State-of-the-Art Report on Fiber Reinforced Concrete*. Review. Farmington Hills: American Concrete Institute American Concrete Institute.

ACI, 2013. *ACI Concrete Terminology*. ACI Standard. Farmington Hills: American Concrete Institute American Concrete Institute.

ASTM A820, 2011. *Standard Specification for Steel Fibers for Fiber-Reinforced Concrete*. ASTM Standard. West Conshohocken Pennsylvania: ASTM International.

ASTM C1018, 1997. *Standard Test Method for Flexural Toughness and First Crack Strength of Fiber-Reinforced Concrete (Using Beam With Third Point Loading)*. Withdrawn ASTM Standard. West Conshohocken Pennsylvani: ASTM International.

ASTM C1399, 2010. *Standard Test Method for Obtaining Average Residual-Strength of Fiber-Reinforced Concrete*. ASTM Standard. West Conshohocken Pennsylvania: ASTM International.

ASTM C1550, 2012. *Standard Test Method for Flexural Toughness of Fiber Reinforced Concrete (Using Centrally Loaded Round Panel)*. ASTM Standard. West Conshohocken Pennsylvania: ASTM International.

ASTM C1609, 2012. *Standard Test Method for Flexural Performance of Fiber-Reinforced Concrete (Using Beam With Third-Point Loading)*. ASTM Standard. West Conshohocken Pennsylvania: ASTM International.

ASTM C78, 2010. *Standard Test Method for Flexural Strength of Concrete (Using Simple Beam with Third-Point Loading)*. ASTM Standard. West Conshohocken Pennsylvania: ASTM International.

Barr, B.I.G., Hasso, E.B.D. & Weiss , V.J., 1986. Effect of specimen and aggregate sizes upon the fracture characteristics of concrete. *The International Journal of Cement Composites and Lightweight Concrete*, 8(2), pp.109-19.

Beaudoin, J., 1990. *Handbook of Fiber-Reinforced Concrete. Principles, Properties, Developments and Applications*. New Jersey: Noyes Publications.

Bernard, E.S., 2002. Correlations in the behaviour of fibre reinforced shotcrete beam and panel specimens. *Materials and Structures*, 35, pp.156-64.

Brandt, A.M., 2009. *Cement-based composites*. 2nd ed. CRC Press.

British Standards Institute, 2006. *BS EN 14889 Part 1. Fibres for concrete - Steel fibres - Definitions, specifications and conformity*. British Standard. London: British Standards Institute British Standards Institute.

British Standards Institute, 2006. *BS EN 14889 Part 2. Fibres for concrete - Polymer fibres - Definitions, specifications and conformity*. British Standard. London: British Standards Institute British Standards Institute.

British Standards Institute, 2007. *BS EN 14651: Test Method for Metallic Fibre Concrete - Measuring the Flexural Tensile Strength*. Standard. London: British Standards Institute.

Buratti, N., Mazzotti, C. & Savoia, M., 2011. Post-cracking behaviour of steel and macro-synthetic fibre-reinforced concretes. *Construction and Building Materials*, 25, pp.2713-22.

Cengiz, O. & Turanli, L., 2004. Comparative evaluation of steel mesh, steel fibre and high-performance polypropylene fibre-reinforced shotcrete in panel test. *Cement and Concrete Research*, 34, pp.1357-64.

Chao, S.-H. et al., 2011. FRC performance comparison: uniaxial direct tensile test, third-point bending test and round panel test. *SP-276. Durability Enhancements in Concrete with Fiber Reinforcement*, 276, pp.1-20.

Concrete Society, 2003. *Technical Report 34 - Concrete Industrial Ground Floors*. 3rd ed. Berkshire: The Concrete Society.

Concrete Society, 2007. *Technical Report No. 63 - Guidance for the Design of Steel-Fibre-Reinforced Concrete*. London: The Concrete Society.

EFNARC, 1996. *European specification for sprayed concrete*. Standard. Aldershot: EFNARC EFNARC.

ERMCO, 2012. *Guidance to fibre concrete - Properties, specification and practice in Europe*. Brochure. European Ready Mixed Concrete Organization.

Hannant, D.J., 1978. *Fibre Cements and Fibre Concretes*. Chichester: John Wiley & Sons, Ltd.

Hannant, D.J., 1998. Durability of polypropylene fibers in Portland-cement based composites: 18 years of data. *Cement and Concrete Research*, 28(12), pp.1809-17.

Hannant, D.J., 2002. Fibres in concrete - a perspective. *Concrete*, 36(8), p.40.

Hathaway, B., 2007. A comparison of macro-synthetic- and steel-fibre-reinforced concrete. *Concrete*, 41(9), pp.43-45.

Illston, & Domone, P.L.J., eds., 2001. *Construction Materials*. 3rd ed. Oxon: Spon Press.

International Federation for Structural Concrete , 2012. *Model Code 2010 Final Draft Volume 1*. Lausanne: International Federation for Structural Concrete (fib).

Kellerman, J., 2009. Manufacture and handling of concrete. In G. Owens, ed. *Fulton's concrete technology*. 9th ed. Midrand: Cement and Concrete Institute. p.241.

Li, V.C., Chan, Y.-W. & Wu, H.-C., 1994. Interface Strengthening Mechanisms in Polymeric Fiber Reinforced Cementitious Composites. In Brandt, A.M., Li, V.C. & Marshall, I.H., eds. *Proc. Int. Symp. Brittle Matrix Composites*. Warsaw, 1994. IKE and Woodhead.

Lin, W.-L., 1992. Toughnes behaviour of fibre reinforced concrete. In Swamy, R.N., ed. *Fibre Reinforced Cement and Concrete. Proceedings of the Fourth RILEM International Symposium*. London, 1992. E & FN Spon.

Li, V.C., Wang, Y. & Backer, S., 1990. Effect of inclining angle, bundling and surface treatment on synthetic fibre pull-out from a cement matrix. *Composites*, 21(2), pp.132-40.

Mindess, S., Chen, L. & Morgan, D.R., 1994. Determination of the first-crack strength and flexural toughness of steel fiber-reinforced concrete. *Advanced Cement Based Materials*, 1(5), pp.201-08.

Nallathambi, P., Karihaloo, B.L. & Heaton, B.S., 1984. Effect of specimen and crack sizes, water/cement ratio and coarse aggregate texture upon fracture toughness of concrete. *Magazine of Concrete Research*, 36(129), pp.227-36.

NT Build 511, 2005. *Wedge Splitting Test Method (WST): Fracture testing of fibre-reinforced concrete (Mode 1)*. Standard Test Method. Norway: Nordon Nordic Innovation Centre.

Parmentier, B., De Grove, E., Vandewalle, L. & Van Rickstal, F., 2008. Dispersion of the mechanical properties of FRC investigated by different bending tests. In J.C. Walraven & D. Stoelhorst, eds. *Tailor Made Concrete Structures*. London: Taylor & Francis Group.

Richardson, A.E., 2005. Bond characteristics of structural polypropylene fibres in concrete with regard to post-crack strength and durable design. *Structural Survey*, 23(2/3), pp.210-30.

Richardson, A.E., 2006. Compressive strength of concrete with polypropylene fibre additions. *Structural Survey*, 24(2), pp.138-53.

SABS, 2012. *SANS 5863: Concrete Tests - Compressive Strength of Hardened Concrete*. South African Standard. Pretoria: South African Bureau of Standards (SABS) Standards Division SABS.

SANS 1083, 2006. *Aggregates from natural sources - Aggregates for concrete*. SABS Standard. Pretoria: Standards South Africa Standards South Africa.

SANS 5862-1, 2006. *Concrete tests - Consistence of freshly mixed concrete - Slump test*. SABS code. Pretoria: Standards South Africa Standards South Africa.

SANS 5864, 2006. *Concrete Tests - Flexural Strength of Hardened Concrete*. South African National Standard. Pretoria: SABS Standards Division SABS.

Singh, S., Shukla, A. & Brown, R., 2004. Pullout behaviour of polypropylene fibers from cementitious matrix. *Cement and Concrete Research*, 34, pp.1919-25.

Soutsos, M.N., Le, T.T. & Lampropoulos, A.P., 2012. Flexural performance of fibre reinforced concrete made with steel and synthetic fibres. *Construction and Building Materials*, 36, pp.704-10.

Vandewalle, L., Van Rickstal, F., Heirman, G. & Parmentier, B., 2008. The round panel test and the 3-point bending test. In *Proceedings of the 7th International RILEM Symposium on Fibre Reinforced Concrete: Design and Applications*. Chennai, 2008. RILEM Publications SARL.

Won, J.P., Lim, D.H. & Park, C.G., 2006. Bond behaviour and flexural performance of structural synthetic fibre-reinforced concrete. *Magazine of Concrete Research*, 58(6), pp.401-10.

Appendix A: Determination of Fibre Equivalent Diameters

The fibres' equivalent diameters were determined by weighing a set amount of fibres, and then assuming a circular cross section and determining the equivalent diameter using Equation [11], repeated here for convenience:

$$d_e = \sqrt{\frac{4000 m_f}{RD\pi l_d}}$$

Table 40 details the measurements taken for the normal length fibres. The individual fibres were measured to verify the group fibre measurements.

Table 40: Normal length fibre equivalent diameter and aspect ratio calculations

Rocstay CXO 50/30 SS			Length:		30 mm	
Individual			Groups			
Sample Number	Mass (g)	d_e (mm)	Number of fibres	Mass (g)	Length (mm)	d_e (mm)
1	0.0238	1.058	20	0.4294	600	1.006
2	0.0194	0.956	40	0.8454	1200	0.998
3	0.0197	0.964	50	1.0402	1500	0.990
4	0.0204	0.981	Average (groups):			0.998
5	0.0250	1.086	Average (individual):			1.017
6	0.0238	1.059	Aspect ratio (groups):			30.05
Geotex 500 series			Length:		50 mm	
Individual			Groups			
Sample Number	Mass (g)	d_e (mm)	Number of fibres	Mass (g)	Length (mm)	d_e (mm)
1	0.0196	0.745	20	0.4042	1000	0.756
2	0.0217	0.784	40	0.8203	2000	0.762
3	0.0223	0.794	50	1.0274	2500	0.762
4	0.0182	0.718	Average (groups):			0.760
5	0.0223	0.794	Average (individual):			0.767
			Aspect ratio (groups):			65.78

110

Table 40 continued:

Geotex 600 series			Length:		50 mm	
Individual			**Groups**			
Sample Number	Mass (g)	d_e (mm)	Number of fibres	Mass (g)	Length (mm)	d_e (mm)
1	0.0251	0.843	20	0.5785	1000	0.905
2	0.0313	0.941	40	1.1623	2000	0.907
3	0.0311	0.938	50	1.4599	2500	0.909
4	0.0310	0.937	**Average (individual):**			0.907
5	0.0297	0.917	**Average (groups):**			0.915
			Aspect ratio (groups):			55.14
Chryso Structural			**Length:**		50 mm	
Individual			**Groups**			
Sample Number	Mass (g)	d_e (mm)	Number of fibres	Mass (g)	Length (mm)	d_e (mm)
1	0.0120	0.583	20	0.2765	1000	0.622
2	0.0112	0.563	40	0.5387	2000	0.614
3	0.0135	0.618	50	0.6645	2500	0.610
4	0.0130	0.606	**Average (groups):**			0.615
5	0.0150	0.651	**Average (individual):**			0.604
			Aspect ratio (groups):			81.27

Table 41 details measurements taken and calculations made to determine the 100 mm (longer length) fibre equivalent diameters for the Rocstay and Geotex 500 series fibres.

Table 41: Longer length fibre equivalent diameter and aspect ratio calculations

Rocstay			Length:		100 mm	
Individual			**Groups**			
Sample Number	Mass (g)	d_e (mm)	Number of fibres	Mass (g)	Length (mm)	d_e (mm)
1	0.0361	0.715	5	0.1738	500	0.701
2	0.0387	0.740	10	0.3545	1000	0.708
3	0.0355	0.709	20	0.6930	2000	0.700
4	0.0283	0.633	**Average (groups):**			0.703
5	0.0346	0.700	**Average (individual):**			0.699
			Aspect ratio (groups):			42.66
Geotex 500 series			**Length:**		100 mm	
Individual			**Groups**			
Sample Number	Mass (g)	d_e (mm)	Number of fibres	Mass (g)	Length (mm)	d_e (mm)
1	0.039	0.743	5	0.2045	500	0.761
2	0.0459	0.806	10	0.4209	1000	0.772
3	0.0412	0.763	20	0.8344	2000	0.768
4	0.0381	0.734	**Average (groups):**			0.767
5	0.0425	0.775	**Average (individual):**			0.764
			Aspect ratio (groups):			65.20

Appendix B: Single Fibre Bond Stress and Pull-out Force Comparisons

Table 42 and Table 43 detail the average pull-out forces and bond stresses for all the fibre types at W/C ratios of 0.4, 0.5 and 0.6. Table 43 also details the standard deviation of each result set. The embedment lengths in brackets are for the Rocstay fibre.

Table 42: Average pull-out forces

W/C	Fibre Type	Embedment Length (mm)			
		12.5 (10)	25 (20)	37.5 (30)	50 (40)
0.4	Rocstay	73.95	139.25	232.15	136.46
	G500	67.51	96.70	150.53	94.25
	G600	32.42	54.35	62.39	107.31
	Chryso	61.64	88.37	108.19	111.17
0.5	Rocstay	85.94	140.08	174.83	134.92
	G500	73.70	108.18	147.61	110.36
	G600	21.99	38.72	60.57	99.39
	Chryso	49.15	79.70	105.95	88.98
0.6	Rocstay	91.72	169.22	211.58	122.66
	G500	71.18	96.61	146.18	126.02
	G600	31.49	43.87	65.87	102.56
	Chryso	50.99	77.40	108.93	122.93

Table 43: Detailed single fibre bond stress results

Rocstay	W/C = 0.4				
	Embedment Length	10 mm	20 mm	30 mm	40 mm
	Number of usable results	8	6	8	8
	Minimum (MPa)	1.67	1.96	2.04	1.52
	Maximum (MPa)	3.68	2.81	3.16	2.47
	Average (MPa)	2.51	2.44	2.51	2.07
	Standard deviation (MPa)	0.79	0.33	0.43	0.35
	COV	0.32	0.14	0.17	0.17
	Rocstay	0.96	1.79	1.66	1.38
	W/C = 0.5, Set 1				
		10 mm	20 mm	30 mm	40 mm
	Number of usable results	8	8	8	7
	Minimum (MPa)	1.69	1.52	1.51	1.54
	Maximum (MPa)	3.84	2.79	2.45	2.35
	Average (MPa)	2.56	2.30	1.90	2.05
	Standard deviation (MPa)	0.60	0.43	0.35	0.36
	COV	0.24	0.19	0.18	0.18
	95% Confidence value (MPa)	1.38	1.45	1.21	1.33
	W/C = 0.5, Set 2				
		10 mm	20 mm	30 mm	40 mm
	Number of usable results	8	7	8	7
	Minimum (MPa)	1.87	1.39	1.32	1.15
	Maximum (MPa)	4.74	2.87	1.91	1.76
	Average (MPa)	3.40	1.94	1.68	1.53
	Standard deviation (MPa)	0.90	0.48	0.20	0.27
	COV	0.27	0.25	0.12	0.18
	95% Confidence value (MPa)	1.63	0.99	1.30	1.00
	W/C = 0.6				
		10 mm	20 mm	30 mm	40 mm
	Number of usable results	8	8	8	7
	Minimum (MPa)	2.47	1.78	1.94	1.36
	Maximum (MPa)	3.77	3.10	2.49	2.16
	Average (MPa)	2.85	2.52	2.27	1.85
	Standard Deviation (MPa)	0.46	0.45	0.18	0.31
	COV	0.16	0.18	0.08	0.17
	95% Confidence value (MPa)	1.95	1.64	1.92	1.24

Table 43 continued:

		W/C = 0.4			
	Embedment Length	12.5 mm	25 mm	37.5 mm	50 mm
	Number of usable results	8	8	8	8
	Minimum (MPa)	1.39	1.40	1.22	0.63
	Maximum (MPa)	2.81	1.96	2.03	0.92
	Average (MPa)	2.05	1.61	1.64	0.80
	Standard deviation (MPa)	0.52	0.18	0.26	0.12
	COV	0.25	0.11	0.16	0.15
	95% Confidence value (MPa)	1.03	1.26	1.13	0.57
		W/C = 0.5			
		12.5 mm	25 mm	37.5 mm	50 mm
	Number of usable results	8	8	8	7
	Minimum (MPa)	1.70	0.99	1.33	0.65
Geotex 500 series	Maximum (MPa)	2.57	2.41	2.04	1.20
	Average (MPa)	2.14	1.79	1.59	0.92
	Standard deviation (MPa)	0.27	0.52	0.28	0.23
	COV	0.13	0.29	0.18	0.25
	95% Confidence value (MPa)	1.61	0.78	1.04	0.46
		W/C = 0.6			
		12.5 mm	25 mm	37.5 mm	50 mm
	Number of usable results	8	8	8	7
	Minimum (MPa)	1.45	1.25	0.98	0.47
	Maximum (MPa)	2.69	2.22	1.90	1.14
	Average (MPa)	2.15	1.66	1.54	0.91
	Standard Deviation (MPa)	0.42	0.32	0.32	0.27
	COV	0.20	0.20	0.21	0.30
	95% Confidence value (MPa)	1.33	1.02	0.91	0.38

Table 43 continued:

Geotex 600 series	W/C = 0.4				
	Embedment Length	12.5 mm	25 mm	37.5 mm	50 mm
	Number of usable results	8	8	8	8
	Minimum (MPa)	0.43	0.40	0.53	0.71
	Maximum (MPa)	1.07	1.28	0.62	0.91
	Average (MPa)	0.81	0.78	0.58	0.81
	Standard deviation (MPa)	0.23	0.27	0.03	0.07
	COV	0.29	0.35	0.06	0.09
	95% Confidence value (MPa)	0.35	0.24	0.51	0.67
	W/C = 0.5				
		12.5 mm	25 mm	37.5 mm	50 mm
	Number of usable results	8	8	8	7
	Minimum (MPa)	0.55	0.21	0.44	0.63
	Maximum (MPa)	1.02	0.67	0.73	0.93
	Average (MPa)	0.68	0.50	0.57	0.75
	Standard deviation (MPa)	0.16	0.13	0.11	0.09
	COV	0.23	0.26	0.18	0.12
	95% Confidence value (MPa)	0.37	0.24	0.36	0.58
	W/C = 0.6				
		12.5 mm	25 mm	37.5 mm	50 mm
	Number of usable results	8	8	8	7
	Minimum (MPa)	0.47	0.47	0.50	0.69
	Maximum (MPa)	0.87	0.72	0.93	0.81
	Average (MPa)	0.72	0.59	0.63	0.76
	Standard Deviation (MPa)	0.13	0.09	0.15	0.05
	COV	0.17	0.15	0.24	0.07
	95% Confidence value (MPa)	0.48	0.41	0.34	0.65

Table 43 continued:

		W/C = 0.4			
	Embedment Length	12.5 mm	25 mm	37.5 mm	45 mm
	Number of usable results	8	8	8	4
	Minimum (MPa)	1.59	1.42	1.15	1.22
	Maximum (MPa)	2.66	2.09	1.67	1.37
	Average (MPa)	2.15	1.70	1.49	1.30
	Standard deviation (MPa)	0.36	0.23	0.16	0.07
	COV	0.17	0.13	0.11	0.05
	95% Confidence value (MPa)	1.44	1.26	1.18	1.17
		W/C = 0.5			
		12.5 mm	25 mm	37.5 mm	45 mm
	Number of usable results	7.00	8.00	7.00	6.00
Chryso Structural	Minimum (MPa)	1.79	1.21	1.12	0.72
	Maximum (MPa)	2.46	2.18	1.66	1.29
	Average (MPa)	1.96	1.71	1.44	1.03
	Standard deviation (MPa)	0.24	0.31	0.20	0.20
	COV	0.12	0.18	0.14	0.20
	95% Confidence value (MPa)	1.49	1.10	1.05	0.63
		W/C = 0.6			
		12.5 mm	25 mm	37.5 mm	45 mm
	Number of usable results	7	8	8	7
	Minimum (MPa)	1.11	1.33	1.23	1.21
	Maximum (MPa)	2.18	1.85	1.69	1.63
	Average (MPa)	1.70	1.57	1.44	1.39
	Standard Deviation (MPa)	0.38	0.22	0.15	0.13
	COV	0.22	0.14	0.11	0.10
	95% Confidence value (MPa)	0.95	1.13	1.14	1.13

Appendix C: Single Fibre Compressive Strength Results,

Figure 96 shows the relationship between the cube density and compressive strength.
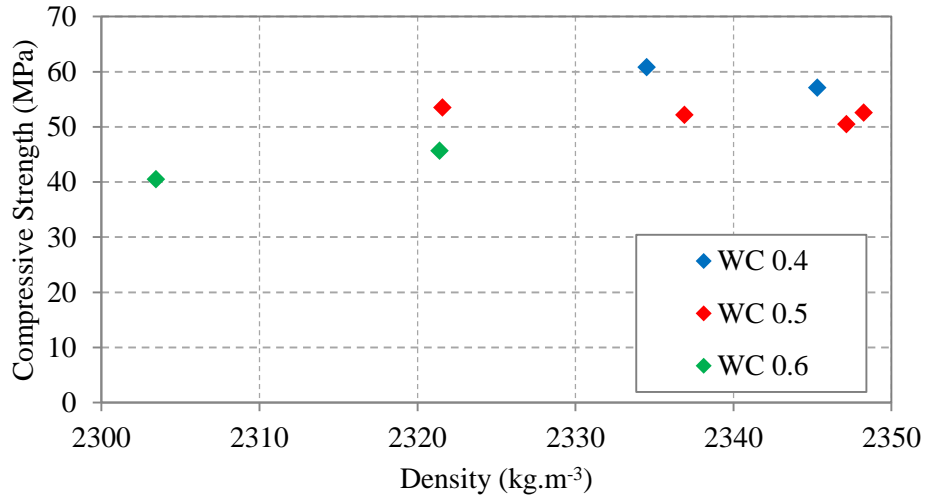
Figure 96: Single fibre pull-out mix designs density compared to compressive strength

Table 44 detail the compressive strength according to SANS 5863 (2012) of the single fibre pull-out mix designs.

The column "Validity Test" is a requirement in Clause 6 of SANS 5863 (2012). The sample is considered valid if the formula below is satisfied:

$$\frac{\sigma_{max} - \sigma_{min}}{\sigma_{average}} \times 100 \leq 15\%$$

Table 44: Single fibre pull-out tests compressive strength results

Cast: 22 August || Tested: 19 September || W/C: 0.4 || Purpose: 0.25L & 0.5L										
Cube	Dimension 1 (mm)	Dimension 2 (mm)	Mass (g)	Density (kg.m^{-3})	Force (kN)	Strength (MPa)	Average (MPa)	Standard Deviation (MPa)	Range (MPa)	Validity Test (%)
1	99.9	101.9	2357.0	2315.4	592.3	58.2	60.8	2.0	Minimum:	7.4
2	100.6	100.1	2348.0	2331.7	608.9	60.5			58.2	
3	101.6	99.8	2373.0	2340.3	635.7	62.7			Maximum:	
4	101.2	100.0	2379.0	2350.8	626.3	61.9			62.7	
Cast: 13 October || Tested: 10 November || W/C: 0.4 Purpose: 0.75L & 1L										
Cube	Dimension 1 (mm)	Dimension 2 (mm)	Mass (g)	Density (kg.m^{-3})	Force (kN)	Strength (MPa)	Average (MPa)	Standard Deviation (MPa)	Range (MPa)	Validity Test (%)
1	98.6	100.0	2328.3	2361.4	551.3	55.9	57.1	1.8	Minimum:	5.8
2	98.5	100.0	2311.7	2346.9	583.1	59.2			55.9	
3	100.3	100.0	2334.7	2327.7	564.4	56.3			Maximum:	
									59.2	

Table 44 continued:

Cube	Dimension 1 (mm)	Dimension 2 (mm)	Mass (g)	Density (kg.m^{-3})	Force (kN)	Strength (MPa)	Average (MPa)	Standard Deviation (MPa)	Range (MPa)		Validity Test (%)
Cast: 21 August || Tested: 18 September || W/C: 0.5 || Purpose: 0.25L & 0.5L											
1	100.9	99.5	2297.5	2288.4	524.0	52.2			Minimum:		
2	100.0	97.5	2280.5	2339.0	536.7	55.0	53.5	1.6	52.2		5.4
3	100.0	98.1	2293.3	2337.7	536.9	54.7			Maximum:		
4	100.2	97.6	2270.1	2321.3	510.3	52.2			55.0		
Cast: 12 October || Tested: 9 November || W/C: 0.5 || Purpose: 0.75L & 1L											
1	100.0	98.6	2337.5	2370.7	519.8	52.7			Minimum:		
2	100.8	100.2	2342.3	2319.1	513.2	50.8	50.5	1.9	48.0		9.3
3	99.9	97.6	2307.2	2366.3	468.0	48.0			Maximum:		
4	101.0	99.2	2337.1	2332.6	504.9	50.4			52.7		

120

Table 44 continued:

Cast: 12 October || Tested: 9 November || W/C: 0.5 || Purpose: Snubbing Effect										
Cube	Dimension 1 (mm)	Dimension 2 (mm)	Mass (g)	Density (kg.m^{-3})	Force (kN)	Strength (MPa)	Average (MPa)	Standard Deviation (MPa)	Range (MPa)	Validity Test (%)
1	96.0	101.0	2348.1	2421.7	514.4	53.1	52.2	0.7	Minimum:	3.2
2	98.9	103.0	2301.4	2259.2	532.3	52.3			51.4	
3	98.5	101.0	2334.6	2346.7	511.0	51.4			Maximum:	
4	99.7	100.0	2313.1	2320.1	519.8	52.1			53.1	
Cast: 6 August || Tested: 3 September || W/C: 0.5 || Purpose: Rocstay Set 2										
Cube	Dimension 1 (mm)	Dimension 2 (mm)	Mass (g)	Density (kg.m^{-3})	Force (kN)	Strength (MPa)	Average (MPa)	Standard Deviation (MPa)	Range (MPa)	Validity Test (%)
1	99.0	100.2	2334.4	2353.3	523.8	52.8	52.6	0.2	Minimum:	0.8
2	99.4	100.1	2336.2	2348.0	523.1	52.6			52.4	
3	99.3	100.0	2335.2	2351.7	522.5	52.6			Maximum:	
4	100.0	100.1	2342.5	2340.2	524.1	52.4			52.8	

121

Table 44 continued:

Cube	Dimension 1 (mm)	Dimension 2 (mm)	Mass (g)	Density (kg.m^{-3})	Force (kN)	Strength (MPa)	Average (MPa)	Standard Deviation (MPa)	Range (MPa)	Validity Test (%)
Cast: 10 October || Tested: 7 November || W/C: 0.6 || Purpose: 0.25L & 0.5L										
1	98.9	100.1	2291.0	2314.2	456.3	46.1	45.7	1.6	Minimum:	7.9
2	100.2	97.9	2278.4	2322.6	455.0	46.4			43.3	
3	100.1	100.3	2339.3	2330.0	434.9	43.3			Maximum:	
4	98.6	100.5	2297.9	2318.9	464.9	46.9			46.9	
Cast: 13 October || Tested: 10 November || W/C Ratio: 0.6 || Purpose: 0.75L & 1L										
1	100.4	100.1	2308.9	2297.4	381.8	38.0	40.5	1.9	Minimum:	10.2
2	97.5	101.0	2301.1	2336.7	393.3	39.9			38.0	
3	100.4	101.2	2320.8	2284.1	427.8	42.1			Maximum:	
4	100.7	100.6	2325.5	2295.6	424.6	41.9			42.1	

122

Appendix D: Macro-Mechanical Behaviour Experiment Mix Designs

The mix designs for the macro-mechanical behaviour are given below in Table 45, with materials quantities in kg.m^{-3}.

Table 45: Macro-mechanical behaviour mix designs, in kg.m^{-3}

Mix number	Water	Cement	W/C ratio	6 mm stone	13 mm stone	19 mm stone	Sand	G600 fibres	G500 fibres	Rocstay fibres	Chryso fibres
1	240.0	400.0	0.6	781.5			926.2				
2	240.0	480.0	0.5	781.5			859.4				
3	240.0	600.0	0.4	781.5			759.3				
4	240.0	400.0	0.6		781.5		926.2	6.67			
5	240.0	400.0	0.6			781.5	926.2	6.67			
6	240.0	600.0	0.4		781.5		759.3				
7	240.0	400.0	0.6	781.5			926.2	5.56			
8	240.0	400.0	0.6	781.5			926.2	6.67			
9	240.0	400.0	0.6	781.5			926.2	7.78			
10	240.0	400.0	0.6	781.5			926.2		5.56		
11	240.0	400.0	0.6	781.5			926.2		6.67		
12	240.0	400.0	0.6	781.5			926.2		7.78		

13	240.0	400.0	0.6	781.5			926.2			5.56	
14	240.0	400.0	0.6	781.5			926.2			6.67	
15	240.0	400.0	0.6	781.5			926.2			7.78	
16	240.0	400.0	0.6	781.5			926.2				5.56
17	240.0	400.0	0.6	781.5			926.2				6.67
18	240.0	400.0	0.6	781.5			926.2				7.78
19	240.0	480.0	0.5		781.5		859.4	6.67			
20	240.0	480.0	0.5			781.5	859.4	6.67			
21	240.0	600.0	0.4		781.5		759.3	6.67			
22	240.0	600.0	0.4			781.5	759.3	6.67			
23	240.0	400.0	0.6	781.5			926.2	3.33			
24	240.0	400.0	0.6	781.5			926.2	10.00			
25	240.0	480.0	0.5	781.5			859.4	6.67			
26	240.0	600.0	0.4	781.5			759.3	6.67			

Appendix E: Macro-Mechanical Behaviour Detailed Results

Table 46 presents the peak forces and MORs for the reference (0 % fibres) beam bending tests.

Table 46: Macro-mechanical reference mix results

Beam number	W/C = 0.4		W/C = 0.5		W/C = 0.6	
	Peak force (kN)	MOR (MPa)	Peak force (kN)	MOR (MPa)	Peak force (kN)	MOR (MPa)
1	16.67	5.26	12.81	4.05	9.47	3.08
2	17.44	5.48	13.72	4.32	9.65	3.24
3	17.46	5.41	13.89	4.38	11.75	3.77
4	17.37	5.33	13.94	4.29	11.87	3.99
5	13.53	4.15	13.77	4.35	10.81	3.73
6	-	-	14.04	4.52	11.11	3.68
Average	16.49	5.13	13.70	4.32	10.78	3.58

Table 47, Table 48, Table 49 and Table 50 present the compressive strength, energy absorbed up to a deflection of 40 mm, and the peak load for each RDPT panel for the fibre dosage effect tests.

Table 47: Rocstay fibre dosage effect RDPT results

0.5 % (Mix 13)	Panel 1	Panel 2	Panel 3	Average	Std. deviation	COV
Cube strength (MPa)	38.34	38.34	39.10	38.72	0.54	0.01
Energy absorbed (40 mm)	156.45	157.23	145.83	153.17	6.37	0.04
Peak load (kN)	23.35	22.35	27.11	24.27	2.51	0.10
0.6 % (Mix 14)	Panel 1	Panel 2	Panel 3	Average	Std. deviation	COV
Cube strength (MPa)	35.66	35.66	31.06	34.13	2.66	0.08
Energy absorbed (40 mm)	167.64	204.70	-	186.17	26.21	0.14
Peak load (kN)	25.33	25.45	-	25.39	0.08	0.00

125

Table 47 continued:

0.7 % (Mix 15)	Panel 1	Panel 2	Panel 3	Average	Std. deviation	COV
Cube strength (MPa)	37.19	37.19	36.39	36.92	0.46	0.01
Energy absorbed (40 mm)	189.17	203.56	-	196.37	10.17	0.05
Peak load (kN)	22.65	25.21	-	22.45	2.86	0.13

Table 48: Geotex 500 series fibre dosage effect RDPT results

0.5 % (Mix 10)	Panel 1	Panel 2	Panel 3	Average	Std. deviation	COV
Cube strength (MPa)	38.09	38.09	37.65	37.94	0.25	0.01
Energy absorbed (40 mm)	180.73	179.00	184.23	181.32	2.67	0.01
Peak load (kN)	24.23	21.76	21.92	22.64	1.38	0.06
0.6 % (Mix 11)	Panel 1	Panel 2	Panel 3	Average	Std. deviation	COV
Cube strength (MPa)	38.81	38.81	40.39	39.49	0.91	0.02
Energy absorbed (40 mm)	-	220.94	194.71	207.82	18.55	0.09
Peak load (kN)	-	21.70	20.24	20.97	1.03	0.05
0.7 % (Mix 12)	Panel 1	Panel 2	Panel 3	Average	Std. deviation	COV
Cube strength (MPa)	37.82	37.82	42.80	39.48	2.88	0.07
Energy absorbed (40 mm)	235.45	255.29	223.89	238.21	15.88	0.07
Peak load (kN)	23.28	22.43	22.92	22.88	0.43	0.02

Table 49: Geotex 600 series fibre dosage effect RDPT results

0.3 % (Mix 23)	Panel 1	Panel 2	Panel 3	Average	Std. deviation	COV
Cube strength (MPa)	38.32	38.32	34.40	37.01	2.26	0.06
Energy absorbed (40 mm)	139.01	109.52	-	124.26	20.86	0.17
Peak load (kN)	23.49	21.44	-	22.47	1.45	0.06

126

Table 49 continued:

0.5 % (Mix 7)	Panel 1	Panel 2	Panel 3	Average	Std. deviation	COV
Cube strength (MPa)	37.41	37.41	34.77	36.53	1.52	0.04
Energy absorbed (40 mm)	272.00	187.34	199.15	219.50	45.85	0.21
Peak load (kN)	24.85	22.58	22.14377	23.19	1.46	0.06
0.6 % (Mix 8)	Panel 1	Panel 2	Panel 3	Average	Std. deviation	COV
Cube strength (MPa)	38.28	38.28	39.18	38.58	0.52	0.01
Energy absorbed (40 mm)	-	306.32	272.75	289.53	23.74	0.08
Peak load (kN)	-	24.47	22.28	23.37	1.55	0.07
0.7 % (Mix 9)	Panel 1	Panel 2	Panel 3	Average	Std. deviation	COV
Cube strength (MPa)	34.59	34.59	36.55	35.24	1.13	0.03
Energy absorbed (40 mm)	350.26	339.21	289.98	326.49	32.09	0.10
Peak load (kN)	23.14	24.75	21.72	23.20	1.52	0.07
0.9 % (Mix 24)	Panel 1	Panel 2	Panel 3	Average	Std. deviation	COV
Cube strength (MPa)	33.87	33.87	34.45	34.06	0.33	0.01
Energy absorbed (40 mm)	390.00	358.16	449.13	399.10	46.16	0.12
Peak load (kN)	23.70	22.58	25.65	23.98	1.55	0.06

Table 50: Chryso Structural fibre dosage effect RDPT results

0.6 % (Mix 17)	Panel 1	Panel 2	Panel 3	Average	Std. deviation	COV
Cube strength (MPa)	35.66	35.66	31.06	34.13	2.66	0.08
Energy absorbed (40 mm)	316.21	285.31	327.48	309.67	21.84	0.07
Peak load (kN)	23.20	21.52	23.22	22.65	0.97	0.04

Table 51, Table 52 and Table 53 present the compressive strength, peak load, modulus of rupture (MOR), mean equivalent force at 2.65 mm (F_3), equivalent flexural tensile strength at 2.65 mm ($f_{eq,3}$) and the $R_{e,3}$ values for each fibre dosage type and dosage variation beam tested. Results highlighted in red were excluded due to testing complications or being abnormally high.

Table 51: Rocstay fibre dosage effect three point beam bending results

0.5 % (Mix 13)	Beam 1	Beam 2	Beam 3	Beam 4	Beam 5	Beam 6	Average	Standard deviation	COV
Cube strength (MPa)	38.34	38.34	39.10	39.10	39.10	39.10	38.80	0.39	0.01
Peak load (kN)	10.57	11.77	13.20	13.15	11.36	13.86	12.01	1.27	0.11
MOR (MPa)	4.70	5.28	5.83	5.92	5.30	6.19	5.41	0.55	0.10
F_3 (kN)	2.09	2.91	3.03	3.43	3.63	5.64	3.02	1.19	0.40
$f_{eq,3}$ (MPa)	0.93	1.31	1.34	1.54	1.69	2.52	1.36	0.54	0.39
$R_{e,3}$ (2.65 mm)	0.20	0.25	0.23	0.26	0.32	0.41	0.25	0.08	0.30
0.6 % (Mix 14)	Beam 1	Beam 2	Beam 3	Beam 4	Beam 5	Beam 6	Average	Standard deviation	COV
Cube strength (MPa)	35.66	35.66	31.06	31.06	31.06	31.06	32.59	2.38	0.07
Peak load (kN)	10.48	12.52	10.53	10.61	11.18	11.00	11.05	0.77	0.07
MOR (MPa)	4.54	5.47	4.76	4.65	4.86	4.90	4.86	0.33	0.07
F_3 (kN)	2.08	4.35	4.34	3.02	2.39	2.52	3.12	1.00	0.32
$f_{eq,3}$ (MPa)	0.90	1.90	1.96	1.32	1.04	1.13	1.38	0.45	0.33
$R_{e,3}$ (2.65 mm)	0.20	0.35	0.41	0.28	0.21	0.23	0.28	0.08	0.30

Table 51 continued:

0.7 % (Mix 15)	Beam 1	Beam 2	Beam 3	Beam 4	Beam 5	Beam 6	Average	Standard deviation	COV
Cube strength (MPa)	37.19	37.19	36.39	36.39	36.39	36.39	36.66	0.41	0.01
Peak load (kN)	11.26	10.23	11.63	11.53	12.70	10.78	11.36	0.84	0.07
MOR (MPa)	5.12	4.56	5.10	5.24	5.44	4.72	5.03	0.33	0.07
F_3 (kN)	4.98	4.56	5.33	3.98	3.82	6.02	4.78	0.84	0.17
$f_{eq,3}$ (MPa)	2.26	2.03	2.34	1.81	1.64	2.63	2.12	0.37	0.17
$R_{e,3}$ (2.65 mm)	0.44	0.45	0.46	0.34	0.30	0.56	0.42	0.09	0.21

Table 52: Geotex 500 series fibre dosage effect three point beam bending results

0.5 % (Mix 10)	Beam 1	Beam 2	Beam 3	Beam 4	Beam 5	Beam 6	Average	Standard deviation	COV
Cube strength (MPa)	38.09	38.09	37.65	37.65	37.65	37.65	37.80	0.23	0.01
Peak load (kN)	11.34	13.04	10.19	10.13	10.71	12.05	11.24	1.14	0.10
MOR (MPa)	5.21	6.09	4.76	4.70	4.71	5.52	5.17	0.56	0.11
F_3 (kN)	3.54	4.30	3.17	2.70	2.94	3.48	3.36	0.56	0.17
$f_{eq,3}$ (MPa)	1.63	1.90	1.48	1.25	1.29	1.60	1.52	0.24	0.16
$R_{e,3}$ (2.65 mm)	0.31	0.31	0.31	0.27	0.27	0.29	0.29	0.02	0.07

Table 52 continued:

0.6 % (Mix 11)	Beam 1	Beam 2	Beam 3	Beam 4	Beam 5	Beam 6	Average	Standard deviation	COV
Cube strength (MPa)	38.81	38.81	40.39	40.39	40.39	40.39	39.86	0.82	0.02
Peak load (kN)	10.88	12.10	10.21	12.28	12.45	11.36	11.55	0.88	0.08
MOR (MPa)	4.92	5.49	4.67	5.68	5.71	5.27	5.29	0.42	0.08
F_3 (kN)	3.02	3.59	2.53	4.21	3.74	2.87	3.33	0.63	0.19
$f_{eq,3}$ (MPa)	1.37	1.63	1.16	1.95	1.72	1.33	1.52	0.29	0.19
$R_{e,3}$ (2.65 mm)	0.28	0.30	0.25	0.34	0.30	0.25	0.29	0.04	0.12
0.7 % (Mix 12)	Beam 1	Beam 2	Beam 3	Beam 4	Beam 5	Beam 6	Average	Standard deviation	COV
Cube strength (MPa)	37.82	37.82	42.80	42.80	42.80	42.80	42.80	2.57	0.06
Peak load (kN)	13.21	14.58	12.17	13.88	13.06	10.95	12.51	1.28	0.10
MOR (MPa)	5.76	6.53	5.26	6.23	6.00	4.98	5.62	0.59	0.10
F_3 (kN)	7.21	8.67	3.26	3.21	4.24	4.14	3.71	2.27	0.61
$f_{eq,3}$ (MPa)	3.14	3.88	1.41	1.44	1.94	1.88	1.67	1.01	0.60
$R_{e,3}$ (2.65 mm)	0.55	0.59	0.27	0.23	0.32	0.38	0.30	0.15	0.50

Table 53: Geotex 600 series fibre dosage three point beam bending results

0.3 % (Mix 23)	Beam 1	Beam 2	Beam 3	Beam 4	Beam 5	Beam 6	Average	Standard deviation	COV
Cube strength (MPa)	38.32	38.32	34.40	34.40	34.40	34.40	35.71	2.02	0.06
Peak load (kN)	9.50	11.12	10.10	12.16	-	10.26	10.63	1.03	0.10
MOR (MPa)	4.43	5.07	4.49	5.53	-	4.64	4.83	0.46	0.10
F_3 (kN)	2.00	2.57	2.68	2.17	-	2.69	2.42	0.32	0.13
$f_{eq,3}$ (MPa)	0.93	1.17	1.19	0.93	-	1.22	1.09	0.15	0.13
$R_{e,3}$ (2.65 mm)	0.21	0.23	0.27	0.17	-	0.26	0.23	0.04	0.18
0.5 % (Mix 7)	Beam 1	Beam 2	Beam 3	Beam 4	Beam 5	Beam 6	Average	Standard deviation	COV
Cube strength (MPa)	37.41	37.41	34.77	34.77	34.77	34.77	35.65	1.36	0.04
Peak load (kN)	10.63	10.64	11.56	11.23	11.38	10.96	11.07	0.39	0.04
MOR (MPa)	4.89	4.95	5.29	5.42	5.02	4.78	5.06	0.25	0.05
F_3 (kN)	4.74	5.84	2.99	3.57	4.12	2.51	3.96	1.21	0.31
$f_{eq,3}$ (MPa)	2.18	2.72	1.37	1.72	1.82	1.17	1.83	0.56	0.31
$R_{e,3}$ (2.65 mm)	0.45	0.55	0.26	0.32	0.36	0.24	0.36	0.12	0.33

Table 53 continued:

0.6 % (Mix 8)	Beam 1	Beam 2	Beam 3	Beam 4	Beam 5	Beam 6	Average	Standard deviation	COV
Cube strength (MPa)	38.28	38.28	39.18	39.18	39.18	39.18	38.88	0.46	0.01
Peak load (kN)	12.63	11.75	9.84	12.33	10.98	10.62	11.36	1.07	0.09
MOR (MPa)	5.74	5.57	4.50	5.67	5.09	4.99	5.26	0.49	0.09
F_3 (kN)	5.24	6.33	3.34	4.85	6.00	4.93	5.12	1.05	0.21
$f_{eq,3}$ (MPa)	2.38	3.00	1.53	2.23	2.78	2.31	2.37	0.51	0.21
$R_{e,3}$ (2.65 mm)	0.41	0.54	0.34	0.39	0.55	0.46	0.45	0.08	0.18
0.7 % (Mix 9)	Beam 1	Beam 2	Beam 3	Beam 4	Beam 5	Beam 6	Average	Standard deviation	COV
Cube strength (MPa)	34.59	34.59	36.55	36.55	36.55	36.55	35.90	1.01	0.03
Peak load (kN)	9.44	10.18	10.84	10.73	9.26	9.84	10.05	0.65	0.07
MOR (MPa)	4.29	4.77	4.86	5.03	4.46	4.55	4.66	0.27	0.06
F_3 (kN)	6.38	5.78	4.90	5.96	3.46	4.18	5.11	1.13	0.22
$f_{eq,3}$ (MPa)	2.90	2.71	2.20	2.79	1.67	1.93	2.37	0.51	0.21
$R_{e,3}$ (2.65 mm)	0.68	0.57	0.45	0.56	0.37	0.42	0.51	0.11	0.22

Table 53 continued:

0.9 % (Mix 24)	Beam 1	Beam 2	Beam 3	Beam 4	Beam 5	Beam 6	Average	Standard deviation	COV
Cube strength (MPa)	33.87	33.87	34.45	34.45	34.45	34.45	34.26	0.30	0.01
Peak load (kN)	11.69	10.02	11.17	10.95	10.15	11.13	10.85	0.64	0.06
MOR (MPa)	5.34	4.58	4.82	5.00	4.70	4.82	4.88	0.27	0.05
F_3 (kN)	5.56	6.50	8.91	6.38	5.20	7.36	6.65	1.34	0.20
$f_{eq,3}$ (MPa)	2.54	2.97	3.85	2.91	2.41	3.19	2.98	0.51	0.17
$R_{e,3}$ (2.65 mm)	0.48	0.65	0.80	0.58	0.51	0.66	0.61	0.12	0.19

Table 54, Table 55 and Table 56 present the compressive strength, energy absorbed and peak load for the RDPT panels involved in W/C ratio and aggregate size effect testing.

Table 54: Aggregate variation at 0.6 W/C ratio

6 mm (Mix 8)	Panel 1	Panel 2	Panel 3	Average	Std. deviation	COV
Cube strength (MPa)	38.28	38.28	39.18	38.73	0.64	0.02
Energy absorbed (40 mm)	-	306.32	272.75	289.53	23.74	0.08
Peak load (kN)	-	24.47	22.28	23.37	1.55	0.07
13 mm (Mix 4)	Panel 1	Panel 2	Panel 3	Average	Std. deviation	COV
Cube strength (MPa)	33.21	33.21	35.28	34.25	1.46	0.04
Energy absorbed (40 mm)	202.30	237.13	217.03	218.82	17.49	0.08
Peak load (kN)	20.26	20.95	19.85	20.35	0.56	0.03
19 mm (Mix 5)	Panel 1	Panel 2	Panel 3	Average	Std. deviation	COV
Cube strength (MPa)	29.38	29.38	28.81	29.10	0.40	0.01
Energy absorbed (40 mm)	145.62	262.00	197.74	201.78	58.30	0.29
Peak load (kN)	19.11	20.51	20.59	20.07	0.83	0.04

Table 55: Aggregate variation at 0.5 W/C ratio

6 mm (Mix 25)	Panel 1	Panel 2	Panel 3	Average	Std. deviation	COV
Cube strength (MPa)	47.45	47.45	48.81	48.13	0.96	0.02
Energy absorbed (40 mm)	339.49	-	352.04	345.77	8.87	0.03
Peak load (kN)	25.66		26.86	26.26	0.85	0.03
13 mm (Mix 19)	Panel 1	Panel 2	Panel 3	Average	Std. deviation	COV
Cube strength (MPa)	45.59	45.59	43.63	44.61	1.39	0.03
Energy absorbed (40 mm)	277.56	232.92	203.78	238.09	37.16	0.16
Peak load (kN)	23.19	23.95	23.03	23.39	0.49	0.02

Table 55 continued:

19 mm (Mix 20)	Panel 1	Panel 2	Panel 3	Average	Std. deviation	COV
Cube strength (MPa)	44.50	44.50	43.64	44.07	0.61	0.01
Energy absorbed (40 mm)	205.58	206.67	180.44	197.56	14.84	0.08
Peak load (kN)	18.43	20.45	22.01	20.30	1.80	0.09

Table 56: Aggregate variation at 0.4 W/C ratio

6 mm (Mix 26)	Panel 1	Panel 2	Panel 3	Average	Std. deviation	COV
Cube strength (MPa)	52.62	52.64	51.77	52.21	0.62	0.01
Energy absorbed (40 mm)	327.83	345.90	411.43	361.72	43.99	0.12
Peak load (kN)	27.99	29.77	28.67	28.81	0.90	0.03
13 mm (Mix 21)	Panel 1	Panel 2	Panel 3	Average	Std. deviation	COV
Cube strength (MPa)	56.39	56.39	58.36	57.38	1.39	0.02
Energy absorbed (40 mm)	251.91	-	286.57	269.24	24.50	0.09
Peak load (kN)	24.03		26.38	25.21	1.67	0.07
19 mm (Mix 22)	Panel 1	Panel 2	Panel 3	Average	Std. deviation	COV
Cube strength (MPa)	55.51	55.51	53.23	54.37	1.61	0.03
Energy absorbed (40 mm)	257.21	257.72	226.06	247.00	18.14	0.07
Peak load (kN)	23.22	24.49	25.45	24.39	1.12	0.05

Table 57, Table 58 and Table 59 present the compressive strength, peak load, MOR, equivalent force (F_3), third equivalent flexural tensile strength $(f_{eq,3})$ and $R_{e,3}$ value for the beams involved in W/C ratio and aggregate size effect testing.

Table 57: Three point beam bending tests aggregate size effect at 0.6 W/C ratio

6 mm (Mix 8)	Beam 1	Beam 2	Beam 3	Beam 4	Beam 5	Beam 6	Average	Standard deviation	COV
Cube strength (MPa)	38.28	38.28	39.18	39.18	39.18	39.18	38.88	0.47	0.01
Peak load (kN)	12.63	11.75	9.84	12.33	10.98	10.62	11.36	1.07	0.09
MOR (MPa)	4.12	4.00	3.22	4.06	3.64	3.58	3.77	0.35	0.09
F_3 (kN)	5.24	6.33	3.34	4.85	6.00	4.93	5.12	1.05	0.21
$f_{eq,3}$ (MPa)	1.71	2.15	1.09	1.60	1.99	1.66	1.70	0.37	0.22
$R_{e,3}$ (2.65 mm)	0.41	0.54	0.34	0.39	0.55	0.46	0.45	0.08	0.18
13 mm (Mix 4)	Beam 1	Beam 2	Beam 3	Beam 4	Beam 5	Beam 6	Average	Standard deviation	COV
Cube strength (MPa)	33.21	33.21	35.28	35.28	35.28	35.28	34.59	1.07	0.03
Peak load (kN)	12.56	11.91	10.96	10.98	10.98	11.70	11.51	0.66	0.06
MOR (MPa)	3.81	3.82	3.43	3.54	3.42	3.74	3.62	0.19	0.05
F_3 (kN)	5.84	4.72	4.58	4.54	4.43	6.58	5.12	0.89	0.17
$f_{eq,3}$ (MPa)	1.77	1.51	1.43	1.46	1.38	2.11	1.61	0.28	0.17
$R_{e,3}$ (2.65 mm)	0.47	0.40	0.42	0.41	0.40	0.56	0.44	0.06	0.14

Table 57 continued:

19 mm (Mix 5)	Beam 1	Beam 2	Beam 3	Beam 4	Beam 5	Beam 6	Average	Standard deviation	COV
Cube strength (MPa)	29.38	29.38	28.81	28.81	28.81	28.81	29.00	0.29	0.01
Peak load (kN)	10.02	9.27	9.48	9.49	9.55	9.65	9.58	0.25	0.03
MOR (MPa)	3.16	2.96	3.06	3.15	3.07	3.08	3.08	0.07	0.02
F_3 (kN)	4.49	3.79	3.84	3.49	4.16	5.20	4.16	0.61	0.15
$f_{eq,3}$ (MPa)	1.41	1.21	1.24	1.16	1.34	1.66	1.34	0.18	0.14
$R_{e,3}$ (2.65 mm)	0.45	0.41	0.40	0.37	0.44	0.54	0.43	0.06	0.13

Table 58: Three point beam bending tests aggregate size effect at 0.5 W/C ratio

6 mm (Mix 25)	Beam 1	Beam 2	Beam 3	Beam 4	Beam 5	Beam 6	Average	Standard deviation	COV
Cube strength (MPa)	47.45	-	-	48.81	48.81	48.81	48.47	0.68	0.01
Peak load (kN)	14.55	-	-	11.79	13.77	13.78	13.47	1.18	0.09
MOR (MPa)	4.72	-	-	3.67	4.41	4.25	4.26	0.44	0.10
F_3 (kN)	4.69	-	-	3.75	3.81	5.37	4.41	0.77	0.18
$f_{eq,3}$ (MPa)	1.52	-	-	1.17	1.22	1.66	1.39	0.24	0.17
$R_{e,3}$ (2.65 mm)	0.32	-	-	0.32	0.28	0.39	0.33	0.05	0.14

Table 58 continued:

13 mm (Mix 19)	Beam 1	Beam 2	Beam 3	Beam 4	Beam 5	Beam 6	Average	Standard deviation	COV
Cube strength (MPa)	45.59	45.59	43.63	43.63	43.63	43.63	44.28	1.01	0.02
Peak load (kN)	10.20	13.45	12.49	12.49	14.25	13.95	12.81	1.47	0.11
MOR (MPa)	3.22	4.32	3.98	3.72	4.38	4.28	3.98	0.45	0.11
F_3 (kN)	3.78	5.69	5.35	4.82	6.19	7.58	5.57	1.29	0.23
$f_{eq,3}$ (MPa)	1.20	1.82	1.70	1.43	1.90	2.33	1.73	0.39	0.23
$R_{e,3}$ (2.65 mm)	0.37	0.42	0.43	0.39	0.43	0.54	0.43	0.06	0.14
19 mm (Mix 20)	Beam 1	Beam 2	Beam 3	Beam 4	Beam 5	Beam 6	Average	Standard deviation	COV
Cube strength (MPa)	44.50	44.50	43.64	43.64	43.64	43.64	43.93	0.44	0.01
Peak load (kN)	11.84	12.97	10.74	11.36	13.97	12.06	12.16	1.16	0.10
MOR (MPa)	3.84	3.89	3.59	3.79	4.50	3.89	3.92	0.31	0.08
F_3 (kN)	4.11	4.52	5.31	2.86	4.91	3.21	4.15	0.96	0.23
$f_{eq,3}$ (MPa)	1.33	1.36	1.78	0.95	1.58	1.03	1.34	0.31	0.23
$R_{e,3}$ (2.65 mm)	0.35	0.35	0.49	0.25	0.35	0.27	0.34	0.09	0.25

Table 59: Three point beam bending tests aggregate size effect at 0.4 W/C ratio

6 mm (Mix 26)	Beam 1	Beam 2	Beam 3	Beam 4	Beam 5	Beam 6	Average	Standard deviation	COV
Cube strength (MPa)	52.62	52.62	51.77	51.77	51.77	51.77	52.05	0.44	0.01
Peak load (kN)	17.22	16.54	17.07	16.41	17.26	18.60	17.18	0.78	0.05
MOR (MPa)	4.99	5.20	5.16	5.08	5.19	5.56	5.20	0.19	0.04
F_3 (kN)	5.17	3.32	5.51	6.77	4.61	4.75	5.02	1.13	0.23
$f_{eq,3}$ (MPa)	1.50	1.05	1.67	2.10	1.39	1.42	1.52	0.35	0.23
$R_{e,3}$ (2.65 mm)	0.30	0.20	0.32	0.41	0.27	0.26	0.29	0.07	0.24
13 mm (Mix 21)	Beam 1	Beam 2	Beam 3	Beam 4	Beam 5	Beam 6	Average	Standard deviation	COV
Cube strength (MPa)	56.39	56.39	58.36	58.36	58.36	58.36	57.70	1.02	0.02
Peak load (kN)	15.18	15.35	16.29	16.18	17.16	14.95	15.85	0.84	0.05
MOR (MPa)	5.03	4.95	5.15	5.21	5.33	4.75	5.07	0.20	0.04
F_3 (kN)	4.05	5.24	5.28	4.26	3.51	3.77	4.35	0.75	0.17
$f_{eq,3}$ (MPa)	1.34	1.69	1.67	1.37	1.09	1.20	1.39	0.24	0.17
$R_{e,3}$ (2.65 mm)	0.27	0.34	0.32	0.26	0.20	0.25	0.28	0.05	0.18

Table 59 continued:

19 mm (Mix 22)	Beam 1	Beam 2	Beam 3	Beam 4	Beam 5	Beam 6	Average	Standard deviation	COV
Cube strength (MPa)	55.51	55.51	53.23	53.23	53.23	53.23	53.99	1.18	0.02
Peak load (kN)	15.44	15.83	17.52	14.93	14.82	14.22	15.46	1.15	0.07
MOR (MPa)	4.83	5.30	5.28	4.85	4.76	4.58	4.93	0.29	0.06
F_3 (kN)	4.13	3.86	3.34	5.25	3.49	7.15	4.54	1.45	0.32
$f_{eq,3}$ (MPa)	1.29	1.29	1.01	1.71	1.12	2.30	1.45	0.48	0.33
$R_{e,3}$ (2.65 mm)	0.27	0.24	0.19	0.35	0.24	0.50	0.30	0.11	0.38